The malate aspartate shuttle in T cell metabolic fitness: Glutamic oxaloacetic transaminase 1 antagonizes T cell exhaustion

Dissertation

submitted to the Combined Faculty of Natural Sciences and Mathematics
of the Ruperto Carola University Heidelberg, Germany
for the degree of Doctor of Natural Sciences

M. Sc. Nina Kathrin Weißhaar
born in Stuttgart, Germany

Dissertation
submitted to the
Combined Faculty of Natural Sciences and Mathematics
of the Ruperto Carola University Heidelberg, Germany
for the degree of
Doctor of Natural Sciences

Presented by
M. Sc. Nina Kathrin Weißhaar
born in Stuttgart, Germany

Oral examination: 22nd July 2020

The malate aspartate shuttle in T cell metabolic fitness: Glutamic oxaloacetic transaminase 1 antagonizes T cell exhaustion

Referees:

Prof. Dr. Ralf Bartenschlager

Dr. Guoliang Cui

Dissertation

submitted to the Combined Faculty of Natural Sciences and Mathematics
of the Ruperto Carola University Heidelberg, Germany
for the degree of Doctor of Natural Sciences

Presented by
M. Sc. Nina Kathrin Weißhaar
born in Stuttgart, Germany

Submitted: 26th May 2020

Acknowledgements

I want to express my gratitude to the people who supported me during this exciting time. The past years have been a journey with ups and downs, and your support made this work possible.

First of all, I would like to thank Dr. Guoliang Cui, who gave me the possibility to join his newly founded lab almost 4 years ago. It has been an exciting time with excellent supervision. His incredible knowledge in immunology combined with his scientific curiosity was stimulating and inspiring, and his continuous support and advice helped me to stay focused and motivated.

I would like to thank my thesis advisory committee and defense committee with Prof. Dr. Ralf Bartenschlager and Prof. Dr. Britta Brügger for their helpful advice and valuable opinions on the progress of this work. Also, I would like to thank Prof. Dr. Hedda Wardemann for participating in my defense as additional referee.

Furthermore, I want to thank my lab colleagues from the T cell metabolism lab, especially Kerstin Mohr, Alaa Madi, Alessa Mieg, Tilo Schlimbach, Dr. Jingxia Wu, Dr. Sicong Ma and Marvin Hering not only for their support in the lab, but also for the great conversations, fun activities, and their continuous support and motivation. You guys kept me going!

Also great thanks to my Azubis Lukas Schmitt, Mareike Munz and Helena Borgers. It was a pleasure working with you! Thank you so much for your contribution and excellent help.

Additionally, I want to say thank you to the students I supervised and co-supervised: Mona Wang, Lisann Müller, Hannah Byren, Mohamed Mahmoud and Maren Baumeister. Thank you for your trust and your hard work.

I would further like to thank the DKFZ flow cytometry core facility, the DKFZ monoclonal antibody core facility, the DKFZ animal core facility and Michael Buettner and Gernot Poschet from the COS for their experimental and scientific support.

Also, a big thank you to all friends from home, and all the friends I made during my time at DKFZ. Thank you so much for all the fun, for motivating me and believing in me, for listening to my complaints and sorrows and for making these years unforgettable.

In the end, my biggest thanks go to my family.

Ich danke meinen Eltern Christine und Rüdiger für ihre uneingeschränkte Liebe und Unterstützung seit meiner Geburt. Ihr habt mich immer begleitet und an mich geglaubt, mir jeden Fehler verziehen, mich bei jeder Entscheidung unterstützt und mir so vieles ermöglicht. Danke auch an meinen Bruder Alexander für seine Motivation und seine positive Energie. Ihr seid mein Vorbild und meine Inspiration. Dafür danke und liebe ich euch.

Zuletzt möchte ich meinem Freund Michael Kircher danken, der mit mir durch die gleiche spannende Zeit gegangen ist. Du hast an mich geglaubt und mich immer unterstützt. Du bist ein Schatz und ich liebe dich.

Abstract

$CD8^+$ T cells play a crucial role in fighting infectious diseases and cancers, but it is frequently observed that $CD8^+$ T cells are functionally compromised or “exhausted” in chronic infections and solid tumors. Exhausted T cells are characterized by the expression of immune checkpoint molecules, reduction in effector cytokine secretion, and alterations in cellular metabolism, such as loss of mitochondrial membrane potential (ΔΨm). Immune checkpoint blockade-based immunotherapies revive exhausted T cells, enhance effector cytokine production, and have achieved clinical success in several types of cancers. It is unknown whether and how ΔΨm regulates T cell exhaustion in chronic infection and cancer. Mitochondrial complexes accept electrons from tricarboxylic acid (TCA) cycle-derived electron carriers, transfer electrons, and pump protons to establish a membrane potential. The malate aspartate shuttle (MAS) produces and transports electron carriers into the mitochondrial matrix and donates electrons to the electron transport chain (ETC). We, therefore, hypothesize that MAS may regulate ΔΨm and antagonize T cell exhaustion.

To test this hypothesis, we have generated a mouse model with T cell-specific deficiency of glutamic oxaloacetic transaminase 1 (*Got1*, encoding the MAS enzyme GOT1). We chose GOT1 because it is a key enzyme of the MAS, and we observed that GOT1 expression was induced by persistent antigenic stimulation in mouse $CD8^+$ T cells and upregulated in $CD8^+$ tumor-infiltrating lymphocytes (TILs) from human colon cancer. T cell-specific ablation of *Got1* impaired tumor-specific effector $CD8^+$ T cell accumulation, effector cytokine production and potential to sustain long term immune responses in a mouse melanoma model. Using the lymphocytic choriomeningitis virus (LCMV) Armstrong acute infection and the LCMV clone 13 chronic infection model, we found that *Got1* deficiency affected the ongoing antiviral effector responses, but not the memory T cell formation after viral clearance, suggesting that $CD8^+$ responses required GOT1 in the presence of persistent, but not transient antigenic stimulation. Further analysis revealed that *Got1* deficiency alone did not affect $CD8^+$ T cell metabolism or ΔΨm when cells were cultured in complete medium. Instead, *Got1* deficiency became only catastrophic for $CD8^+$ T cells when extracellular nutrients were restricted, and antigenic stimulation was persistent. *Got1* deficiency reduced the NAD^+/NADH ratio, increased reactive oxygen species (ROS) production and decreased ΔΨm. This study reveals, GOT1 selectively supports effector $CD8^+$ T cells that are nutrient restricted and chronically stimulated.

Summarized, the presented work revealed that persistent stimulation with tumor and viral antigens induced GOT1 expression on $CD8^+$ T cells. GOT1 was shown to desensitize $CD8^+$ T cells to environmental nutrient limitation and persistent antigenic stimulation-induced loss of ΔΨm and T cell exhaustion. These results present an example of how immune cells alter their metabolic pathways to adapt to nutrient and antigen availability.

Zusammenfassung

Die körpereigene Bekämpfung von Infektionen und Krebs geschieht hauptsächlich durch zytotoxische $CD8^+$ T-Zellen. Es wird regelmäßig beobachtet, dass $CD8^+$ T-Zellen bei chronischen Infektionen und Tumoren in ihrer Funktion eingeschränkt und „erschöpft“ sind. Charakteristisch für erschöpfte T-Zellen sind die Expression von Immun-Checkpoint Molekülen, die eingeschränkte Ausschüttung von Effektorzytokinen und Veränderungen im Metabolismus (z.B. Verlust des mitochondriellen Membranpotentials $\Delta\Psi m$). Immuntherapien basierend auf der Blockierung von Immun-Checkpoint Molekülen, können erschöpfte T-Zellen reaktivieren und haben bei einigen Krebsarten zu klinischen Erfolgen geführt. Allerdings ist nicht bekannt, ob und wie $\Delta\Psi m$ die Erschöpfung von $CD8^+$ T-Zellen in chronischen Infektionen und bei Krebs beeinflusst. Die Atmungskette im Mitochondrium transportiert Elektronen von Reduktionsäquivalenten des Citratzyklus und erhöht durch das Pumpen von Protonen das Membranpotential. Das Malat-Aspartat Shuttle (MAS) transportiert Elektronen aus dem Cytosol in die mitochondrielle Matrix zur Elektronentransportkette. Daher nahmen wir an, dass MAS $\Delta\Psi m$ beeinflusst und damit auch potentielle Auswirkungen auf T-Zell Erschöpfung hat. Um diesen Zusammenhang zu untersuchen, nutzten wir ein Mausmodell mit T-Zell spezifischem Mangel an Glutamat-Oxalacetat-Transaminase 1 (GOT1). GOT1 interessierte uns als Schlüsselenzym des MAS und da die Expression durch chronische Antigenstimulation in murinen $CD8^+$ T-Zellen induziert wurde. Wir detektierten GOT1 auch in tumorinfiltrierenden Lymphozyten aus humanem Colonkarzinom. Der T-Zell-spezifische Mangel von GOT1 beeinträchtigte die Zahl und Effektorfunktion von tumorspezifischen $CD8^+$ T-Zellen in einem Maus Melanom Modell. GOT1-Mangel beeinflusste auch die Effektorfunktion, aber nicht die immunologische Gedächtnisbildung in viralen Infektionsmodellen, induziert mit den akuten und chronischen lymphozytären Choriomeningitis Virusstämmen *Armstrong* und *clone 13.* Die Ergebnisse zeigen, dass $CD8^+$ T-Zellen bei chronischer, aber nicht akuter Antigenstimulation, von GOT1 abhängig sind. Weitere Untersuchungen ergaben, dass der Verlust von GOT1 den Metabolismus und $\Delta\Psi m$ nicht beeinflusste, wenn Zellen in einem Vollmedium kultiviert wurden. GOT1 erwies sich aber als essentiell, wenn die Zellen in einem nährstoffarmen Minimalmedium stimuliert wurden. GOT1-Mangel führte zu einem Abfall des NAD^+/NADH Verhältnis, erhöhte die Level von reaktiven Sauerstoffspezies und verringerte $\Delta\Psi m$.

Zusammenfassend zeigt diese Arbeit, dass die Stimulation mit Tumor- und Virusantigenen die Expression von GOT1 in $CD8^+$ T-Zellen induzierte, und dass GOT1 $CD8^+$ T-Zellen gegenüber Nährstofflimitation desensibilisierte und damit dem Verlust an $\Delta\Psi m$ und dem Fortschreiten der T-Zell Erschöpfung entgegenwirkte. Damit liefern die Ergebnisse ein Beispiel dafür, wie $CD8^+$ T-Zellen metabolische Stoffwechselwege an die Nährstoffverfügbarkeit und Präsenz von Antigenen anpassen.

Table of contents

Acknowledgements ..... **I**

Abstract ..... **III**

Zusammenfassung ..... **V**

1. Introduction **1**

1.1. The immune system 1
1.1.1. The innate immune system 1
1.1.2. The adaptive immune system 2

1.2. T-Lymphocytes 4
1.2.1. T cell activation 6
1.2.2. T cell metabolism 8
1.2.3. T cell exhaustion 10

1.3. Immunotherapy 13
1.3.1. Immunotherapy in cancer 14
1.3.2. Immunotherapy in chronic infections 15

1.4. The malate aspartate shuttle (MAS) 15
1.4.1. GOT1 in T cell biology 16

1.5. Aim of this work 17

2. Materials **19**

2.1. Chemicals and reagents 19

2.2. Commercial kits 23

2.3. Buffers and solutions 24

2.4. Cell culture media composition 26

2.5. Antibodies 27

2.6. Proteins, enzymes and peptides 30

2.7. Biological material 31
2.7.1. Cell lines 31
2.7.2. Viral strains 31
2.7.3. Mouse strains 31
2.7.4. Human material 32

2.8. Consumables 32

2.9. Instruments 33

2.10. Software 35

3. Methods 37

3.1. Cell biology 37
3.1.1. General cell culture practice 37
3.1.2. Virus production of LCMV strains Arm and cl-13 38
3.1.3. Primary cell preparation from mouse organs 39
3.1.4. Preparation of tumor infiltrating lymphocytes (TILs) from mouse tumors 39
3.1.5. T cell isolation from human tissue samples 40
3.1.6. T cell isolation from primary cell suspensions 40
3.1.7. *In vitro* culture of primary cells 41
3.1.8. Staining for flow cytometry 42

3.2. Molecular biology 44
3.2.1. Quantitative real-time PCR (qRT-PCR) analysis of RNA expression in TILs 44
3.2.2. Western blot 44

3.3. Metabolic analysis 46
3.3.1. Seahorse analysis of $Got1^{flox/flox}$Cd4-cre^{-} and $Got1^{flox/flox}$Cd4-cre^{+} P14 T cells 46
3.3.2. Metabolic tracing with ^{13}C-labeled metabolites 49
3.3.3. NAD^{+}/NADH determination by luminescence 51

3.4. *In vivo* studies 51
3.4.1. General mouse genotyping 51
3.4.2. Immune characterization of $Got1^{+/+}$Cd4-cre^{+} or $Got1^{flox/flox}$Cd4-cre^{+} mice 53
3.4.3. Viral infection experiments 53
3.4.4. Tumor experiments 54

4. Results 55

4.1. Breeding and quality control of *Got1*-deficient mouse lines 55

4.2. Naïve mice with *Got1*-deficient T cells develop a normal immune system 56

4.3. GOT1 expression correlates with TCR stimulation *in vitro* 58

4.4. GOT1 is expressed in antitumoral T cells in mice and humans 61

4.5. GOT1 is required for effector cell differentiation, but not for memory formation after acute viral infections 62

4.6. GOT1 is required for the persistence of exhausted T cells after chronic viral infections 66

4.7. GOT1 is required for antigen-specific anti-tumor T cell responses 70

4.8. *Got1*-deficient T cells show metabolic defects *in vivo* after viral infection 79

4.9. The loss of GOT1 does not impair the utilization of extracellular nutrients 81

4.10. GOT1 does not influence electron flux in the ETC 83

4.11. GOT1-associated phenotypes correlate with nutrient withdrawal *in vitro* 84

4.12. Loss of GOT1 correlates with bioenergetic insufficiencies 86

4.13. GOT1-associated phenotypes can be rescued *in vitro* 87

4.14. Pyruvate and α-KG supplementation restored GOT1-associated phenotypes *in vivo* 90

5. Discussion 95

5.1. The expression of *Got1* is dependent on TCR stimulation, but delayed compared to TCR-associated pathways 96

5.2. *In vitro* and *in vivo* studies of *Got1*-deficient T cells 97

5.3. GOT1 is dispensable in environments of excessive nutrient availability 97

5.4. GOT1 is required to maintain cellular metabolic fitness during nutrient restriction 98
5.4.1. GOT1 mediates redox balance and ROS expression 99
5.4.2. GOT1 maintains mitochondrial fitness and desensitizes T cells to oxidative stress and apoptosis 100
5.4.3. GOT1 desensitizes T cells to extracellular nutrient availability 102

5.5. GOT1 maintains T cell effector functions and antagonizes T cell exhaustion 105
5.5.1. GOT1 is required for effector but not memory T cell formation 105
5.5.2. GOT1 antagonizes T cell exhaustion 106

5.6. Conclusion 109

References 113

Supplementary figures 127

List of figures 129

List of tables 131

Abbreviations 133

List of publications 137

1. Introduction

The human body encounters millions of pathogenic and non-pathogenic microorganisms, bacteria or viruses. Also, own body cells can mutate and become aggressively growing tumors. To distinguish between friend or foe, “self” and “non-self”, and to defend the organism against potentially harmful or fatal diseases, a complex and multilayered defense mechanism developed: the immune system [1]. The immune system is a well-orchestrated collaboration between various cell-types, tissues and soluble factors, with the aim to protect from the invasion and multiplication of pathogens or cancerous growths, and to establish memory to be prepared for reoccurring encounters.

1.1. The immune system

Host defense mechanisms evolved in all organisms [2] with different complexities and can even be found in plants [3]. In many organisms, they can be subdivided in two major branches, which closely interact with each other: the innate and the adaptive immune system [4].

1.1.1. The innate immune system

The innate immune system serves as the first line of defense of the organism. Invading pathogens face a network of chemical and physical boundaries (e.g. epithelia, pH barriers or mucus [4]) to hinder the entrance into the tissues. Specialized innate immune cells and soluble proteins (e.g. antimicrobial defensins [5] and complement factors [6]) respond to, and eliminate, a large variety of pathogens. Antigen recognition of the innate immune systems relies on the recognition of characteristic pathogen-associated molecular patterns (PAMP) by specialized pattern recognition receptors (PRR), that recognize for example oligosaccharides, lipopolysaccharides, or non-methylated nucleic acids [7]. Prominent extracellular PRRs are Toll-like receptors (TLRs) [8], while intracellular recognition can be mediated by nucleotide-binding oligomerization domain-like receptors (NOD-like) [9].

An important class of innate immune cells are phagocytic cells like dendritic cells (DCs) or macrophages (MΦs). These cells develop from the myeloid lineage. The major function of phagocytes is the absorption and elimination of pathogens upon PRR-binding, and to present

fragments of these acquired antigens on the cell surface through surface receptors, referred to as major histocompatibility complex (MHC) class I and II (see 1.1.2), to activate T lymphocytes [10]. Therefore, they are also referred to as antigen-presenting cells (APCs) and pose an important link between the innate and adaptive immune system. Another class of innate cells develop from the lymphoid lineage and are referred to as innate lymphoid cells (ILCs), which compose of group 1, 2 and 3 ILCs and natural killer cells (NK cells). The specialty of the latter is the killing of cells with altered expression of MHC I molecules [11]. Innate cells can also express a variety of immunomodulatory receptors, cytokines or chemokines to shape emerging immune responses.

Interestingly, there are also immune cells sharing features of innate and adaptive immune cells, referred to as innate-like lymphocytes (ILLs) [12]. Examples are invariant natural killer T cells (iNKT), γδ-T cells or mucosal-associated invariant T (MAIT) cells. Although the roles of some of these cells have not been completely understood yet, their existence blurs the line between innate and adaptive immunity.

1.1.2. The adaptive immune system

Adaptive immune responses are mediated by B and T lymphocytes, that develop from the lymphoid lineage in the bone marrow (B cells) or thymus (T cells) [13-15]. During development, lymphocytes have to undergo strict positive and negative selection processes, to ensure self-tolerance and to prevent the development of auto-reactive cells that could cause autoimmunity [16-19].

Antigen recognition yields powerful humoral and cellular responses, once the respective B and T cell receptors (BCR and TCR, respectively, **Figure 1.1 A**) are engaged. The BCR resembles an antibody, that is attached to the membrane by a transmembrane tail domain [20]. The antigen recognition is mediated by highly variable loops (complementary determining regions) that are formed by the heavy and light variable (V) chains. The constant (C) chains do not mediate antigen recognition. In contrast, the TCR resembles the Fab-fragment of the BCR and is formed by one α- and β-chain, that are linked together by a disulfide bond. The huge repertoire of BCRs and TCRs is achieved by somatic recombination of the receptor loci during cell maturation [21, 22]. Activated B cells can differentiate into antibody producing plasma cells, or become long-lasting memory B cells [23].

Even though TCR and BCR are structurally related, their target recognition is very different. While B-cells recognize the antigen in its native structure, T cells can only recognize their cognate antigen in a processed form, bound to MHC [24].

Classical MHC I molecules (**Figure 1.1 B**) are composed of an α-chain and β_2 microglobulin, that is non-covalently attached. MHC II is composed of a non-covalent interaction of one α- and β-chain. Both MHC types form a cavity for antigen binding, but preferentially bind to different substrates: MHC I prefer peptides with 8-10 amino acids, while MHC II can bind longer peptides with at least 13 amino acids or longer [25]. MHC I molecules are expressed on all nucleated body cells and mainly present intracellular peptides, including intracellular pathogens, that are degraded in the cytosol by the proteasome. The peptides are transported into the endoplasmic reticulum (ER) by ATP-dependent transporters (TAP1/2) where they bind to partially folded MHC I. The now stabilized MHC I – peptide complex is translocated to the cell membrane. Through cross-presentation, MHC I can also present extracellular proteins obtained from the extracellular space through retro-translocation [4].

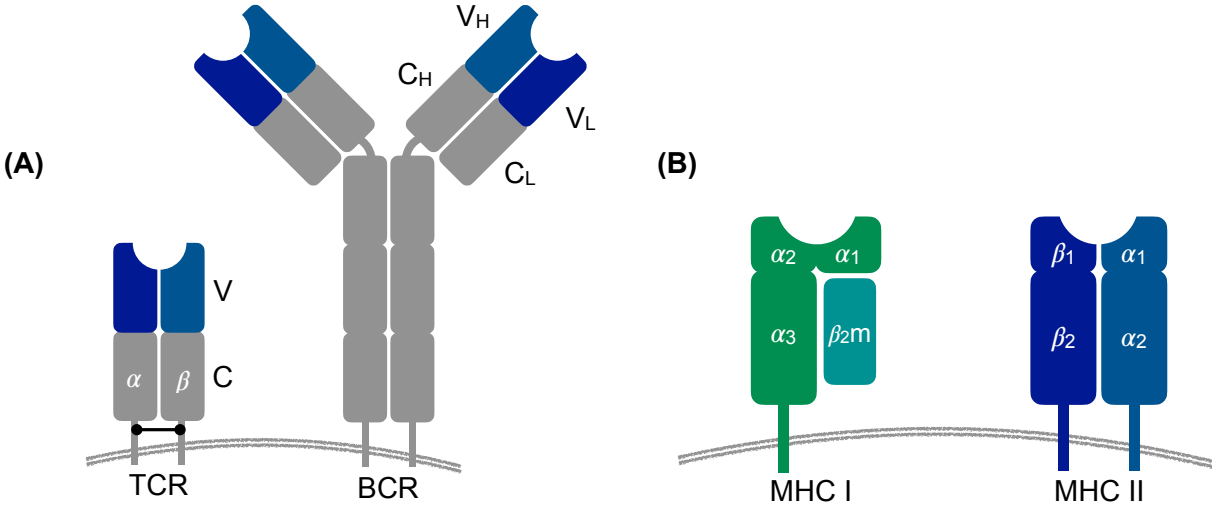

Figure 1.1: Schematic representation of TCR, BCR and MHC. *A: The BCR consists of a heavy (H) and light (L) chain, with constant (C) and variable (V) regions for antigen binding. The TCR is made of α- and β-chains and forms a constant and variable region for antigen binding. B: Schematic representation of MHC I and II molecules. MHC I is formed by one α-chain, bound to β_2m. Peptide binding occurs in a cavity formed by α_1 and α_2 domains. MHC II is formed by one α- and β -chain. Peptide binding occurs in a cavity formed by α_1 and β_1 domains. β_2m = β_2 microglobulin. Image inspired from [4].*

In contrast, peptides for MHC II presentation are created in acidic endosomes by peptidases, and thus mainly present peptides from extracellular proteins and pathogens. MHC II is mainly expressed on phagocytes, adaptive immune cells and epithelial cells in the thymus. Empty MHC II are stabilized by an invariant chain (CLIP) that binds to the peptide cavity, and transported in vesicles that fuse to the endosomes, where CLIP is exchanged to the antigenic peptide. The MHC II – peptide complex is then translocated to the cell membrane to initiate the activation of T cells [4].

1.2. T-Lymphocytes

T-lymphocytes can be grouped in two major classes based on the expression of the glycoproteins CD4 and CD8 [26].

$CD4^+$ T cells recognize MHC II bound peptides. After activation by APCs, the naïve T cells differentiate into subsets, mediated by the cytokine milieu (**Figure 1.2**) [27, 28].

A major subclass of $CD4^+$ cells are helper T cells. T-BET transcription initiates T_H1 cell differentiation in the presence of IL-12 and IFNγ, to enhance cellular immune responses by the activation of $CD8^+$ T cells, and thus are contributing to antiviral immune responses. IL-4 stimulates T_H2 differentiation in a GATA-3-dependent fashion to enhance humoral immune responses, by stimulating B cell differentiation, antibody production and antibody class switch. T_H1 and T_H2 cytokines are inhibiting the differentiation of each other. Follicular helper cells (T_{FH}) express BCL-6 and enhance the germinal center reaction of B cells, to produce antibodies with higher affinity. They are mainly induced by IL-6 and IL-21. In combination with Tgfβ, IL-6 induces the differentiation of T_H17 cells by RORγt. T_H17 are pro-inflammatory cells that produce IL-17, and have been implicated in the development of autoimmune diseases [29].

Regulatory $CD4^+$ T cells (T_{Reg}) are negative regulators of immune responses and can restrain pro-inflammatory T cells. T_{Reg} defects correlate with the development of autoimmune diseases [30]. The signature transcription factor of T_{Reg} is FOXP3, and the differentiation is dependent on Tgfβ and supported by IL-2. The inhibitory function of T_{Reg} is mediated by several mechanisms. The expression of surface receptor CTLA-4 (see 1.2.3) scavenges co-stimulatory receptors from APCs to prevent T cell stimulation. T_{Reg} furthermore express the anti-inflammatory cytokines Tgfβ and IL-10 and can deplete IL-2 from the extracellular space [31]. Due to the negative impact on effector T cell function, high levels of T_{Reg} in tumors correlate with enhanced tumor growth [32].

$CD8^+$ cytotoxic T lymphocytes (CTLs) are the main force of cellular adaptive immunity and recognize antigenic peptides bound to MHC I. CTLs mediate killing of target cells by secreting cytotoxic molecules (e.g. granzymes and perforins [33, 34]) and proinflammatory cytokines (e.g. TNFα and IFNγ [35, 36]). They are also the major contributors during antitumoral and antiviral immune responses and eliminate mutated or infected target cells. After antigen recognition (for example due to an acute viral infection), CTLs expand rapidly (expansion phase) and mediate the killing of infected cells **(Figure 1.3 A**). This phase is followed by a contraction phase where the majority of CTLs undergo apoptosis. A small fraction of T cells can differentiate into long-lived memory cells that mount powerful secondary responses after re-infection with the same pathogen [37, 38]. Some viral infections are characterized by chronic antigen persistence. Chronic viral infections are characterized by lack of viral clearance

(**Figure 1.3 B**) and foster the development of dysfunctional “exhausted” T cells, as explained later in 1.2.3.

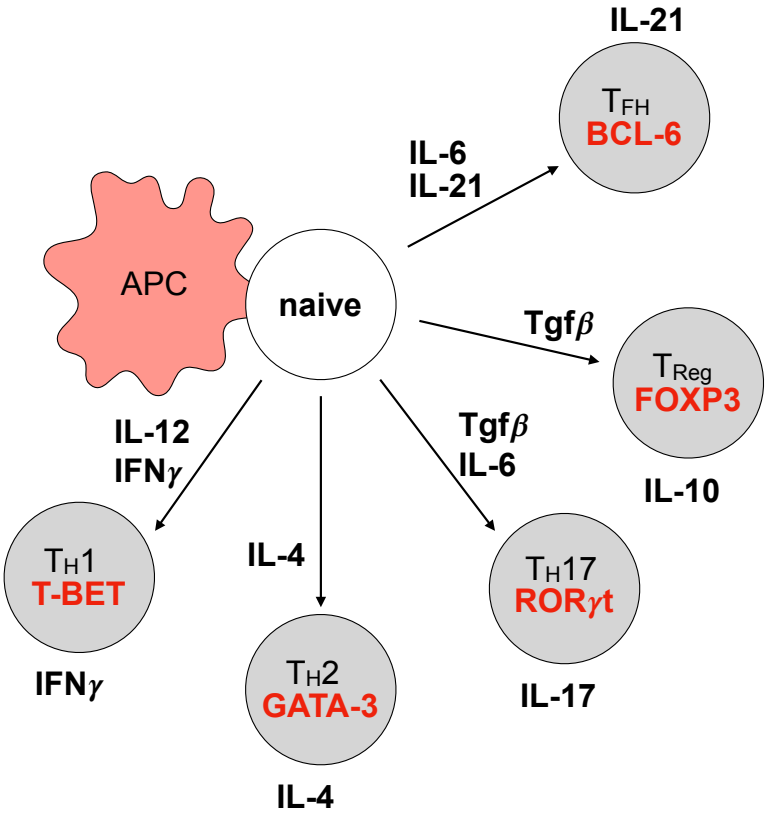

Figure 1.2: Overview over CD4⁺ T cell subsets. *Differentiation of naïve CD4⁺ T cells after engagement with APCs into various subsets, depending on the cytokine milieu, and the resulting key cytokines they produce. Signature transcription factors are highlighted in red. Image inspired from [39].*

$CD4^+$ and $CD8^+$ T cells can differentiate into memory cells to protect from reoccurring antigens [40]. They are subdivided into three major classes, characterized by specific surface molecules and their localization in the body [41]. Longevity of memory cells is supported by homeostatic cytokines like IL-7 and IL-15, and metabolic adaptations (see 1.2.2) [42-44].

Central memory T cells (T_{CM}) express chemokine receptor 7 (CCR7), the lymph node homing receptor L-selectin (CD62L) and the IL-7 receptor IL-7Rα (CD127) [45]. This class of memory cells is mainly found in peripheral and lymphoid tissues. In contrast, effector memory T cells (T_{EM}) express CD127, but lack CCR7 and CD62L, and are therefore found mainly in peripheral tissues [45].

Tissue resident memory T cells (T_{RM}) are a recently discovered group of non-circulating memory cells, that reside in the tissues [46, 47]. General T_{RM} markers are surface molecules that promote tissue homing (e.g. CD103 and CD69). Additionally, tissue-specific markers have been acknowledged [48].

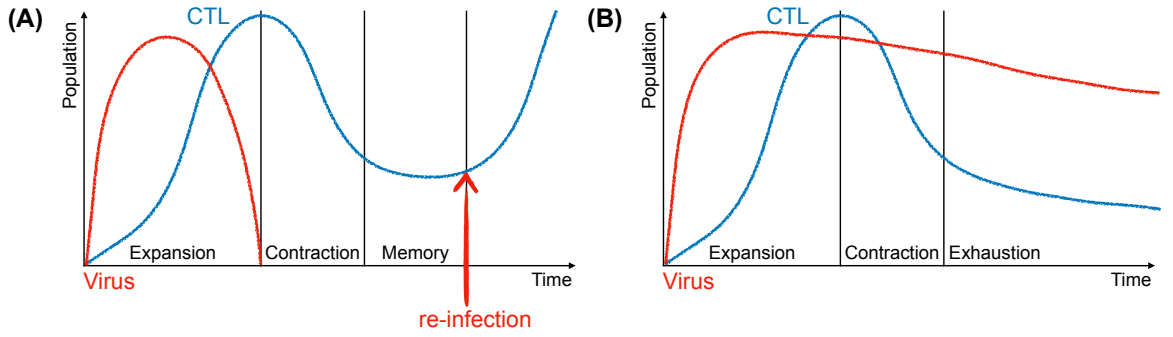

Figure 1.3: Kinetics of CTLs (blue line) over time following a viral infection (red line). *A: During an acute viral infection, T cells undergo initial expansion, followed by a contraction phase, while a fraction of T cells remains as long-lived memory cells, to mount a secondary response after re-infection with the same antigen (red arrow). B: Chronic viral infections are characterized by viral persistence and the development of dysfunctional exhausted CTLs. Images inspired from [39] and [49].*

1.2.1. T cell activation

The activation of T cells is initiated by three major signals (signal 1-3). Signal 1 requires the specific recognition of an antigenic peptide bound to MHC by the TCR:CD3 complex of the T cell. The complex is formed by the TCR itself (**Figure 1.1**), associated with a homodimer of intracellular ζ-chains which each possess three immunoreceptor tyrosine-based activation motifs (ITAMs) for intracellular signal transduction. The TCR complex is completed by interaction with CD3:δε and CD3:γε dimers, which also possess intracellular ITAM domains [50-53]. TCR, ζ-chains and CD3 associate to the TCR:CD3 complex by non-covalent electrostatic interactions of the transmembrane domains [54]. The binding of the TCR:CD3 complex to an APC is completed by interaction of the co-receptors CD4 or CD8 with the respective MHC molecules of the interacting cell. Signal 2 is provided by co-stimulation conferred by binding of CD28 on T cells to CD80 (B7.1) or CD86 (B7.2) on APCs. Finally, inflammatory cytokines (e.g. IL-12 and type I interferons (IFN)) have been appreciated to contribute to T cell function by providing a third signal [55, 56].

One central element of T cell activation is the engagement of three key transcription factors (**Figure 1.4**), that mediate the production of IL-2, a key cytokine for the effector and memory function of T cells, and other cytokines [57]. After TCR stimulation, the tyrosine residues of intracellular ITAMs of the TCR:CD3 complex are phosphorylated by membrane-associated protein tyrosine kinases of the Src-family (Lck and Fyn) [58, 59]. The phosphorylation events enable the binding of Zeta-chain-associated protein kinase 70 (ZAP70) to the ITAMs, and its activation by Lck-dependent phosphorylation [60]. ZAP70 phosphorylates and activates several scaffolding and linker proteins like linker for activation of T cells (LAT) or SLP-76 (not shown) for the mobilization of phospholipase C-γ1 (PLCγ1) [61]. PLCγ1 converts the membrane lipid phosphatidylinositol-4,5-bisphosphate (PIP_2) to the second messengers inositol-1,4,5-trisphosphate (IP_3) and diacylglycerol (DAG) [62]. IP_3 enables the opening of

calcium-channels of the ER and plasma membrane to increase cytoplasmic calcium (Ca^{2+}) concentrations. The ions activate calmodulin (CaM), which forms a complex with the serine-threonine phosphatase calcineurin (CaN) for the dephosphorylation of the transcription factor nuclear factor of activated T cells (NFAT), which then translocates to the nucleus for the initiation of NFAT-specific gene transcription [63].

DAG diffuses through the membrane and activates, among others, Ras guanyl nucleotide-releasing protein (RasGRP), which initiates a mitogen-activated protein kinase (MAPK) cascade by Ras activation [64]. The MAPK cascade triggers the nuclear translocation of the transcription factor activating protein 1 (AP-1), which is composed of a dimer from proteins of the Fos and Jun family [65]. A second target of DAG is the activation of protein kinase Cθ (PKCθ) [66]. Through several steps, PKCθ induces the degradation of inhibitor of NFκB (IκB) to release the transcription factor NFκB, a dimer of the Rel family, for nuclear translocation.

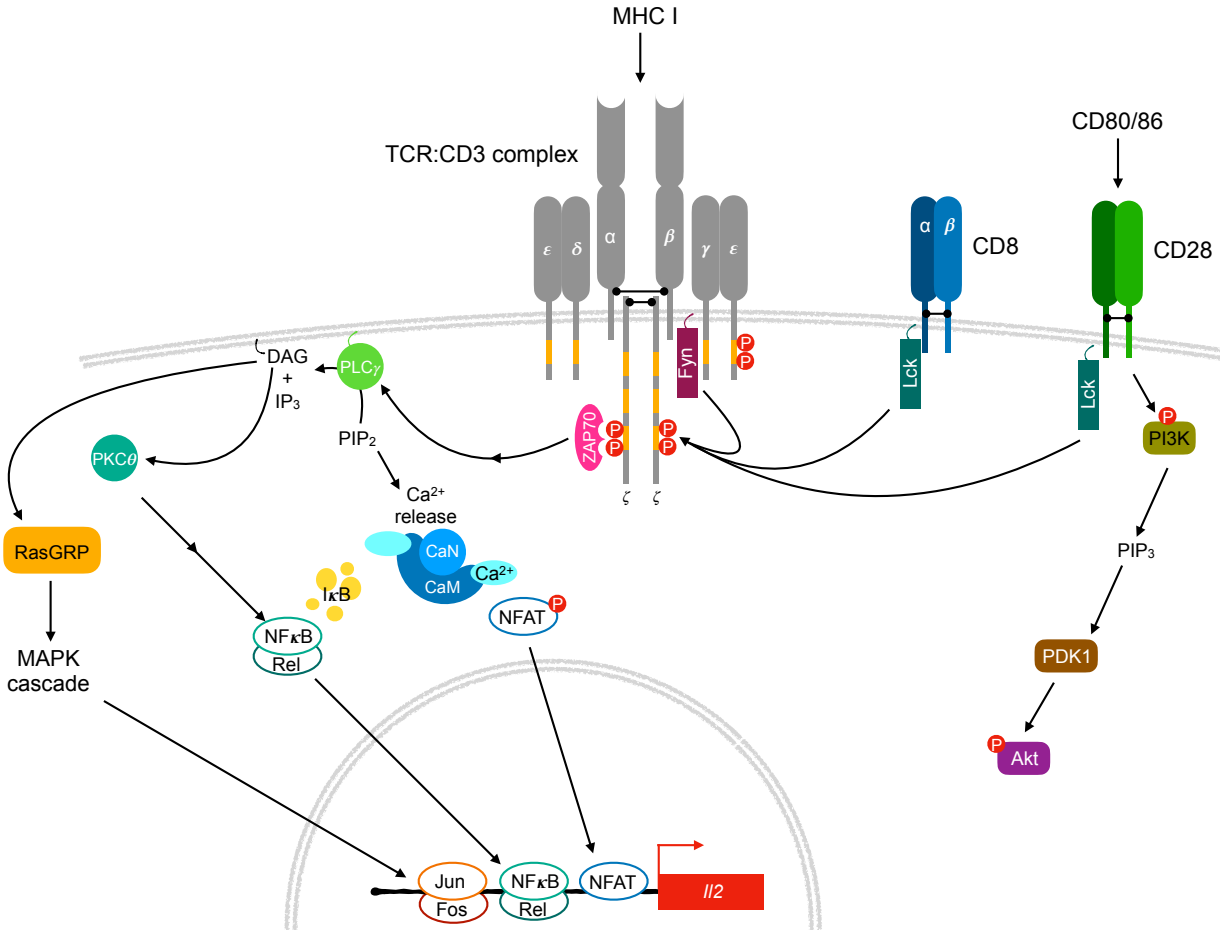

Figure 1.4: Simplified representation of key T cell receptor signaling pathways. *T cell activation is initiated by peptide-MHC:TCR interaction (signal 1) and CD28 co-stimulation (signal 2). ITAM sequences of the TCR:CD3 complex are highlighted in orange. The shown key pathways initiate the transcription of IL-2 and other pro-inflammatory cytokines, representative for $CD8^+$ T cells.*

The CD28 mediated co-stimulation can activate Lck to support TCR signaling [67]. Secondly, engagement of CD28 leads to phosphorylation of a cytoplasmic tyrosine residue, which mobilizes and activates PI-3-kinase (PI3K), to produce phosphatidylinositol-3,4,5-triphosphat

(PIP_3) [68]. PIP_3 mediates the phosphorylation of protein kinase B (Akt) through phosphoinositide-dependent kinase 1 (PDK1) and the activation of mechanistic target of Rapamycin (mTOR) for proliferation and survival [69]. PDK1 can also activate PKCθ [70]. The phosphorylation of CD28 can furthermore induce a Ras-mediated MAPK cascade through the GTP-exchange factor SOS (not shown) [71].

Signal 1 and 2 (stimulation and co-stimulation) are necessary for successful T cell activation. T cells that lack sufficient co-stimulation become anergic [72] or undergo activation-induced cell death (AICD) [73]. This mechanism is central for self-tolerance and prevents T cells from attacking body cells that lack the expression of co-stimulatory receptors.

1.2.2. T cell metabolism

The activation of T cells after stimulation and co-stimulation initiates dramatic metabolic changes, to support the increase in cell proliferation. T cell subsets engage distinct metabolic pathways to meet their biogenetic and biosynthetic demands.
Resting naïve T cells in general can be considered as catabolic [74]. To meet their bioenergetic demands, they preferably feed glucose-derived pyruvate to the tricarboxylic acid cycle (TCA cycle), to support ATP production by oxidative phosphorylation (OXPHOS) [75] in the electron transport chain (ETC, **Figure 1.5**, left panel). After TCR engagement, effector T cells are rapidly activated and become anabolic. They start to divide as short as every 8 h [76], consuming large amounts of ATP and metabolites. To meet the increasing bioenergetic and biosynthetic requirements, a metabolic switch is induced, and these metabolic changes are already detectable within minutes after TCR engagement [77]. Effector T cells prefer to perform Warburg metabolism: similar to other fast dividing cells (e.g. cancer cells [78]), they are converting glucose derived pyruvate to lactate by aerobic glycolysis, to maintain a pool of metabolites for the synthesis of macromolecules including amino acids, membrane lipids or nucleotides (**Figure 1.5**, middle panel) [75]. Effector T cells also consume extracellular lipids [79] and extracellular amino acids. Especially the uptake of extracellular glutamine, which is available in high concentrations in the tissues and blood, and its utilization by glutaminolysis have been shown to support T cell activation [80]. Glutaminolysis supports cellular metabolism by creating intermediates to replenish the TCA cycle by anaplerotic reactions. It should be noted that, even though effector T cells require high levels of glycolysis, also ongoing OXPHOS is necessary to reach full effector potential [81-83].

As described above (see 1.2), immune responses can form protective memory cells with specific metabolic requirements. Even though the metabolic signature of quiescent memory T cells is more similar to naïve T cells than effector cells, they are more dependent on the

utilization of extracellular lipids, or the oxidation of intracellular lipids for OXPHOS-based energy production **(Figure 1.5,** right panel) [84, 85]. Memory cells are also characterized by an enhanced spare respiratory capacity [79], which could explain their enhanced proliferative and effector potential after recall [86]. Furthermore, memory cells can rapidly engage glycolysis for enhanced effector function during recall responses [87, 88].

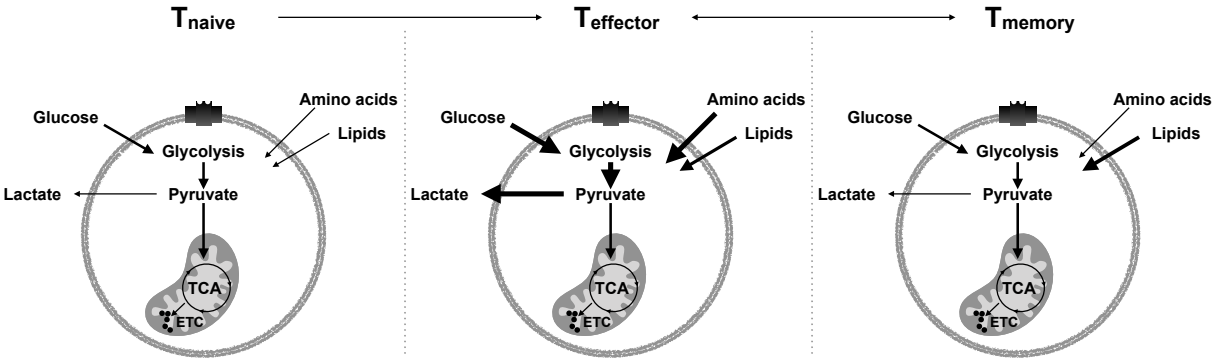

Figure 1.5: T cell metabolism in different T cell subsets. *Naïve T cells primarily utilize glucose for OXPHOS-derived energy production. Effector T cells perform aerobic glycolysis for energy production and anabolism, and consume extracellular amino acids, but also lipids. Memory T cells use lipid oxidation for OXPHOS-derived energy production. Image inspired from [75].*

The described metabolic switches are induced by several transcriptional activators and intracellular pathways. For example, the transcription factor c-Myc is induced by TCR activation, and drives the transcription of glycolytic genes, the glucose transporter GLUT1, glutaminase and glutamine transporters [75, 89]. Therefore, c-Myc contributes to the glycolytic switch, as well as to increased glutamine utilization [89].

A central pathway which supports the metabolic changes during T cell activation is the activation of mTOR signaling with the two signaling complexes mTORC1 and mTORC2 [69]. CD28/PI3K-dependent Akt phosphorylation inhibits TSC1/2, which leads to the activation of mTORC1 [90]. One of the main results of mTORC1 activation is the promotion of protein synthesis by phosphorylation of the kinase P70S6 (pS6) and inactivation of 4E-BP1, to release eIF-4e for the initiation of translation [91, 92]. PI3K can also upregulate mTORC2, which in turn activates Akt to enhance mTORC1 through a positive feedback loop. It has been shown that mTOR activation can further increase the activity of c-Myc and other transcription factors implicated in cell metabolic changes (e.g. Hypoxia-inducible factor 1α (HIF-1α)). Therefore, mTOR activation plays an important role in the glycolytic switch of activated T cells [69].

The anabolic pathways stimulated by mTOR can be negatively regulated by the AMP-activated protein kinase (AMPK). APMK drives catabolic metabolism and restricts immune cell activation, when energy availability is limited. When the cellular ATP/AMP ratio decreases, AMPK is activated to engage energy production for example by fatty acid oxidation (FAO) [93].

1.2.3. T cell exhaustion

The chronic presence of antigen during certain viral infections or during cancer progression has a negative impact on respective effector T cells and can impair their survival and effector function. This process is termed “T cell exhaustion”. Exhausted T cells (T_{Ex}) differ from their effector and memory counterparts by the expression of inhibitory receptors, altered metabolic state, a distinct transcriptome and epigenetic profile, and the failure to maintain effector function and memory differentiation [94, 95]. T cell exhaustion probably evolved as a protective mechanism to prevent the development of autoimmunity due to hyper-activated T cells, and to maintain self-tolerance [95].

T cell exhaustion in CTLs was first described in mice being infected with a variant of the lymphocytic choriomeningitis virus (LCMV), termed clone 13 (cl-13) [96-98], but the findings have been confirmed for other chronic infections (e.g. hepatitis B and C virus (HBV/HCV) [99-101], human immunodeficiency virus (HIV) [102-106]) and various tumor entities [107-114] in humans as well. T cell exhaustion is the result of profound cellular reprogramming, and some key features of $CD8^+$ T cell exhaustion are discussed below. $CD4^+$ T cells can also become exhausted and share features of exhausted CTLs [115], even though the processes are incompletely understood.

1.2.3.1. Loss of cytotoxicity and effector function

T_{Ex} are characterized by the hierarchical loss of cytokine and effector molecule secretion. With the progression of exhaustion, effector T cells first lose the ability to secrete IL-2, then TNFα and IFNγ [116, 117]. The severity of exhaustion correlates with the antigen burden and the lack of help by $CD4^+$ T cells.

1.2.3.2. Upregulation of inhibitory receptors

Key signature of exhausted T cells is the co-expression of multiple inhibitory surface molecules on T cells. Ligands of these receptors are expressed by APCs and other immune cells, various tissues and cancer cells, and lead to the downregulation of effector functions and rewiring of intracellular pathways in the effector cell.

CD152, a member of the immunoglobulin superfamily termed cytotoxic T-lymphocyte-associated protein 4 (CTLA-4) was one of the first described negative regulators of T cells. Even though already discovered in 1987 [118], its impact on in the immune system was confirmed several years later by two independent research groups. Genetic mouse models with CTLA-4 deficiency showed lethal lymphoproliferative disorders and an autoimmune phenotype in mice, and revealed the importance of the negative regulatory function for tolerance [119, 120]. CTLA-4 belongs to the immunoglobulin superfamily and is expressed as

a homodimer, linked by a disulfide bond. It binds to the co-stimulatory ligands CD80 and CD86 with great affinity and avidity, thereby competing out CD28 for ligation [121-123].
Even though the immunosuppressive potential of CTLA-4 was discovered several years ago, its exact mechanism of action remains controversial. One mode of action might be the removal of CD80/86 from APCs by trans-endocytosis [124]. Another explanation is the recruitment of intracellular phosphatases SHP-1, SHP-2 and PP2A, that interfere with TCR signaling (**Figure 1.6**) [122]. Furthermore, the activity of PP2A was shown to interfere with the PI3K/Akt signaling cascade, probably downstream of PI3K [125].
Another prominent example is CD279, or programmed cell death protein (PD-1). PD-1 also belongs to the immunoglobulin superfamily and was discovered and characterized by Tasuku Honjo and colleagues [126]. Two ligands of the B7 family have been identified for PD-1: PD-L1 and PD-L2 [127-130]. In contrast to CTLA-4, PD-1-deficient mouse models showed non-lethal autoimmune phenotypes [131, 132]. PD-1 is already expressed early after T cell activation [133] and is regulated by a positive feedback loop through FoxO1-mediated transcription during the progression of exhaustion, when mTOR activity decreases [134].
The exact inhibitory mechanism of PD-1 is still debated, but probably mainly mediated by the intracellular tail, which contains two phosphorylation sites in the immunoreceptor tyrosine-based inhibition motif (ITIM) and immunoreceptor tyrosine-based switch motif (ITSM). Both domains can be bound by intracellular phosphatases (SHP-1 and SHP-2), and it is believed that the major inhibitory function is conferred by SHP-2 binding to the ITSM (**Figure 1.6**) [135]. The action of the intracellular phosphatases likely hinders distal and proximal TCR signaling cascades, for example by the dephosphorylation of ZAP70, Lck, CD28 or PI3K [135, 136]. PD-1 can also increase the phosphatase activity of phosphatase and tensin homolog (PTEN) to interfere with PI3K/Akt signaling [137].
It has also been shown that PD-1 can upregulate an E3-ubiquitin ligase, that can induce TCR down-modulation by initiating proteasomal degradation [138].

The expression of CTLA-4 or PD-1 alone is not enough to define a T cell as exhausted, but the co-expression of several inhibitory receptors is a hallmark of T_{Ex} [139]. Other recently discovered inhibitory receptors include T cell immunoreceptor with Ig and ITIM domains (TIGIT) [140], Lymphocyte-activation gene 3 (LAG-3) [141], T-cell immunoglobulin and mucin-domain containing-3 (TIM-3) [142] or CD244 (2B4) [143].

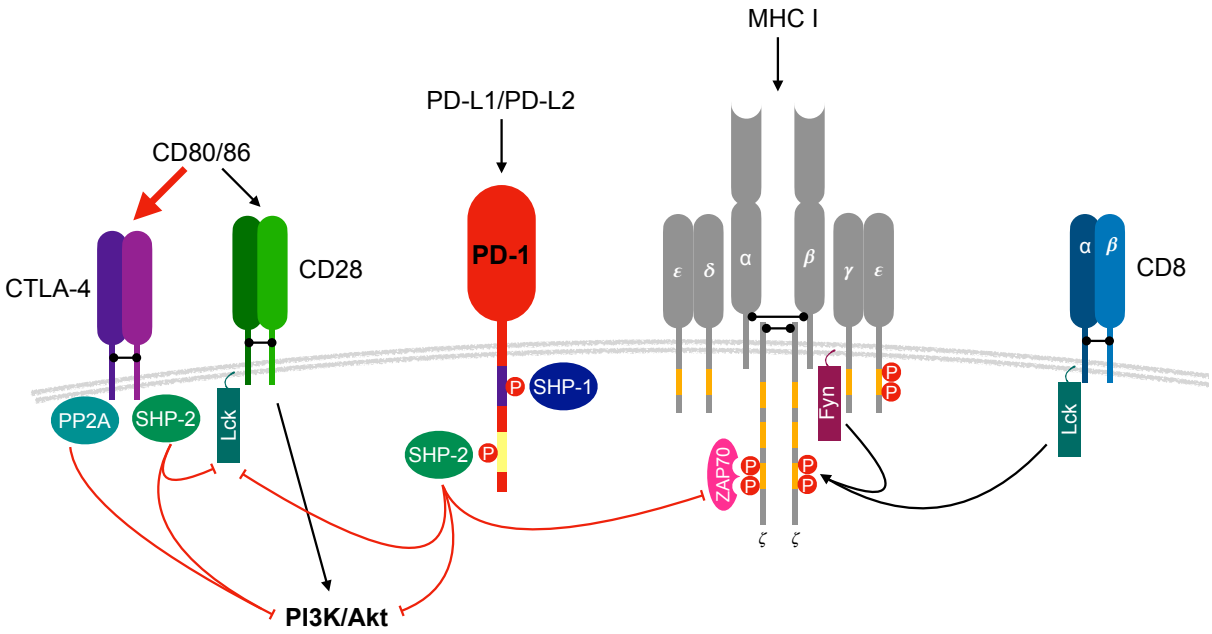

Figure 1.6: Inhibitory receptors interfere with T cell activation. *Simplified potential mechanism of action of inhibitory signals conferred by PD-1 and CTLA-4. The PD-1 ITIM is highlighted in purple. The PD-1 ITSM is highlighted in yellow. The CD3:TCR complex-associated ITAMs are highlighted in orange.*

1.2.3.3. Impaired homeostasis and memory differentiation and altered expression of transcription factors

The cytokines IL-7 and IL-15 are well known to support the survival and differentiation of memory T cells. During the development of exhaustion, T_{Ex} lose the ability to integrate IL-7 and IL-15 signals for homeostatic proliferation and, are unable to develop memory cells that confer long-lasting immune responses [144].

Instead, a small population of “stem cell-like” T cells has been identified, which is characterized by the co-expression of transcription factors T cell factor 1 (TCF1) and Eomesodermin (EOMES), and CXC chemokine receptor type 5 (CXCR5). These stem cell-like cells give rise to progeny with residual effector response. The daughter cells become terminally exhausted over time and express high levels of PD-1, EOMES and TIM-3, but downregulate the expression of TCF1 and CXCR5 [145-147].

Additionally, the transcription factor thymocyte selection-associated HMG box protein (TOX) was shown to be highly expressed in T_{Ex} [148-153]. Several independent publications found TOX to be a driver of the exhaustion phenotype by suppression of TCF1, effector function and altered epigenetic fate. However, T cell specific deletion of TOX led to T cell apoptosis. Thus, TOX is regarded as a rheostat to prevent T cell overstimulation and drives exhaustion to prevent antigen induced cell death (AICD) and immunopathology.

1.2.3.4. Metabolic alterations during T cell exhaustion

During T cell exhaustion, the downregulation of PI3K/Akt/mTOR skews T_{Ex} from aerobic glycolysis towards a more oxidative metabolism and the utilization of fatty acids [154-156]. This metabolic switch can be induced by negative regulation of TCR signaling events through PD-1 [135], CTLA-4 or other inhibitory receptors, as described above.

It was recently recognized, that early T_{Ex} fail to meet their bioenergetic and biosynthetic demands already during the first week of chronic LCMV cl-13 infection [157].

Early T_{Ex} showed reduced capacities of performing OXPHOS and glycolysis, even though several metabolic genes were initially upregulated in these cells. Moreover, early T_{Ex} displayed elevated levels of defective (depolarized) mitochondria with reduced mitochondrial membrane potential ($\Delta\Psi m$) and increased production of potentially toxic reactive oxygen species (ROS). It was shown that PD-1 could suppress glucose consumption and the proliferator-activated receptor gamma co-activator 1α (PGC1α), and overexpression of PGC1α at least partially restored metabolic fitness [157]. PGC1α was also repressed in exhausted tumor infiltrating lymphocytes (TILs), resulting in reduced mitochondrial mass and mitochondrial biogenesis and reduced effector function [158].

1.2.3.5. Transcriptional and epigenetic alterations

The application of novel sequencing techniques, for example RNA sequencing and assay for transposase-accessible chromatin (ATAC) sequencing for the analysis of chromatin accessibility, revealed T_{Ex} displayed a distinct accessibility profile for several thousand loci [159]. T_{Ex} cells strongly differed from T_{Mem} and T_{Eff} cells, but the profiles of exhausted cells derived from tumors and chronic viral infections were closely related, implying a common exhaustion phenotype between the different morbidities.

The observed epigenetic changes directly impacted the functionality of the cells. It was for example appreciated, that during chronic viral infections, the gene locus and enhancer regions of *Pdcd1* (encoding for PD-1) were chronically demethylated and enabled the sustained expression of PD-1 [160].

1.3. Immunotherapy

Inhibitory receptors and other key players that regulate the onset and development of exhaustion, are termed “immune checkpoints”. These molecules are of great interest for clinical intervention, to reinitiate the lost effector function of exhausted cells [161, 162].

1.3.1. Immunotherapy in cancer

The immune system plays a pivotal role in fighting cancer, and immunocompromised patients have an elevated risk to develop certain malignancies [163]. Especially CTLs have been appreciated to be a major contributor to antitumoral immune responses, and the amount of TILs is correlated with better prognosis for the patients [164].
Cancer cells have developed strategies to evade the destruction through CTLs by decreasing the immunogenicity through immunoediting [165] and upregulation of immunosuppressive mechanisms in the tumor microenvironment (TME), for example by recruitment of immunosuppressive T_{Reg}, tumor-associated MΦs (TAMs) or myeloid derived suppressor cells (MDSCs), as well as deprivation of nutrients and secretion of immunosuppressive metabolites and the expression of inhibitory surface molecules to directly impact T cell function [166]. The combination of these factors along with chronic antigen presence and TCR stimulation drives the exhaustion of CTLs and leads to tumor progression. The aforementioned immunosuppressive mechanisms are all under investigation for potential clinical intervention. Immunotherapy aims to overcome the negative influence of the TME to convert immunologically “cold” tumors with low CTL infiltration to “hot” tumors with enhanced antitumoral immune reactions.

A promising approach to enhance the effector function of CTLs is immune checkpoint blockade (ICB). ICB aims to interfere with immune checkpoints on the surface of the T cell, or the ligands of inhibitory receptors on accessory cells or tumor cells by targeted blocking with monoclonal antibodies. Especially the interference with CTLA-4 and PD-1/PD-L1 proved to be of clinical significance [167, 168].
The first FDA approved ICB was the development of Ipilimumab, a monoclonal antibody against CTLA-4 for the treatment of melanoma. Ipilimumab treatment showed clinical benefit in form of enhanced CTL infiltration and decreased tumor sizes, especially in patients whose tumors showed high mutational burden [169]. However, CTLA-4 blockade could lead to severe immune-related adverse effects in a proportion of treated patients [170].
The second generation of ICBs targeted the inhibition of the PD-1/PD-L1 axis. Monoclonal antibodies were developed against PD-1 (Nivolumab, Pembrolizumab) or PD-L1, which is widely expressed in various cancer entities [171] (Atezolizumab, Avelumab, Durvalumab). These antibodies were FDA approved for a range of cancer entities, including melanoma, colorectal cancer, non-small cell lung cancer and many other solid tumors [172]. Targeting of the PD-1/PD-L1 axis showed reduced occurrence of severe immune-related side effects, compared to Ipilimumab [173].
Even though monotherapies targeting CTLA-4 and PD-1/PD-L1 proved clinical success with durable response rates, a large fraction of patients failed to respond to treatment. Combination

therapies of Ipilimumab and PD-1/PD-L1 antagonists proved beneficial over monotherapies for the treatment of melanoma, renal cell carcinoma and colorectal cancer [174].
Since the response rate of combination therapies showed favorable outcome for several cancer entities, ICBs targeting other inhibitory receptors implicated in T cells exhaustion are under development and tested in clinical trials.

1.3.2. Immunotherapy in chronic infections

T cell exhaustion also occurs frequently during chronic viral infections (see 1.2.3). Therefore, the effect of ICB is also tested for the treatment of HIV, HBV, HCV and others [175], however most of these studies have been performed *in vitro* or *ex vivo*, and to this time there are only very few ongoing clinical trials for the treatment of chronic viral infections using ICBs.
For example $CD4^+$ T cells from HIV-infected patients showed enhanced functionality after combination of antibodies targeting TIGIT and PD-L1 *ex vivo* [176]. Also, first evidence showed that ICB treatment might help to relief HIV-latency to enable viral clearance [177].
For hepatitis infections, in mouse models using the woodchuck hepatitis virus as a model for persistent infection, anti-PD-L1 or anti-PD-L2 treatment partially restored T cell function [178]. However, especially during the treatments of hepatitis, adverse effects of ICB could have negative impact on the disease progression, by elevated liver inflammation that could lead to hepatitis exacerbation or the development of hepatocellular carcinoma [179, 180].
In summary, ICB might be helpful to treat chronic viral infections, but needs to be studied further before clinical application.

1.4. The malate aspartate shuttle (MAS)

The immune system requires rapid metabolic adaptions to support proliferating cells. As described in 1.2.2, T cells require glycolysis and OXPHOS to unleash full effector potential, and disturbances in the metabolism are associated with the development of exhaustion. Mitochondrial shuttle systems are required to connect the cytosolic metabolism (e.g. glycolysis) to the mitochondrial metabolism (e.g. TCA and ETC).
The inner mitochondrial membrane is impermeable for electrons and reductive equivalents like nicotinamide adenine dinucleotide (NAD). The MAS is a system of enzymes and membrane transporters, that facilitates the shuttling of electrons produced by glycolysis in the cytoplasm through the inner mitochondrial membrane, to feed into OXPHOS. Malate is transported through the inner mitochondrial membrane by a malate – α-ketoglutarate (α-KG) antiporter [181, 182]. In the matrix, malate is oxidized to oxaloacetate (OAA) by a mitochondrial malate dehydrogenase (MDH), while NAD^+ is simultaneously reduced to NADH. This reaction is part

of the TCA cycle, and the electrons transferred to NADH can enter the ETC to produce ATP [183].

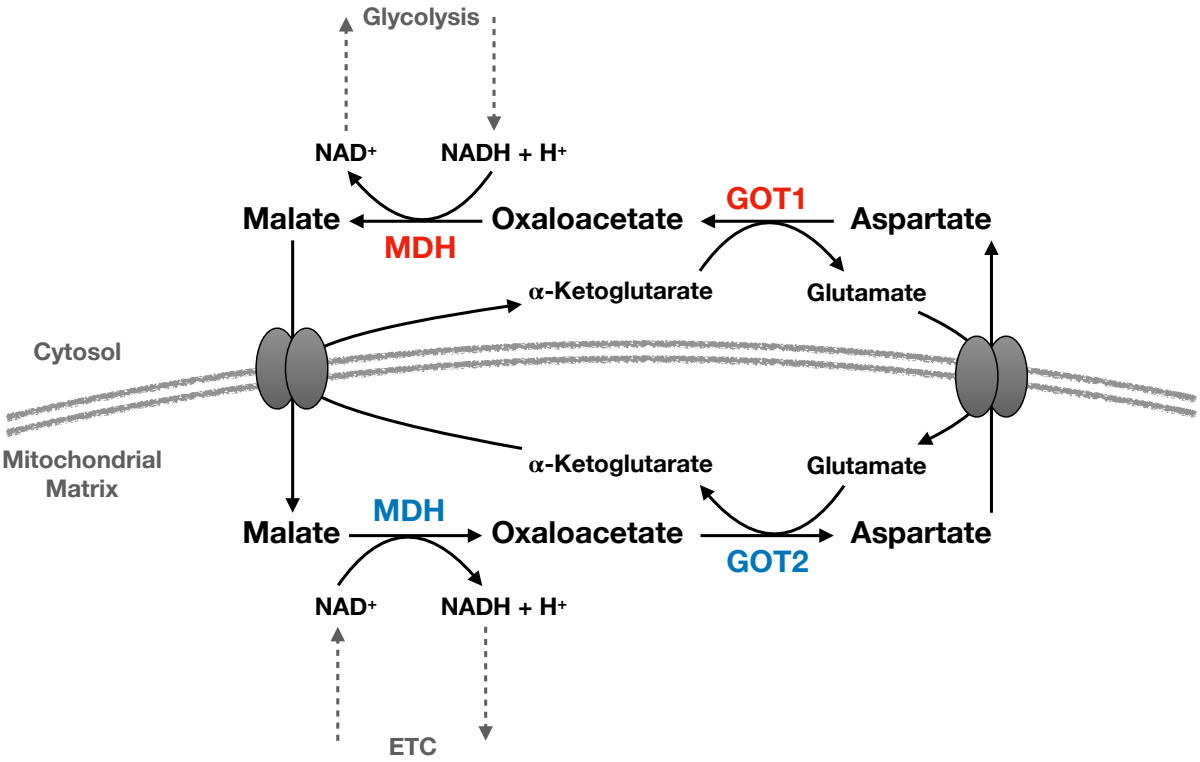

Figure 1.7: The MAS connects cytosolic and mitochondrial metabolism. *MAS enables indirect electron transport from the cytoplasm to the mitochondrial matrix, in form of NAD⁺ and NADH, using a network of redox reactions and membrane transporters.*

The mitochondrial glutamic oxaloacetic transaminase 2 (GOT2) is mediating the transamination from an amino group of glutamate to OAA, to form aspartate and α-KG. Aspartate is transported back into the cytosol by a glutamate – aspartate antiporter [184, 185], where the reverse transamination from aspartate to α-KG is performed by the cytosolic glutamic oxaloacetic transaminase 1 (GOT1). The resulting OAA is reduced to malate by the cytosolic MDH, using electrons from NADH that is produced by glycolysis. This closes the loop of redox reactions, and the cycle can start again.

1.4.1. GOT1 in T cell biology

GOT1 mediates the reversible transamination from aspartate to α-KG to create OAA and glutamate in the cytosol. Thus, it is one of the key enzymes of the MAS. The catalytical function of GOT1 is dependent on the cofactor pyridoxal 5'-phosphate (PLP) [186].

The role of GOT1 in $CD8^+$ T cells is poorly understood. Recent publications implicated, that GOT1 might contribute to the balance between T_{Reg} and T_H17 cells through an epigenetic mechanism [187-189]. Using the small molecule inhibitor (aminooxy)acetic acid (AOA), the differentiation of T_H17 cells was redirected to induce T_{Reg} cells. GOT1-mediated transamination

increased the levels of 2-hydroxyglutarate, which caused the hypermethylation of the gene locus of FOXP3 and inhibited T_{Reg} differentiation to produce T_H17 cells. GOT inhibition by AOA prevented the hypermethylation and promoted T_{Reg} differentiation. This improved the symptoms of experimental autoimmune encephalomyelitis in mice [188].
In Jurkat cells, an immortalized line of human T lymphocytes, GOT1 was identified in a CRISPR-based genetic screen as essential to maintain cell viability during treatment with the ETC complex I inhibitor phenformin. It was discovered that GOT1, when the ETC was blocked, reversed the transamination reaction in order to produce aspartate in the cytosol to sustain proliferation [190].

It was also recently appreciated that metabolic enzymes, including *Got1* are highly expressed in exhausted T cells after chronic viral infection with the virus LCMV cl-13 [157]. However, none of the works mentioned so far investigated the contribution of GOT1 and the MAS to $CD8^+$ T cell effector function or T cell exhaustion.

1.5. Aim of this work

T cell exhaustion impairs the clearance of chronic viral infections and antitumoral immune responses. Recent advances in immune therapies were able to (at least partially) restore the function of T_{Ex} in different cancer entities. However, not all patients and cancer types react to the use of checkpoint inhibitors. Simultaneously, the use of immune therapies can induce severe side effects.
Metabolism and T cell function are tightly entwined. Recent research in the field of immune metabolism has strengthened and pointed out the meaning and the changes of metabolic alterations in activated and exhausted T cells. Thus, the identification of metabolic checkpoints and the development of metabolic checkpoint inhibitors for clinical use to improve or complement already available immune checkpoint therapies, is one of the main focuses of immune cell metabolic research. Still, the meaning of many metabolic pathways is not yet studied in T cells or T cell subtypes, and the roles of many metabolic enzymes during the development of effector function and exhaustion of T cells are not clear to this time.

We chose to study the role of metabolic pathways, mainly the MAS, in T cells. Based on aforementioned metabolic phenotypes that arise during T cell exhaustion, like the accumulation of depolarized mitochondria, we reasoned, that the lost membrane potential might have resulted from altered function of the ETC complexes. As mentioned above, the MAS is a key metabolic system to shuttle electrons across the inner mitochondrial matrix. Since the MAS therefore links cytosolic to mitochondrial metabolism, it could influence $\Delta\Psi m$

in T cells. Also due to its aberrantly high expression during the onset of exhaustion, we targeted the MAS enzyme GOT1 for further investigation in T cell biology and to detect potential links to the development of T cell exhaustion.
We studied the role of GOT1 during T cell effector responses, memory formation and T cell exhaustion. Therefore, we used genetically modified mouse strains to remove GOT1 selectively from T cells. Using different viral strains of LCMV to induce acute (LCMV Arm) or chronic (LCMV cl-13) infection and syngeneic melanoma tumor models, we investigated the role of GOT1 in TILs.

This work aims to shed a light on the contribution of GOT1 and the MAS during T cell activation, antiviral and antitumoral responses and exhaustion, in order to evaluate its potential as a metabolic checkpoint.

2. Materials

2.1. Chemicals and reagents

Deionized water was taken from the laboratory water supply. Double deionized water (ddH_2O) was purified by an ion-exchanger (TKA GenPure, JWT, Jena, Germany).

Table 1: Overview over used chemicals and reagents. *Standard chemicals that are not listed were purchased from Sigma-Aldrich/Merck KGaA (Darmstadt, Germany).*

Material	Company	Identifier
$^{13}C_5$-glutamine	Sigma-Aldrich/ Merck KGaA (Darmstadt, Germany)	605166
$^{13}C_6$-glucose	Sigma-Aldrich/ Merck KGaA (Darmstadt, Germany)	389374
2-Deoxy glucose	Cayman Chemical (Ann Arbor, MI, USA)	14325-5
3-Nitrophenylhydrazine hydrochloride	Sigma-Aldrich/ Merck KGaA (Darmstadt, Germany)	N21804
30% Acrylamide/Bis Solution, 29:1	Serva (Heidelberg, Germany)	10687.01
Adenosine 5′-diphosphate monopotassium salt dihydrate (ADP)	Sigma-Aldrich/ Merck KGaA (Darmstadt, Germany)	A5285
Ammonium Persulfate (APS)	Bio-Rad Laboratories (Hercules, CA, USA)	161-0700
Antimycin A	Sigma-Aldrich/ Merck KGaA (Darmstadt, Germany)	A8674
Blasticidine S hydrochloride	Sigma-Aldrich/ Merck KGaA (Darmstadt, Germany)	15205
Bovine Serum Albumin (BSA)	Sigma-Aldrich/ Merck KGaA (Darmstadt, Germany)	A9647

Bovine Serum Albumin (Fatty Acid free)	Capricorn Scientific (Ebsdorfergrund, Germany)	BSA-FAF-1U
Brefeldin A Solution	Abcam (Cambridge, UK)	Ab193369
Carbonyl cyanide 4-(trifluoromethoxy)phenylhydrazone (FCCP)	Cayman Chemical (Ann Arbor, MI, USA)	15218-50
CD90.1 MicroBeads, mouse and rat	Milteny Biotec (Bergisch Gladbach, Germany)	130-121-273
Clarity™ Western ECL Substrate	Bio-Rad Laboratories (Hercules, CA, USA)	1705060S
Crystal Violet	TCS Biosciences (Buckingham, UK)	HD1295-25
Cyclosporin A	Santa Cruz Biotechnology (Santa Cruz, CA, USA)	sc-3503
Dialyzed Fetal Bovine Serum	Sigma-Aldrich/ Merck KGaA (Darmstadt, Germany)	F0392-100ML
Dimethyl-2-oxoglutarate	Sigma-Aldrich/ Merck KGaA (Darmstadt, Germany)	349631-5G
Disodium succinate	Sigma-Aldrich/ Merck KGaA (Darmstadt, Germany)	W327700
Dodecyltrimethylammoniumbromide (DTAB)	Sigma-Aldrich/ Merck KGaA (Darmstadt, Germany)	D8638
eBioscience™ Foxp3/transcription factor staining buffer set	Thermo Fischer Scientific (Waltham, MA, USA)	00-5523-00
Fetal bovine serum (FBS)	Sigma-Aldrich/ Merck KGaA (Darmstadt, Germany)	F0804
Fixation Buffer	BioLegend (San Diego, CA, USA)	420801
G-418 Sulfate	Sigma-Aldrich/ Merck KGaA (Darmstadt, Germany)	345810-1GM
Gibco® 0.25 % Trypsin-EDTA (1X)	Thermo Fischer Scientific (Waltham, MA, USA)	25200-055
Gibco® 2-Mercaptoethanol (1000X)	Thermo Fischer Scientific (Waltham, MA, USA)	21985-023
Gibco® ACK Lysis Buffer	Thermo Fischer Scientific (Waltham, MA, USA)	A10492-01

Gibco® DMEM (1X) (4,5 g/l D-Glucose, L-Glutamine, no pyruvate)	Thermo Fischer Scientific (Waltham, MA, USA)	41965-039
Gibco® DPBS (1X)	Thermo Fischer Scientific (Waltham, MA, USA)	14040-091
Gibco® MEM NEAA (100X)	Thermo Fischer Scientific (Waltham, MA, USA)	11140050
Gibco® Pen Strep	Thermo Fischer Scientific (Waltham, MA, USA)	14140-122
Gibco® RPMI Medium 1640	Thermo Fischer Scientific (Waltham, MA, USA)	21875-034
Invitrogen™ Permeabilization Buffer 10X	Thermo Fischer Scientific (Waltham, MA, USA)	00-8333-56
4x Laemmli Sample Buffer	Bio-Rad Laboratories (Hercules, CA, USA)	1610747
L-ascorbic acid sodium	Sigma-Aldrich/ Merck KGaA (Darmstadt, Germany)	A4034
L-Glutamine solution	Sigma-Aldrich/ Merck KGaA (Darmstadt, Germany)	G7513-100ML
L-Glutathione reduced	Sigma-Aldrich/ Merck KGaA (Darmstadt, Germany)	G6013-5G
Live/dead fixable dead cell stain kit	Thermo Fischer Scientific (Waltham, MA, USA)	L23102
Malic acid	Sigma-Aldrich/ Merck KGaA (Darmstadt, Germany)	PHR1273
Methoxyamine hydrochloride	Sigma-Aldrich/ Merck KGaA (Darmstadt, Germany)	226904
MitoSOX™ Red Mitochondrial Superoxide Indicator	Thermo Fischer Scientific (Waltham, MA, USA)	M36008
MitoTracker™ Deep Red FM	Thermo Fischer Scientific (Waltham, MA, USA)	M22426
MitoTracker™ Green FM	Thermo Fischer Scientific (Waltham, MA, USA)	M7514
MojoSort™ Streptavidin Nanobeads	BioLegend (San Diego, CA, USA)	76447
N, N, N′, N′-tetramethyl-p-phenylenediamine (TMPD)	Sigma-Aldrich/ Merck KGaA (Darmstadt, Germany)	T7394

N-Acetyl-L-cysteine (NAC)	Sigma-Aldrich/ Merck KGaA (Darmstadt, Germany)	A9165-5G
Nicotinamide Riboside (NR)	Cayman Chemical (Ann Arbor, MI, USA)	23132
N-tert-Butyldimethylsilyl-N-methyltrifluoroacetamide (MTBSTFA)	Sigma-Aldrich/ Merck KGaA (Darmstadt, Germany)	394882
Oligomycin	Merck Millipore (Burlington, MA, USA)	495455-10mg
6x Orange DNA Loading Dye	Thermo Fischer Scientific (Waltham, MA, USA)	R0631
PageRuler™ Prestained Protein Ladder	Thermo Fischer Scientific (Waltham, MA, USA)	26616
Percoll™	GE Healthcare (Chalfont, UK)	17-0891-01
Propidium Iodide Solution	BioLegend (San Diego, CA, USA)	421301
Poly D-Lysine	Merck Millipore (Burlington, MA, USA)	A-003-E
Pyridine	Sigma-Aldrich/ Merck KGaA (Darmstadt, Germany)	270970
Rapamycin	Enzo Life Sciences	BML-A275-0005
RIPA Lysis Buffer System	Santa Cruz Biotechnology (Santa Cruz, CA, USA)	sc-24948
Rotenone	Cayman Chemical (Ann Arbor, MI, USA)	13995-5
RPMI 1640 (no L-Glutamine, no D-Glucose)	Biological Industries (Beit HaEmek, Israel)	01-101-1A
Seahorse XF Plasma Membrane Permeabilizer (PMP)	Agilent Technologies (Santa Clara, CA, USA)	102504-100
SeaKem® ME Agarose	Lonza (Basel, Switzerland)	50014
Skim milk powder	GERBU Biotechnik (Heidelberg, Germany)	16020500
Sodium $^{13}C_3$-lacate	Sigma-Aldrich/ Merck KGaA (Darmstadt, Germany)	490040
Sodium Azide	Sigma-Aldrich/ Merck KGaA (Darmstadt, Germany)	S2002-5G

Sodium Pyruvate	Sigma-Aldrich/ Merck KGaA (Darmstadt, Germany)	P5280
SYBER safe DNA stain	Thermo Fischer Scientific (Waltham, MA, USA)	S33102
SYBR Green Master Mix	Thermo Fischer Scientific (Waltham, MA, USA)	A25742
TEMED	Bio-Rad Laboratories (Hercules, CA, USA)	161-0801
Triton™ X-100	Sigma-Aldrich/ Merck KGaA (Darmstadt, Germany)	X100-500ML
Trypan Blue solution	Sigma-Aldrich/ Merck KGaA (Darmstadt, Germany)	T81544-100ML
XF Base Medium	Agilent Technologies (Santa Clara, CA, USA)	102353-100
XF Calibrant	Agilent Technologies (Santa Clara, CA, USA)	100840-000

2.2. Commercial kits

Table 2: Commercially available kits used in the study.

Kits	Company	Identifier
$CD4^+$ T cell Isolation Kit	Milteny Biotec (Bergisch Gladbach, Germany)	130-104-454
$CD8^+$ T cell Isolation Kit	Milteny Biotec (Bergisch Gladbach, Germany)	130-104-075
NAD/NADH-Glo™ Assay	Promega (Madison, WI, USA)	G9071
Pierce™ BCA™ Protein Assay kit	Thermo Fischer Scientific (Waltham, MA, USA)	23225
Qiagen RNase-Free DNase Set	Thermo Fischer Scientific (Waltham, MA, USA)	79254
Qiagen RNeasy Mini Kit	Thermo Fischer Scientific (Waltham, MA, USA)	74106
SuperScript™ III system	Thermo Fischer Scientific (Waltham, MA, USA)	18080051

2.3. Buffers and solutions

Table 3: Overview over used buffers and solutions and the respective composition.

Buffer/Solution	Composition
1x Annexin V staining buffer	0.01 M HEPES 0.14 M NaCl 2.5 mM $CaCl_2$ pH 7.4
Complete RPMI	10 % (v/v) FBS 1 % (v/v) PenStrep 1 % (v/v) NEAA 0.1 % (v/v) 2-Mercaptoethanol RPMI 1640
FACS buffer	2 % FBS 0.1 % (w/v) NaN_3 PBS
Freezing medium	10 % (v/v) DMSO FBS
MACS buffer	2 % FBS PBS
1x Mitochondrial assay solution (1x MAS)	70 mM Sucrose 220 mM Mannitol 10 mM KH_2PO_4 5 mM $MgCl_2$ 2 mM HEPES 1 mM EGTA 0.2 % (w/v) Fatty acid-free BSA pH 7.2
Minimal RPMI	10 % (v/v) Dialyzed FBS 1 % (v/v) Pen Strep 6.7 mM Glucose RPMI 1640 (no L-Glutamine, no D-Glucose)
NAD^+/NADH lysis buffer	1 % (w/v) DTAB 0.2 M NaOH
1x Phosphate-buffered saline (1x PBS)	137 mM NaCl 8.1 mM KCl 2.7 mM Na_2HPO_4

	1.5 mM KH_2PO_4
	pH 7.4
PBS-T	0.01 % (v/v) Triton X-100
	PBS
Plaque assay buffer	1 % (w/v) Crystal violet
	20 % MeOH
1 % RPMI	1 % (v/v) FBS
	1 % (v/v) Pen Strep
	RPMI 1640
1x SDS running buffer	25 mM Tris base
	0.19 M Glycine
	1 % (w/v) SDS
SDS-PAGE Resolving gel (15 %)	15 % (v/v) Acrylamide/Bis Solution
	375 mM Tris-HCl pH 8.8
	0.1 % (w/v) SDS
	0.1 % (w/v) APS
	0.04 % (v/v) TEMED
SDS-PAGE Stacking gel (5 %)	5 % (v/v) Acrylamide/Bis Solution
	125 mM Tris-HCl pH 6.8
	0.1% (w/v) SDS
	0.1% (w/v) APS
	0.01% (v/v) TEMED
1x Tris acetate EDTA buffer (1x TAE)	40 mM Tris base
	1 mM EDTA
	pH 7.4
1.0 M Tris-HCl pH 6.8	1.0 M Tris base
	pH 6.8
1.5 M Tris-HCl pH 8.8	1.5 M Tris base
	pH 8.8
Tumor digest buffer	200 µg/ml DNase I
	0.5 µg/ml Collagenase D
	RPMI 1640
1x Western blot transfer buffer	25 mM Tris base
	190 mM Glycine
	20 % (v/v) MeOH or EtOH

2.4. Cell culture media composition

Table 4: Cell culture medium composition for immortalized cell lines.

Cell line	Medium composition
B16F10-GFP-OVA	10 % (v/v) FBS 1 % (v/v) PenStrep 2.5 µg/ml Blasticidine DMEM
B16F10-gp_{33-41}	10 % (v/v) FBS 1 % (v/v) PenStrep 200 µg/ml G-418 DMEM
Baby hamster kidney (BHK)	10 % (v/v) FBS 1 % (v/v) PenStrep DMEM
Vero	10 % (v/v) FBS 1 % (v/v) PenStrep DMEM
YUMM-gp_{33-41}	10 % (v/v) FBS 1 % (v/v) PenStrep 200 µg/ml G-418 DMEM

2.5. Antibodies

Table 5: Fluorescence-labeled antibodies for flow cytometry and used dilutions.

Antibody	Company	Identifier	Dilution
AF488 Donkey anti-rabbit IgG	BioLegend (San Diego, CA, USA)	406416	1:1000
APC anti-mouse CD25	BioLegend (San Diego, CA, USA)	101910	1:400
APC anti-mouse CD45.1	BioLegend (San Diego, CA, USA)	110714 RRID:AB_313503	1:400
APC anti-mouse T-bet	Milteny Biotec (Bergisch Gladbach, Germany)	130-098-607	1:100
APC/Cy7 anti-mouse CD4	Becton Dickinson (Franklin Lakes, NJ, USA	552051	1:400
APC/Cy7 anti-mouse CD45.1	BioLegend (San Diego, CA, USA)	110716	1:400
APC/Cy7 anti-mouse/human CD44	BioLegend (San Diego, CA, USA)	103028 RRID:AB_830785	1:400
APC/Vio770 anti-mouse CD45.2	Milteny Biotec (Bergisch Gladbach, Germany)	130-118-951	1:200
BV421 anti-mouse CD4	BioLegend (San Diego, CA, USA)	562891 RRID:AB_2737870	1:400
BV421 anti-mouse CD44	BioLegend (San Diego, CA, USA)	103040 RRID:AB_2616903	1:400
BV421 anti-mouse CD45.1	BioLegend (San Diego, CA, USA)	110732	1:400
BV421 anti-mouse CD45.2	BioLegend (San Diego, CA, USA)	109832	1:400
BV421 Donkey anti-rabbit IgG	BioLegend (San Diego, CA, USA)	406410	1:1000
BV650 anti-mouse CD45.2	BioLegend (San Diego, CA, USA)	109835	1:400
BV711 anti-mouse CD45	BioLegend (San Diego, CA, USA)	103147	1:400
BV711 anti-mouse CD45.1	BioLegend (San Diego, CA, USA)	110739	1:400

FITC Annexin V	Milteny Biotec (Bergisch Gladbach, Germany)	130-093-060	1:200
FITC anti-mouse CD4	BioLegend (San Diego, CA, USA)	100406 RRID:AB_312691	1:400
FITC anti-mouse TCR-vα2	BioLegend (San Diego, CA, USA)	127806	1:400
FITC anti-mouse TNF-α	Milteny Biotec (Bergisch Gladbach, Germany)	130-102-294	1:200
PE anti-mouse CD45.2	BioLegend (San Diego, CA, USA)	109808 RRID:AB_313445	1:400
PE anti-mouse Eomes	Milteny Biotec (Bergisch Gladbach, Germany)	130-102-419	1:100
PE anti-mouse IL-7Rα	BioLegend (San Diego, CA, USA)	135010 RRID:AB_1937251	1:400
PE anti-mouse TIGIT	BioLegend (San Diego, CA, USA)	142104	1:400
PE anti-mouse TNF-α	BioLegend (San Diego, CA, USA)	506306 RRID:AB_315427	1:400
PE/Cy7 anti-mouse CD62L	BioLegend (San Diego, CA, USA)	104418 RRID:AB_313103	1:400
PE/Cy7 anti-mouse IFN-γ	BioLegend (San Diego, CA, USA)	505826 RRID:AB_2295770	1:400
PE/Cy7 anti-mouse PD-1	BioLegend (San Diego, CA, USA)	135216	1:400
PerCP anti-human CD3	BioLegend (San Diego, CA, USA)	317306 RRID:AB_571907	1:200
PerCP anti-human CD8a	BioLegend (San Diego, CA, USA)	300922 RRID:AB_1575072	1:200
PerCP/Cy5.5 anti-mouse CD8a	BioLegend (San Diego, CA, USA)	100734 RRID:AB_2075238	1:200

Table 6: Biotinylated and HRP-conjugated antibodies and respective dilutions.

Antibody	Company	Identifier	Dilution
Biotin anti-mouse CD8a (53-6.7)	BioLegend (San Diego, CA, USA)	100704	1:1000
HRP Donkey anti-rabbit IgG	BioLegend (San Diego, CA, USA)	406401	1:5000
HRP Goat anti-mouse IgG	BioLegend (San Diego, CA, USA)	405306	1:5000

Table 7: Unconjugated antibodies and respective dilutions.

Antibody	Company	Identifier	Dilution
Anti-human aspartate aminotransferase	Abcam (Cambridge, UK)	ab104265	1:200 for flow cytometry
β-Actin (C4)	Santa Cruz Biotechnology (Santa Cruz, CA, USA)	sc-47778	1:1000
CD4 (GK1.5)	Provided by the DKFZ core facility	monoclonal antibody	400 µg/animal
GOT1 (E4A4O)	Cell Signaling Technology (Danvers, MA, USA)	34423S	1:500
GRP94 (D6X2Q)	Cell Signaling Technology (Danvers, MA, USA)	20292	1:1000
Phospho-S6 Ribosomal Protein (Ser240/244) (D68F8)	Cell Signaling Technology (Danvers, MA, USA)	5364 RRID:AB_10694233	1:1000
TCF1/TCF7 (C63D9)	Cell Signaling Technology (Danvers, MA, USA)	2203S	1:1000 for flow cytometry
Ultra-LEAF™ Purified anti-mouse CD3	BioLegend (San Diego, CA, USA)	100238	0.2 µg/ml
Ultra-LEAF™ Purified anti-mouse CD16/32	BioLegend (San Diego, CA, USA)	101330	1:400
Ultra-LEAF™ Purified anti-mouse CD28	BioLegend (San Diego, CA, USA)	122022	0.1 µg/ml

2.6. Proteins, enzymes and peptides

Table 8: Overview over used enzymes, proteins and peptides.

Proteins, enzymes, peptides	Company	Identifier
Collagenase D	Sigma-Aldrich/ Merck KGaA (Darmstadt, Germany)	11088882001
DNase I	Sigma-Aldrich/ Merck KGaA (Darmstadt, Germany)	D4527
GP(33-41) peptide	GenScript (Piscataway Township, NJ, USA)	RP20091
IFNα	PeproTech (Rocky Hill, NJ, USA)	300-02A
IFNβ	PeproTech (Rocky Hill, NJ, USA)	300-02BC
IFNγ	PeproTech (Rocky Hill, NJ, USA)	315-05-20
Recombinant Mouse IL-2 (carrier-free)	BioLegend (San Diego, CA, USA)	575408
Recombinant Mouse IL-12 (p70) (carrier-free)	BioLegend (San Diego, CA, USA)	577004
Recombinant Mouse IL-15 (carrier-free)	BioLegend (San Diego, CA, USA)	566304
5x Taq Master Mix	New England Biolabs (Ipswich, MA, USA)	M0285L

2.7. Biological material

2.7.1. Cell lines

Table 9: Immortalized cell lines for tumor implantation and virus replication.

Cell line	Provided by
B16F10-gp_{33-41}	Prof. Dr. Hanspeter Pircher (University Freiburg, Freiburg, Germany)
B16F10-GFP-OVA	Dr. Rafael Carretero (German Cancer Research Center, Heidelberg, Germany)
BHK	Prof. Dr. Susan Kaech (Salk Institute for Biological Sciences, La Jolla, CA, USA)
Vero	
YUMM-gp_{33-41}	Dr. Ping-Chih Ho (University Lausanne, Lausanne, Switzerland)

2.7.2. Viral strains

Table 10: Viral strains for in vivo infections.

Viral strain	Reference	Provided by
LCMV Armstrong (Arm)	[191]	Prof. Dr. Susan Kaech (Salk Institute for Biological Sciences, La Jolla, CA, USA)
LCMV clone 13 (cl-13)	[192]	

2.7.3. Mouse strains

Mice were housed in the pathogen-free facility at DKFZ. Age- and sex-matched littermates (age of ~6-12 weeks) were used in the experiments. The studies were performed after approval at the Regierungspräsidium Karlsruhe.

Table 11: Used mouse lines.

Mouse strain	Short name	Provider, Reference	Identifier
C57BL/6		Charles River	027
C57BL/6N-Got1tm1c$^{(EUCOMM)Hmgu/H}$	Got1$^{flox/flox}$	MRC Harwell Institute	GOT-TM1C-B6n
Tg(Cd4-cre)1Cwi/BfluJ	Cd4-cre	[193, 194]	017336
Tg(TcrLCMV)327Sdz	P14	[195]	MGI:2665105

2.7.4. Human material

Human colon cancer tissues and healthy non-cancer adjacent tissues were obtained from the tissue bank of the National Center for Tumor Diseases (NCT) in Heidelberg, after approval of the ethics committee of the Heidelberg University.

2.8. Consumables

Table 12: Overview over consumables used in the study.

Consumable	Company	Identifier
Cellstar® White 96 Well Cell Culture Microplate	Greiner Bio-One (Kremsmünster, Austria)	655073
Costar® 50 ml Reagent Reservoir	Coring (Corning, New York, USA)	4870
Falcon™ 15 ml Polypropylene Conical Tube	Thermo Fischer Scientific (Waltham, MA, USA)	352096
Falcon™ 5 ml Polystyrene Round-Bottom Tube	Thermo Fischer Scientific (Waltham, MA, USA)	352054
Falcon™ 50 ml Polypropylene Conical Tube	Thermo Fischer Scientific (Waltham, MA, USA)	352070
Falcon™ Cell Strainer 70 µm Nylon	Thermo Fischer Scientific (Waltham, MA, USA)	352350
LS colums	Milteny Biotec (Bergisch Gladbach, Germany)	130-042-401
Millex®-GS Filter Unit 0.22 µm	Merck Millipore (Burlington, MA, USA)	SLGS033SS
NORM-JECT®-F Luer Solo Syringe	B.Braun (Melsungen, Germany)	NJ-9166017
Nylon Mesh SEFAR NITEX	Sefar (Edling, Germany)	3A03-0150-115-00
Pierce™ Blotting Paper	Thermo Fischer Scientific (Waltham, MA, USA)	LC2010
PVDF membrane	Santa Cruz Biotechnology (Santa Cruz, CA, USA)	sc-358811
Safe Lock Tube 0,5 ml	Eppendorf (Eppendorf, Germany)	0030121023
Safe Lock Tube 1,5 ml	Eppendorf (Eppendorf, Germany)	0030120086

Safe Lock Tube 2 ml	Eppendorf (Eppendorf, Germany)	0030120094
Safe Lock Tube 5 ml	Eppendorf (Eppendorf, Germany)	0030119487
Seahorse XFe96 FluxPak	Agilent Technologies (Santa Clara, CA, USA)	102416-100
TipOne 10 µl Graduated Tip	StarLab (Hamburg, Germany)	S1111-3700
TipOne 1000 µl Graduated Tip	StarLab (Hamburg, Germany)	S1111-6701
TipOne 200 µl Yellow Tip	StarLab (Hamburg, Germany)	S1111-0706
Zellkulturflasche 75cm^2	Techno Plastic Products TPP (Trasadingen, Switzerland)	90076
Zellkulturtestplatte 6 Well	Techno Plastic Products TPP (Trasadingen, Switzerland)	92006
Zellkulturtestplatte 96U Well	Techno Plastic Products TPP (Trasadingen, Switzerland)	92697

2.9. Instruments

Table 13: Instruments for analysis and experiments.

Instrument	Company
Cell incubator Heraeus Hera cell 150	Thermo Fischer Scientific (Waltham, MA, USA)
Centrifuges:	
Centrifuge 5810R	Eppendorf (Eppendorf, Germany)
Centrifuge 5920R	
Megafuge3.0RS	Heraeus (Hanau, Germany)
Chemi-Smart 5100	Vilber Lourmat (Eberhardzell, Germany)
Flow cytometers:	
FACS Canto II	Becton Dickinson (Franklin Lakes, NJ, USA)
FACS Fortessa	
FACS LSR II	
Heatblock:	
VWR Digital Heatblock	VWR (Radnor, DE, USA)
Block heater SBH130D	Cole-Parmer (Staffordshire, UK)
Thermomixer compact	Eppendorf (Eppendorf, Germany)
Horizon®11.14 Gibco BRL Gel Electrophoresis Apparatus	Thermo Fischer Scientific (Waltham, MA, USA)

Manual pipettes:	
Research® Plus (0.1-2.5µl; 1-10µl; 2-20µl;10-100µl; 20-200µl; 100-1000µl)	Eppendorf (Eppendorf, Germany)
Rainin Classic™ Pipette (1-10µl; 10-100µl; 100-1000µl)	Mettler-Toledo (Columbus, OH, USA)
Transferpette®S-12 and S-8 (20-200µl)	Brand (Wertheim, Germany)
Measures:	
Sartorius Universal Sartorius Analytic	Sartorius (Göttingen, Germany)
Microscope brightfield Nikon eclipse TS100	Nikon (Minato, Japan)
Microwave R-941STW	Sharp (Osaka, Japan)
Mini-PROTEAN® Tetra cell	Bio-Rad Laboratories (Hercules, CA, USA)
Molecular Imager GelDoc XR+	Bio-Rad Laboratories (Hercules, CA, USA)
Orion L Micorplate Luminometer	Berthold Detection Systems (Pforzheim, Germany)
PCR machine:	
T100™ Thermal Cycler	Bio-Rad Laboratories (Hercules, CA, USA)
Mastercycler	Eppendorf (Eppendorf, Germany)
PH meter ProfiLine pH 3210	Consort (Turnhout, Belgium)
Pipetboy acu	Integra biosciences (Zizers, Switzerland)
Power supply:	
Electrophoresis Power supply E864	Consort (Turnhout, Belgium)
peQPOWER	VWR (Radnor, DE, USA)
PowerPac	Bio-Rad Laboratories (Hercules, CA, USA)
Seahorse XFe96 analyzer	Agilent (Santa Clara, CA, USA)
Shaker	Edmund Bühler (Bodelshausen, Germany)
Stirrer D-6010	NeoLab (Heidelberg, Germany)
Table centrifuges:	
Hearaeus Pico17 (for 24 tubes)	Thermo Fischer Scientific (Waltham, MA, USA)
Centrifuge 5415R (for 24 tubes)	Eppendorf (Eppendorf, Germany)
Vortexer Vortex Genie 2	Scientific industries (Bohemia, NY, USA)
Waterbath WNE 7	Memmert (Schwabach, Germany)

2.10. Software

Table 14: Used software and software versions.

Software	Company
Chemi Capt version 15.01	Vilber Lourmat (Eberhardzell, Germany)
EndNote X.7.7.1	Thomson Reuters (Toronto, Canada)
FACS Diva™	Becton Dickinson (Franklin Lakes, NJ, USA)
FlowJo V10.1	Becton Dickinson (Franklin Lakes, NJ, USA)
Graph Pad Prism 7.04	GraphPad Software (San Diego, CA, USA)
ImageJ 1.52a	NIH (Bethesda, MD, USA)
Keynote 10.0	Apple (Cupertino, CA, USA)
Microsoft Office Professional Plus 2013	Microsoft (Redmond, WA, USA)
Wave 2.6.0	Agilent (Santa Clara, CA, USA)

3. Methods

3.1. Cell biology

3.1.1. General cell culture practice

3.1.1.1. Cell culture

Cell culture was performed under sterile conditions using a Heraeus Hera Safe laminar flow hood (Thermo Fisher Scientific, Waltham, MA, USA).
BHK, Vero, YUMM-gp_{33-41} (YUMM-gp33), B16F10-gp_{33-41} (B16-gp33), B16-GFP-OVA (B16-OVA) cells or primary cells were cultured at 37 °C with 5 % CO_2 in a humidified incubator in the respective growth media (**Table 4**). Fetal bovine serum (FBS) for the growth medium was heated for 30 min at 56 °C to inactivate complement factors. Immortalized cell lines were cultivated in 75 cm^2 cell culture treated polystyrene flasks. Cell growth of immortalized cell lines was monitored daily by microscopy and cell lines were passaged when they reached 90 % confluency at a dilution from 1:2 to 1:20. To detach adherent cell lines from the culture flasks, the medium was removed, and cells were rinsed carefully with 5 ml PBS. Cells were digested with 2 ml 0.25 % Trypsin-EDTA for 2-5 min and collected in 10 ml cell culture medium.

Centrifugation of the cells (e.g. for pelleting or washing steps) was performed at 2000 rpm (684-818 g) for 2 min at room temperature (RT), if not specified else.

3.1.1.2. Determination of cell numbers

Cell numbers were determined using a Brand™ Neubauer counting chamber (Thermo Fischer Scientific, Waltham, MA, USA). To discriminate between living and dead cells, the cells were stained with Trypan Blue solution at a 1:10 to 1:100 dilution. Only the uncolored cells were counted for calculation of the total cell number.

3.1.1.3. Freezing and thawing of eukaryotic cell lines

Cells were frozen at 1-5x10^6 cells/ml in 1 ml freezing medium in cryotubes. For gentle freezing (stepwise decrease of temperature, 1 °C/min), tubes were frozen in a Thermo Scientific™ Mr. Frosty™ Freezing Container (Thermo Fischer Scientific, Waltham, MA, USA) at -80 °C.
Frozen cells were thawed rapidly in a 37 °C water bath. To remove the DMSO, the cell suspension was transferred to a 50 ml conical tube and washed with 5 ml of the respective cell culture medium. The cells were seeded in 20 ml medium and cultivated as described above. 24 h after thawing, medium was changed to remove the dead cells.

3.1.2. Virus production of LCMV strains Arm and cl-13

3.1.2.1. Virus inoculation

For virus production of LCMV Arm or LCMV cl-13, BHK cells were used. One day prior to virus inoculation, BHK cells were plated as 5x10^5 cells/well in 1.5 ml medium in 6-well plates. The cells were infected with virus at a multiplicity of infection (MOI) of 0.001. The cell plates were incubated at 37 °C for 1.5 h. 3 ml pre-warmed medium were added to each well and the infected cells were incubated for 4 days. The supernatant was harvested and centrifuged to remove residual cells from the virus-containing supernatant. The supernatants were aliquoted and stored at -80 °C.

3.1.2.2. Plaque assay

The viral titer of the viral stocks was determined by plaque assays. Therefore, Vero cells were seeded in 6 well plates with 5x10^5 cells/well in 1.5 ml cell culture media per well, one day prior to the assay. On the day of the assay, 100 µl of the virus stock or 100 µl of 1:10 serial dilutions prepared in cell culture medium were added to the Vero cells and gently mixed by tilting the plate. The cells were incubated for 1.5 h at 37 °C. A 1 % (w/v) agarose solution in plain DMEM was prepared and mixed 1:1 with cell culture medium. The mixture was cooled down to 37 °C and 4 ml agarose solution was carefully overlaid to each well. The plates were left to cool down at RT for 10 min, and then incubated for 4 days. The agarose was carefully removed from each well. Using a transfer pipet, 2 ml plaque assay buffer were added to each well and incubated for 10 min at RT. The buffer was removed, and residual buffer was rinsed out with tab water. The plates were dried at RT and the plaques were counted to calculate the viral titer as plaque forming units per ml (pfu/ml).

3.1.3. Primary cell preparation from mouse organs

To prepare single cell suspensions from the organs of interest, mice were sacrificed by cervical dislocation and the respective organs (e.g. spleen, lymph nodes, Peyer's patches or thymus) were removed and collected in 1 ml 1 % RPMI. The organs were grinded in a 70 µm cell strainer using the plunger of a 1 ml syringe. After flushing the cell strainer with 5-10 ml 1 % RPMI, cells were pelleted. The supernatant was removed.

For the spleen, to remove red blood cells, the cell pellet was resuspended with 1 ml ACK Lysing buffer for 1 min. The reaction was stopped by adding 4 ml complete RPMI. The cell pellet was resuspended in 1 ml complete RPMI and filtered through nylon mesh to a fresh 15 ml conical tube.

Bone marrow was prepared from the femurs of the hind legs. The bone ends were cut open with scissors, and the marrow was flushed out with 1 % RPMI using a needle and syringe. The cell suspension was treated with ACK Lysing buffer and prepared similar to the splenocytes, as described above.

3.1.4. Preparation of tumor infiltrating lymphocytes (TILs) from mouse tumors

3.1.4.1. Yale University Mouse Melanoma gp33 tumors (YUMM-gp33)

YUMM-gp33 tumors were collected in 1 ml tumor digest buffer, and the tumor was cut to 2-3 mm sized pieces using surgical scissors. The fragments were digested at 37 °C for 30-60 min. The tubes were gently inverted every 15 mins. The digested tissue was smashed through a 70 µm cell strainer using the plunger of a syringe. After flushing the cell strainer with 15-20 ml 1 % RPMI, cells were pelleted. The supernatant was removed, and the cell suspension was resuspended in 10 ml 40 % Percoll™ diluted in plain DMEM. The suspension was overlaid to 5 ml 80 % Percoll™ diluted in plain DMEM in a conical 15 ml tube. The gradient was centrifuged for 30 min at 2000 rpm (684-818 g), RT, with the breaking speed reduced to 2. The middle layer containing the TILs was collected using a transfer pipette and transferred to a fresh conical 15 ml tube and the cells were washed once with 1 % RPMI. The resulting pellet was resuspended with 1 ml ACK Lysing buffer for 1 min. The reaction was stopped by adding 4 ml complete RPMI. Cells were pelleted, and the supernatant was removed. The pellet was resuspended in 1 ml complete RPMI. Cells were counted and used directly for subsequent experiments.

3.1.4.2. B16-gp33 and B16-OVA melanoma

B16 tumors were collected in 1 ml 1 % RPMI. The tumors were smashed through a 70 µm cell strainer using the plunger of a syringe. After flushing the cell strainer with 15-20 ml 1 % RPMI,

cells were pelleted. The supernatant was removed, and the cell suspension was resuspended in 10 ml 40 % Percoll™ diluted in plain DMEM. The suspension was overlaid to 5 ml 80 % Percoll™ diluted in plain DMEM in a conical 15 ml tube. The gradient was centrifuged for 30 min at 2000 rpm (684-818 g), RT, with the breaking speed reduced to 2. The middle layer containing the TILs was collected in a fresh conical 15 ml tube and washed once with 1 % RPMI. The resulting pellet was resuspended with 1 ml ACK Lysing buffer for 1 min. The reaction was stopped by adding 4 ml complete RPMI. Cells were pelleted and the supernatant was removed. The pellet was resuspended in 1 ml complete RPMI. Cells were counted and used directly for subsequent experiments.

3.1.5. T cell isolation from human tissue samples

Human tissues (colon tumor and non-tumor adjacent tissues) were cut into small pieces and digested with collagenase D (0.2 mg/ml in plain RPMI) at 37 °C for 30 minutes. The tissues were smashed through a 70 µm cell strainer. The suspension was resuspended in 10 ml 40 % Percoll™ diluted in plain RPMI and overlaid to 5 ml 80 % Percoll™ diluted in plain RPMI in a conical 15 ml tube. The gradient was centrifuged for 30 min at 2000 rpm (684-818 g), RT, with the breaking speed reduced to 2. The middle layer containing the TILs was collected in a fresh conical 15 ml tube and washed once with 1 % RPMI. Cells were used directly for flow cytometry staining.

3.1.6. T cell isolation from primary cell suspensions

3.1.6.1. $CD8^+$ positive selection

Positive selection of $CD8^+$ T cells was performed using MojoSort™ Streptavidin Nanobeads. $2x10^7$ cells (e.g. splenocyte suspension) were resuspended in 1 ml MACS buffer in a 5 ml FACS tube. 1 µl Biotin anti-CD8a antibody was added, mixed and incubated at RT for 15 min. The tube was washed with 2 ml MACS buffer. The supernatant was discarded, and the cell pellet was dissolved in 1 ml MACS buffer. 1 µl beads were added, thoroughly mixed and incubated at RT for 15 min. 2 ml MACS buffer were added and the cells were mixed. The tube was incubated for 2 min at RT on a MojoSort™ magnetic stand (BioLegend, San Diego, CA, USA). The supernatant was decanted without removing the tube from the stand. 3 ml MACS buffer were added and gently mixed by inverting the tube. Incubation on the magnetic stand, decanting of the supernatant and the subsequent washing step with 3 ml MACS buffer were repeated 2 more times. Cells were counted and then frozen or used directly for subsequent experiments.

3.1.6.2. Isolation of donor TILs

To recover donor TILs from B16 tumors after adoptive transfer, positive selection with CD90.1 MicroBeads was performed, after isolation of the TILs (as described in 3.1.4.2), according to manufacturer's description. Briefly, the cells were resuspended in the indicated volume of MACS buffer and incubated with positive selection antibody cocktail for 10 min at 4 °C. The mixture was loaded on LS separation columns fixed on a QuadroMACS™ separator (Milteny Biotec, Bergisch Gladbach, Germany) and washed once with MACS buffer. The cells were flushed from the column and used directly for subsequent RNA extraction.

3.1.6.3. $CD4^+$ or $CD8^+$ negative selection

$CD8^+$ and $CD4^+$ T cells were isolated from spleen cell suspensions using the $CD8^+$ or $CD4^+$ T Cell Isolation Kit, according to manufacturer's description. Briefly, cells were resuspended in the indicated volume of MACS buffer and incubated with a CD8 or CD4 negative selection antibody cocktail for 5 min at 4 °C. The samples were further diluted with MACS buffer and incubated with biotin microbeads for 10 min at 4 °C. The mixture was loaded on LS separation columns fixed on a QuadroMACS™ separator and the flow through and subsequent wash, containing the desired cells, were collected and combined. The cells were pelleted, and the resulting pellet was dissolved in 1 ml complete RPMI. Cells were counted and then frozen or used directly for subsequent experiments.

3.1.7. *In vitro* culture of primary cells

3.1.7.1. *In vitro* activation with anti-CD3 and anti-CD28

For stimulation of pan $CD4^+$ or $CD8^+$ T cells, 96-well plates with round bottom were coated with 0.2 µg/ml anti-CD3 and 0.1 µg/ml anti-CD28 in 50 µl PBS for 2 h at 37 °C. The wells were washed once with 100 µl PBS, before $5x10^5$ $CD4^+$ or $CD8^+$ T cells were seeded in 200 µl complete RPMI. Cells were incubated for 3 days.

3.1.7.2. *In vitro* activation of P14 cells with antigen

For stimulation of P14 cells, $5x10^5$ splenocytes from a P14 mouse were incubated in 96-well plates with round bottom in 200 µl complete RPMI with 10 ng/µl IL-2 and gp_{33-41} (gp33). Cells were incubated for 3 days.

Additional drugs or chemicals used during cell culture were added at the indicated concentration.

3.1.7.3. *In vitro* co-culture and *in vitro* rescue

A 1:1 mixture of $2.5x10^4$ P14 wildtype and $2.5x10^4$ *Got1*-deficient P14 T cells in 200 µl complete RPMI or minimal RPMI/well, supplemented with 10 ng/µl gp33 was established in 96-well plates with round bottom.
Additional drugs or chemicals used during cell culture were added at the indicated concentration. Cells were incubated for 3 days.
After 3 days, each well was split into 3 parts, and the ratio between wildtype and *Got1*-deficient cells, apoptosis, reactive oxygen species (ROS) production and the levels of depolarized mitochondria were investigated by flow cytometry.

3.1.8. Staining for flow cytometry

3.1.8.1. General surface staining

The single cell suspension was transferred to a round bottom 96-well plate (not more than $2x10^6$ cells/well) and briefly centrifuged for 2 min at 2000 rpm (684-818 g), RT. Fc-blocking was performed with 1:400 anti-CD16/32 in MACS for 5 min at RT. The antibodies of choice were diluted in FACS buffer to their indicated dilution (**Table 5, Table 7**). 50 µl of the respective staining solution was added to each well and gently mixed using a multi-channel pipette. The mixture was incubated for 15 min (RT). Cells were washed once with 200 µl FACS buffer/well, and then resuspended in 50-100 µl FACS buffer/well, prior to acquisition or subsequent intracellular staining.

3.1.8.2. Staining for apoptotic markers

To determine the apoptotic state of the cells, surface staining of annexin V (AnxV) and propidium iodide (PI) (1:200) and other surface markers of interest was carried out in annexin V staining buffer, similar to the general staining protocol described above. Cells were kept on ice and were acquired fresh without prior fixation.

3.1.8.3. Staining of ROS

The levels of ROS were determined using MitoSOX™ Red Mitochondrial Superoxide Indicator. 50 µl per well of a staining solution containing 5 µM MitoSOX™ Red and other surface staining antibodies of interest in FACS buffer were incubated for 30 min at 37 °C. The cells were washed once with 200 µl FACS buffer/well, and then resuspended in 50-100 µl FACS buffer/well. Cells were kept on ice and acquired fresh without prior fixation.

3.1.8.4. Staining of mitochondria

To determine the polarization state of mitochondria, a combination of membrane potential dependent (MitoTracker™ Deep Red FM) and independent dyes (MitoTracker™ Green FM) was used. 50 µl per well of a staining solution containing 50 nM MitoTracker™ dyes and other surface staining antibodies of interest in FACS buffer were incubated for 30 min at 37 °C. The cells were washed once with 200 µl FACS buffer/well, and then resuspended in 50-100 µl FACS buffer/well. Cells were kept on ice and acquired fresh without prior fixation.

3.1.8.5. General fixation

After surface staining was completed, cells that were not immediately analyzed on the flow cytometer, or cells that were to be stained with intracellular markers, were fixed.
For fixation and intracellular staining, cells were fixed with 50 µl Fixation Buffer/well at RT for 5 min and washed twice with 200 µl FACS buffer/well before subsequent analysis or intracellular staining.
For transcription factor staining, cells were fixed with 100 µl eBioscience™ Fixation/Permeabilization solution/well at 4 °C for at least 1 h (but not exceeding 24 h). Cells were washed twice with 200 µl FACS buffer/well before subsequent analysis or intracellular staining.

3.1.8.6. General permeabilization and intracellular staining

For transient permeabilization of the plasma membrane, cells were washed twice with 200 µl Permeabilization Buffer/well. The respective intracellular staining antibodies were diluted in Permeabilization Buffer and 50 µl staining solution was incubated for 15 min at RT. The cells were washed once with 200 µl Permeabilization Buffer/well, resuspended in 50-100 µl Permeabilization Buffer/well and acquired on a flow cytometer.

3.1.8.7. *In vitro* re-stimulation for cytokine analysis

For the analysis of intracellular cytokines, primary cells were re-stimulated with the LCMV-specific peptide gp33 (10 ng/ml) in the presence of 5 µg/ml Brefeldin A (BFA), to prevent proteins from being secreted, in 200 µl complete RPMI/well in a round bottom 96-well plate. The cells were incubated for 4-12 h. Unstimulated cells incubated in 200 µl complete RPMI/well were included as negative controls.

3.2. Molecular biology

3.2.1. Quantitative real-time PCR (qRT-PCR) analysis of RNA expression in TILs

3.2.1.1. RNA extraction and cDNA synthesis

RNA was extracted using Qiagen RNAeasy mini kit according to manufacturer's instructions. A DNA digestion step using the Qiagen RNase-Free DNase Set was included, before mRNA was eluted. 1.5 µg RNA/sample were used for reverse-transcription to cDNA using the SuperScript™ III system, according to manufacturer's description.

3.2.1.2. qRT-PCR reaction

The PCR reaction was performed in triplicates with a reaction mix prepared of 1 µl forward and reverse primer mix (5 µM stock), 12.5 µl Power SYBR® Green PCR Master Mix, 2 µl cDNA and 9.5 µl ddH_2O, using an ABI Prism 7500 sequence detection system (Thermo Fischer Scientific, Waltham, MA, USA) in 96-well format, following the cycling conditions from **Table 15**.

The following primers for *Got1* (Got1-qPCR-Fw 5'-GACCATGAGATCCGAACTCA-3'; Got1-qPCR-Re 5'-TGACCAAATACTCGACCTGC-3') and *β-Actin* as housekeeping gene for internal control (bActin-qPCR-Fw 5'-GGCTGTATTCCCCTCCATCG-3'; bActin-qPCR-Re 5'-CCAGTTGGTAACAATGCCATGT-3') were used. The levels of cDNA were determined by calculating the $2^{\Delta C_t(\beta Actin - Got1)}$ values. To compare the mRNA expression levels, the $2^{\Delta C_t(\beta Actin - Got1)}$ values of each group were normalized to those of the cells before transfer.

Table 15: PCR program for qRT-PCR reaction.

Step	Time	Temperature [°C]	
1	2 min	50	
2	10 min	60	
3	15 sec	95	40 repeats
4	1 min	60	

3.2.2. Western blot

3.2.2.1. Sample preparation

Cells to be analyzed by Western blot were pelleted by centrifugation (13000 rpm, (16100 - 17000 g), RT, 1 min) and the supernatant was removed. The cell pellet was lysed with 50 µl RIPA lysis buffer per 10^6 cells for 10 min at -80 °C. The sample was thawed, and the debris

was pelleted by centrifugation (13000 rpm, (16100 - 17000 g), RT, 1 min). 2 µl lysate were used for measuring the protein concentration in triplicates with the Pierce™ BCA™ Protein Assay kit, according to the manufacturer instructions. 10-40 µg protein per sample were mixed with respective amount of 4x LLB and boiled for 15 min at 95 °C. The samples were cooled on ice for 2 min, centrifuged (13000 rpm, (16100 - 17000 g), RT, 1 min) and loaded on denaturating SDS gels.

3.2.2.2. Gel preparation and electrophoresis

SDS-Page gels were casted by hand using casting chambers (Bio-Rad Laboratories, Hercules, CA, USA). First, the resolving gel mixture was prepared and poured between the glass slides (with 1.5 mm spacer) using a serological pipette. To smoothen the surface, the gel was overlayed with 200 µl isopropanol. After 15-30 min of polymerization, the isopropanol was removed from the now solid gel. The stacking gel mixture was poured on top of the resolving gel using a serological pipette. A 10 or 15-well comb was carefully inserted. After 15-30 min of polymerization, the gel was either used immediately or stored in wetted tissue paper in the fridge at 4 °C for up to one week. The gel was installed in a Mini-PROTEAN Tetra Cell (Bio-Rad Laboratories, Hercules, CA, USA) and the chamber was filled with 500 ml SDS running buffer. The combs were carefully removed, and the individual wells were flushed clean using a pipette. The sample or 5 µl PageRuler™ Prestained Protein Ladder were loaded to the wells. Gel run was performed at 70 V for 30 min and then 60-90 min at 100 V, until the desired separation was reached.

3.2.2.3. Transfer and blot

After separation, the gel was removed from the glass slides and the stacking gel was cut away. Proteins were transferred on PVDF membranes by wet transfer. Therefore, the membrane was activated with 100 % EtOH for 30 s and then equilibrated in Wet blot transfer buffer together with 2 sheets of filter paper. The blotting sandwich was assembled with 1 layer of pre-soaked filter paper, the membrane, the gel and the second filter paper. The transfer was performed in 500 ml Wet blot transfer buffer at 400 mA for 90 min. The membrane was blocked with 5 % skim milk powder in PBS-T or 5 % BSA in PBS-T (when phosphorylated proteins were investigated) for 60 min at RT on a shaker. The membrane was washed with PBS-T and incubated with the respective primary antibodies diluted in 5 % BSA with PBS-T with 0.2 mg/ml NaN_3 over night at 4 °C on a shaker.

3.2.2.4. Development and imaging

Probed blots were washed 3x 15 min with PBS-T at RT on a shaker. The HRP-conjugated secondary antibody was diluted to the indicated concentration (**Table 6**) in 5 % skim milk

powder in PBS-T or 5 % BSA in PBS-T (when phosphorylated proteins were investigated) and incubated for 60 min at RT on a shaker. The blots were washed 3x 15 min with PBS-T at RT on a shaker. For detection, 1 ml Clarity™ Western ECL Substrate was applied to the membrane and the signals were imaged in a chemiluminescence imager.

3.2.2.5. Stripping of membranes

To remove the detection antibodies, membranes were incubated with 0.2 M NaOH for 20 min at RT on a shaker. The membrane was blocked, re-incubated with the selected antibody and imaged as described above.

3.3. Metabolic analysis

3.3.1. Seahorse analysis of Got1$^{flox/flox}$Cd4-cre^{-} and Got1$^{flox/flox}$Cd4-cre^{+} P14 T cells

Seahorse mitochondrial and glycolytic stress tests were performed to determine the oxygen consumption and extracellular acidification rates (OCR and ECAR) of wildtype or *Got1*-deficient T cells. Mitochondrial coupling assays were performed to determine the degree of coupling between OXPHOS and the ETC. Electron flux assays were performed to assess the electron transport between the single complexes. A Seahorse XFe96 analyzer was used for the experiments.

3.3.1.1. Mitochondrial and glycolytic stress test

The respective wildtype or *Got1*-deficient P14 cells were *in vitro* activated in complete RPMI at a cell density of 0.5-1x10^6 cells/ml in 6 wells plates with 10 ng/ml gp33 and IL-2 for 2-3 days. The cells were skewed with different conditions at a cell density of 0.5-1x10^6 cells/ml in 6 well plates with Seahorse base medium, supplemented with 10 % dialyzed FBS, 6.7 mM glucose and 1 % PenStrep in the presence of gp33 for 12-24h (after 2 days of activation) or complete RPMI with 10 ng/ml IL-2 for 12-24h (after 3 days of activation).

Seahorse Cartridges were hydrated according to manufacturer's description. Seahorse 96 well cell culture plates were coated with 50 µl Poly-D-Lysine (1:20 diluted in XF calibrant buffer) and incubated at 4°C overnight.

After *in vitro* activation, the cell pellets were collected in 1 ml plain SH medium and 5x10^5 cells/well were seeded in 180 µl plain Seahorse medium (glycolytic stress test) or 180 µl Seahorse medium with 6.7 mM glucose (mitochondrial stress test of minimal medium

cultivated cells) or 10 mM glucose (mitochondrial stress test of complete RPMI cultivated cells). Therefore, the Poly-D-Lysine buffer was removed from the cell culture plate, and the plate was washed once with 100 µl plain Seahorse base medium. After seeding of the cells, the culture plate was spun for 1 min at 2000 rpm (684-818 g), RT and incubated for 30-60 mins in a 37 °C incubator without CO_2. The Seahorse cartridge was loaded with the respective drugs as described in **Table 16** and **Table 17**, and run on the analyzer follwing the program in **Table 18**.

Table 16: Portal injections for the mitochondrial stress test [in Seahorse medium + 6.7 mM-10 mM glucose].

Port	Drug	Final concentration [µM]	Injection volume [µl]
A	Oligomycin	1.5	20
B	FCCP	2	22
C	Rotenone	1.5	25

Table 17: Portal injections for the glycolytic stress test [in plain Seahorse medium].

Port	Drug	Final concentration [µM]	Injection volume [µl]
A	Glucose	6.7 or 10 mM	20
B	Oligomycin	1.5	22
C	2-DG	10 mM	25

Table 18: Assay program mitochondrial and glycolytic stress tests.

Step	Time	Repeats
Calibration	Standard	-
Equilibration	Standard	-
Baseline	Mix 5 min Measure 5 min	3
Injection Port A	Mix 5 min Measure 5 min	3
Injection Port B	Mix 5 min Measure 5 min	3
Injection Port C	Mix 5 min Measure 5 min	3
Final measurement	Mix 5 min Measure 5 min	3

3.3.1.2. Seahorse mitochondrial coupling analysis

Wildtype or *Got1*-deficient P14 cells were *in vitro* activated in complete RPMI at a cell density of 0.5-1x10^6 cells/ml in 6 wells plates with 10 ng/ml gp33 and IL-2 for 3 days. The cells were skewed with complete RPMI and 10 ng/ml IL-2 for 12-24h. Seahorse Cartridges and Seahorse 96 well cell culture plates were prepared as described in 3.3.1.1.

At the day of the assay, the cells were harvested and washed once in 1x MAS buffer. 5x10^5 cells/well were seeded in 1x MAS with 10 mM disodium succinate, 2 µM rotenone and 1 nM PMP. The Poly-D-Lysine buffer was removed from the cell culture plate, and the plate was washed once with 100 µl 1x MAS. After seeding the cells, the culture plate was spun for 1 min at 2000 rpm (684-818 g), RT and immeadiately measured with the drugs injected according to **Table 19** with the measurement schedule described in **Table 20**.

Table 19: Portal injections for the mitochondrial coupling assay.

Port	Drug	Final concentration	Injection volume [µl]
A	ADP	4 mM	20
B	Oligomycin	3.2 µM	22
C	FCCP	4 µM	25
D	Antimycin A	4 µM	27

Table 20: Assay program for coupling and electron flow assay.

Step	Time	Repeats
Calibration	Standard	-
Equilibration	Standard	-
Baseline	Mix 1 min Measure 2 min	3
Injection Port A	Mix 1 min Measure 2 min	3
Injection Port B	Mix 1 min Measure 2 min	3
Injection Port C	Mix 1 min Measure 2 min	3
Injection Port D	Mix 1 min Measure 2 min	3
Final measurement	Mix 1 min Measure 2 min	3

3.3.1.3. Seahorse electron flux assay

The cells were cultivated as in 3.3.1.2. $5x10^5$ cells/well were seeded in 1x MAS with 4 mM ADP, 4 µM FCCP, 10 mM sodium pyruvate, 2 mM malic acid and 1 nM PMP. The assay was performed as in 3.3.1.2. with the injection ports loaded as in **Table 21**.

Table 21 Portal injections for the mitochondrial coupling assay.

Port	Drug	Final concentration	Injection volume [µl]
A	Rotenone	2 µM	20
B	Sodium succinate	10 mM	22
C	Antimycin A	4 µM	25
D	Ascorbate	10 mM	27
	TMPD	100 µM	

3.3.2. Metabolic tracing with ^{13}C-labeled metabolites

3.3.2.1. Metabolic labeling

P14 cells from Got1$^{flox/flox}$Cd4-cre^{+} and Got1$^{flox/flox}$Cd4-cre^{-} mice were activated *in vitro* for 3 days at a cell density of $5x10^5$ cells/ml in 6 wells plates with 10 ng/ml gp33 and IL-2. The gp33 was washed out and the cells were expanded in complete RPMI with IL-2 for 2 days at a cell density of $3x10^5$ cells/ml in 6 wells plates. The cells were harvested and washed once with 10 ml cold PBS. 10^7 cells in 500 µl PBS with 1 % FBS were used for each condition:
To 10^7 cells from each mouse, either 5 µl 1 M D-Glucose-$^{13}C_6$ or 5 µl 200 mM L-Glutamine-$^{13}C_5$ or 5 µl 1M Na-Lactate-$^{13}C_3$ or 5 µl PBS were added and gently mixed. The cells were incubated for 60 min at 37 °C and then quenched by addition of 1 ml cold 0.9 % NaCl. The tubes were inverted 3 times and spun for 1 min, 13000 rpm (16100 - 17000 g) at 4 °C. The pellets were washed once with 1 ml 0.9 % NaCl, the supernatant was completely removed, the pellet was frozen on dry ice and stored at -80 °C until analysis.

3.3.2.2. Gas chromatography/mass spectrometry (GC/MS) analysis

Analysis and method description were kindly performed and provided by Michael Buettner; Centre for Organismal Studies (COS), University of Heidelberg, Heidelberg, Germany.

Sample material (frozen pellets corresponding to 10^7 cells) was extracted in 360 µl of 100 % methanol for 15 min at 70 °C with vigorous shaking. As internal standard 20 µl Ribitol (0.2 mg/ml) were added to each sample. After the addition of 200 µl chloroform, samples were shaken at 37 °C for 5 min. To separate polar and organic phases, 400 µl ddH_2O were added and samples were centrifuged for 10 min at 11000 g. For the derivatization, 700 µl of the upper

(polar) phase were transferred to a fresh tube and dried in a vacuum concentrator without heating. For the derivatization (Methoximation and Silylation), pellets were re-dissolved in 30 µl methoximation reagent containing 20 mg/ml methoxyamine hydrochloride in pyridine and incubated for 90 min at 55 °C with shaking. For silylation, 30 µl MTBSTFA were added to each sample. After incubation for 60 min at 55 °C, samples were transferred to glass vials for GC/MS analysis. A GC/MS-QP2010 Plus (Shimadzu®, Kyoto, Japan) fitted with a Zebron ZB 5MS column (Phenomenex®, Torrance, CA, USA; 30 m x 0.25 mm x 0.25 µm) was used for GC/MS analysis.
The GC was operated with an injection temperature of 250 °C and 1 µL sample was injected with split mode (1:5). The GC temperature program started with a 2 min hold at 100 °C followed by a 10 °C/min ramp to 300 °C, a 60 °C/min ramp to 330 °C and a bake-out for 1 min at 330 °C, using Helium as carrier gas with constant linear velocity. The MS was operated with ion source and interface temperatures of 250 °C, a solvent cut time of 5 min and a scan range (m/z) of 40 – 700 with an event time of 0.1 s. The DExSI software [196] was used for data processing.

3.3.2.3. Ultra-performance liquid chromatography (UPLC) analysis

We want to thank the Metabolomics Core Technology Platform of the Excellence cluster "CellNetworks" (University of Heidelberg) and the Deutsche Forschungsgemeinschaft (grant ZUK 40/2010-3009262) for support with HPLC-based metabolite quantification.
Analysis and method description were kindly performed and provided by Gernot Poschet; Centre for Organismal Studies (COS), University of Heidelberg, Heidelberg, Germany.

Determination of organic acids was adapted from [197]. In brief, $1x10^6$ cells per sample were extracted in 100 µl ice cold methanol with sonication on ice. For derivatization, 50 µl extract was mixed with 25 µl 140 mM 3-Nitrophenylhydrazine hydrochloride, 25 µl methanol and 100 µl 50 mM Ethyl-3-(3-dimethylaminopropyl) carbodiimide hydrochloride and incubated for 20 min at 60 °C.
Separation was carried out by reversed phase chromatography on a Acquity H-class UPLC system coupled to a QDa mass detector (Waters, Milford, MA, USA) using an Acquity HSS T3 column (100 mm x 2.1 mm, 1.8 µm, (Waters, Milford, MA, USA)) which was heated to 40 °C. Separation of derivates was achieved by increasing the concentration of 0.1 % formic acid in acetonitrile (B) in 0.1 % formic acid in water (A) at 550 µl/min as followed: 2 min 15 % B, 2.01 min 31 % B, 5 min 54 % B, 5.01 min 90 % B, hold for 2 min, and return to 15 % B in 2 min. Mass signals for the following compounds were detected in single ion record (SIR) mode using negative detector polarity and 0.8 kV capillary voltage: lactate (224.3 m/z; 25 V CV), malate (403.3 m/z; 25 V CV), succinate (387.3 m/z; 25 CV), fumarate (385.3 m/z; 30 V), citrate (443.3

m/z; 10 V), pyruvate (357.3 m/z; 15 V) and α-ketoglutarate (550.2 m/z; 25 CV). Data acquisition and processing was performed with the Empower3 software suite (Waters, Milford, MA, USA).

3.3.3. NAD^+/NADH determination by luminescence

The levels of NAD^+ and NADH were determined using the NAD/NADH-Glo™ Assay according to manufacturer's description. 10^6 cells (fresh or frozen pellet stored at -80 °C) were used per sample. Briefly, samples were lysed with 30 µl NAD^+/NADH lysis buffer and split in 2 separate 1.5 ml tubes (15 µl each). For NAD^+ measurement, 7.5 µl 0.4 M HCl were added. After 15 min incubation at 60 °C, 7.5 µl Tris base were added. For NADH measurement, samples were incubated for 15 min at 60 °C, before 15 µl Tris-HCl were added. After adding a luciferin detection reagent, luciferase signal was measured after 30 min incubation for 1 s with a luminescence detector. NAD^+ and NADH concentration were calculated using standard curves that were included in the measurement.

3.4. *In vivo* studies

3.4.1. General mouse genotyping

3.4.1.1. Genotyping by PCR

DNA was isolated from ear biopsies. The tissue was boiled with 100 µl 50 mM NaOH at 95 °C for 30 min and then neutralized with 50 µl 1 M Tris-HCl (pH 7.8). The DNA was stored at 4 °C. A PCR mix was prepared from 1 µl forward and reverse primer mix (10 µM stock), 4 µl 5x Taq Master Mix, 1 µl DNA and 14 µl ddH_2O. The genomic DNA was amplified following the PCR protocol shown in **Table 22**. Oligomers (**Table 23**) were synthesized by Eurofins Scientific (Luxemburg, Luxemburg). After the amplification, the PCR product was mixed with 4 µL 6x Loading Dye and 10 µl were loaded on a 1 % agarose gel containing 0.005 % SYBER safe DNA stain in TBE, and separated with 120 V for 30-40 min. The agarose gel was then imaged using an agarose gel documentation system.

For $Got1^{flox/flox}$ genotyping, the combination from primers P1 and P2 resulted in a 209 bp fragment for wildtype, and in two fragments (114 and 200 bp) for floxed animals. Additionally, the combination of P1 and P3 yielded a 114 bp fragment, and P7 and P8 a 218 bp fragment in floxed animals. The PCR result for Cd4-cre resulted in a 600 bp band in cre positive animals. For P14 genotyping, the mix from all primers resulted in a 400 bp band for P14 positive animals, and a 200 bp fragment as internal positive control.

Table 22: Standard PCR program for genotyping.

Step	Time	Temperature [°C]	
1	5 min	94	
2	30 s	94	34 repeats
3	30 s	58	
4	40 s	68	
5	10 min	68	
6	Forever	4	

Table 23: Primer for Got1$^{flox/flox}$ genotyping (row 1-5), Cd4-cre genotyping (row 6, 7), P14 genotyping (row 8-11).

Primer name	Sequence (5'-3')
P1 GOT1-5arm-WTF	CAA ACC TGT TGG GTC GTG TT
P2 GOT1-Crit-WTR	TGC CAC AAA CTC AGG TCA AG
P3 tm1a (5mut-R1)	GAA CTT CGG AAT AGG AAC TTC G
P7 tm1c (5'CAS-F1)	AAG GCG CAT AAC GAT ACC AC
P8 tm1c (5'CAS-R1)	CCG CCT ACT GCG ACT ATA GAG A
CD4 cre Fw	CCC AAC CAA CAA GAG CTC
CD4 cre Re	CCC AGA AAT GCC AGA TTA CG
oIMR0244	CAT GGA GGC TGC AGT CAC CC
oIMR0245	GTT TGT TTG CGA GCT CTG TTT TGA TGG CTC
oIMR8744	CAA ATG TTG CTT GTC TGG TG
oIMR8745	GTC AGT CGA GTG CAC AGT TT

3.4.1.2. Genotyping by flow cytometry

Genotyping of congenic markers was performed from blood samples. 50 µl blood were transferred from a sodium-citrate containing collection tube to a round bottom 96-well plate and spun at 2000 rpm, 2 min, RT. The supernatant was discarded, and the pellets were resuspended with 200 µl ACK Lysing buffer to remove the red blood cells. After 1 min incubation, the plate was spun at 2000 rpm (684-818 g), 2 min, RT and the supernatant was discarded. The ACK lysis was repeated 2 times and the final pellet was washed once with 200 µl FACS buffer. The cells were stained using the standard panel from **Table 24** as described in 3.1.8.1.

Table 24: Standard flow cytometry staining for genotyping.

Antigen	Fluorophore	Dilution
CD8a	Percp-Cy5.5	1:400
TCR-vα2	FITC	1:400
CD45.1	APC	1:400
CD45.2	PE	1:400
CD90.1	BV421	1:400
CD90.2	PE-Cy7	1:400

3.4.2. Immune characterization of Got1$^{+/+}$Cd4-cre^{+} or Got1$^{flox/flox}$Cd4-cre^{+} mice

Naïve Got1$^{+/+}$Cd4-cre^{+} and Got1$^{flox/flox}$Cd4-cre^{+} mice of both genders were sacrificed and the lymphocyte phenotype in spleen, mesenteric lymph nodes, Peyer's patches, bone marrow (from both femurs) and thymus were investigated by flow cytometry.

3.4.3. Viral infection experiments

3.4.3.1. LCMV Arm

Mice were infected with 2x10^{5} pfu LCMV Arm (i.p. in 200 µl RPMI). The mice were sacrificed 8 days or 30 days post infection (dpi), and the splenic T cells were stained for flow cytometry.

3.4.3.2. LCMV cl-13

Mice were infected with 2x10^{6} pfu LCMV cl-13 (i.v. in 200 µl RPMI). CD4^{+} T cells were depleted by injection of anti-CD4 (GK1.5) i.p. (in total 0.4 mg/animal) in 200 µl PBS. The mice were sacrificed 8 or 21 dpi, and the splenic T cells were stained for flow cytometry.

3.4.3.3. Adoptive T cell transfer and LCMV infection

Got1$^{flox/flox}$Cd4-cre^{-} P14 or Got1$^{flox/flox}$Cd4-cre^{+} P14 T cells of donor mice with mismatched congenic markers (CD45.1 or CD45.2) were purified as described above.

A 1:1 mix of 5000 Got1$^{flox/flox}$Cd4-cre^{-} P14 and 5000 Got1$^{flox/flox}$Cd4-cre^{+} P14 T cells in 200 µl plain RPMI was i.v. injected into recipient C57BL/6 mice, and the animals were infected with LCMV Arm as described above.

A 1:1 mix of 500 Got1$^{flox/flox}$Cd4-cre^{-} P14 and 500 Got1$^{flox/flox}$Cd4-cre^{+} P14 T cells in 200 µl plain RPMI was i.v. injected into recipient C57BL/6 mice, and the animals were infected with LCMV cl-13 as described above.

3.4.4. Tumor experiments

3.4.4.1. Tumor implantation

B16-gp33, B16-OVA or YUMM-gp33 cells were cultivated in respective cell culture medium and passaged 3-4 times before inoculation. Prior to inoculation, the cells were washed twice with plain medium, to remove residual FBS from the culture. For tumor inoculation, mice were anesthetized with 1.5-3 % isoflurane. The injection site was shaved and 0.2-0.4x10^6 B16-gp33, B16-OVA or YUMM-gp33 cells in 200 µl plain DMEM were subcutaneously injected above the right flank, or simultaneously in the right and left flank.

3.4.4.2. Tumor measurements

Tumor growth was monitored with a digital caliper every 2-3 days. The tumor volume was calculated by $V = D \times d \times \frac{1}{2} d$ (V = tumor volume, D = larger tumor diameter, d = smaller diameter).

3.4.4.3. Adoptive T cell transfer on tumor bearing mice

T cells were transferred when tumors were palpable (ca. day 9-11 after implantation).
For adoptive transfer of P14 cells to tumor bearing mice, the P14 cells were *in vitro* activated for 3 days in complete RPMI with gp33 and IL-2 (each 10 ng/ml). The gp33 was washed out and the cells were expanded in complete RPMI with 10 ng/ml IL-2 for additional 24 hours. Prior to adoptive transfer, the cells were washed twice with plain RPMI. 0.3-1x10^6 Got1$^{flox/flox}$Cd4-cre$^-$ P14, Got1$^{flox/flox}$Cd4-cre$^+$ P14 or a 1:1 mix of 3x10^5 wildtype and 3x10^5 *Got1*-deficient P14 T cells in 200 µl plain RPMI were i.v. injected into tumor bearing mice. In certain cases, naïve P14 cells were transferred, instead of pre-activated cells.
Mice were sacrificed 4 days after adoptive transfer, or when the termination criteria (tumor size of 1.5 cm diameter) was met. TILs were prepared as described in 3.1.4 and analyzed by flow cytometry.

3.4.4.4. *In vitro* treatment and adoptive transfer on tumor bearing mice

T cells were transferred when tumors were palpable (ca. day 9-11 after implantation).
Wildtype or *Got1*-deficient P14 T cells were *in vitro* cultivated in minimal RPMI with 10 ng/ml gp33 and supplemented with a vehicle, 1 mM sodium pyruvate or 10 mM dimethyl-2-oxoglutarate (membrane permeable α-KG) for 24 h. 3x10^5 cells were adoptively transferred in plain RPMI on mice bearing B16-gp33 tumors. TILs and splenocytes were prepared as described in 3.1.3 and 3.1.4 and stained and analyzed by flow cytometry.

4. Results

4.1. Breeding and quality control of *Got1*-deficient mouse lines

To selectively deplete GOT1 in T cells, we bred mice with exon 2 of the *Got1* coding sequence flanked by loxP sites ($Got1^{tm1a(EUCOMM)Hmgu}$ which has been converted to $Got1^{flox/flox}$ using Flp recombinase, **Figure 4.1 A**) to mice bearing a cre recombinase under the control of *Cd4* (Tg(Cd4-cre)1Cwi/BfluJ), further referred to as Cd4-cre [198, 199]. This combination allowed the selective deletion of functional *Got1* in $CD4^+$ and $CD8^+$ T cells during thymic T cell development (**Figure 4.1 B**). The mice were subsequently bred to Tg(TcrLCMV)327Sdz [200], a strain further referred to as P14. This strain bears a transgenic TCR against the gp_{33-41} epitope of LCMV and allowed us to study the antigen-dependent and $CD8^+$ T cell-intrinsic role of GOT1. As wildtype controls in the experiments, littermates were used which were either $Got1^{+/+}$ or $Cd4\text{-}cre^-$, as indicated in the respective experiment. GOT1 protein was effectively deleted in $CD8^+$ and $CD4^+$ T cells from $Got1^{flox/flox}Cd4\text{-}cre^+$ animals, as well as in $CD8^+$ T cells from $Got1^{flox/flox}Cd4\text{-}cre^+$ P14 mice (**Figure 4.1 C** and **D**).

The International Mouse Phenotyping Consortium (IMPC) found homozygous lethality for *Got1* germline deficient mice. However, T cell specific deletion did not cause embryonic lethality or other breeding defects in the mice. We investigated the immune system of naïve *Got1*-deficient and *Got1* wildtype mice, to assess for potential alterations caused by the deletion of *Got1*.

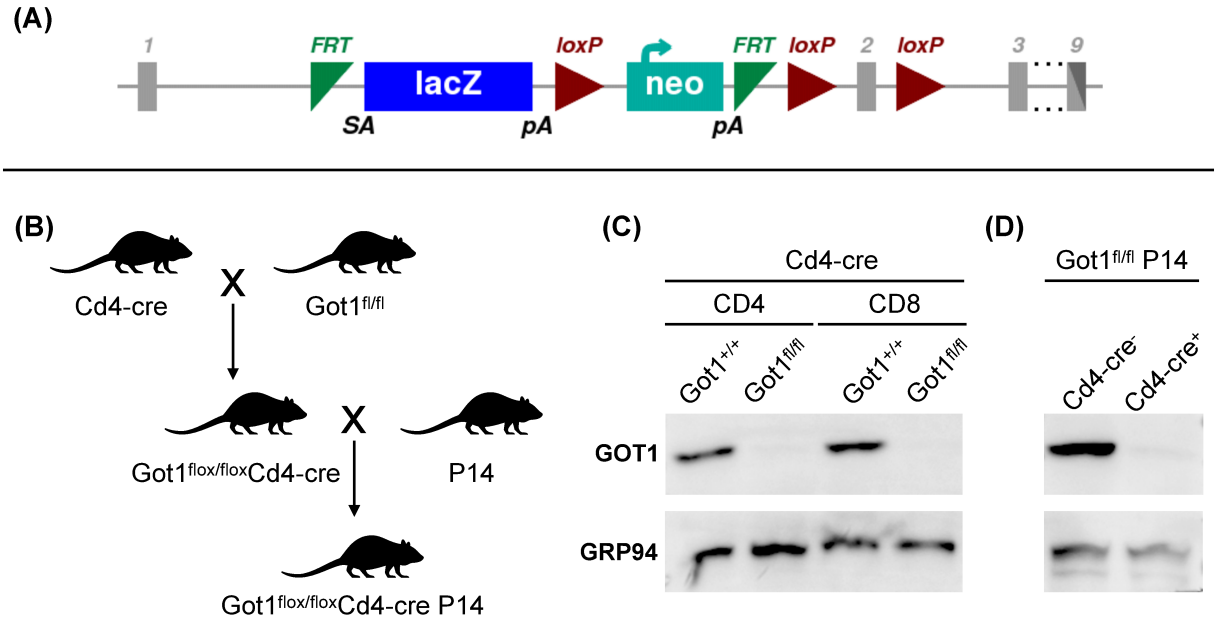

***Figure 4.1: Overview of the investigated Got1-deficient mouse lines**. A: Construction of the Got1$^{tm1a(EUCOMM)Hmgu}$ allele, picture obtained from [201]. B: Breeding scheme. C: Western blot of GOT1 protein expression in Got1-deficient CD4$^+$ or CD8$^+$ T cells after in vitro stimulation with anti-CD3/CD28. D: Western blot of GOT1 protein expression in Got1-deficient P14 T cells compared to wildtype control samples after in vitro stimulation with gp33 and IL-2. GRP94 was used as loading control in C and D.*

4.2. Naïve mice with *Got1*-deficient T cells develop a normal immune system

We compared the immune system of naïve *Got1* wildtype or -deficient mice of both genders by analyzing a panel of commonly investigated markers for T cell activation, differentiation and others in primary and secondary lymphoid organs (thymus, spleen, mesenteric lymph nodes (mLN), bone marrow and the Peyer's patches) by flow cytometry (**Figure 4.2**). Naïve mice displayed similar absolute cell numbers in all investigated organs (**Figure 4.2 A**), and a similar distribution of CD4$^+$ and CD8$^+$ T cells (**Figure 4.2 B** and **C**). We investigated the expression of CD62L and CD44 and found no difference in the frequency of CD62L^{high}CD44^{low} naïve T cells, CD62L^{high}CD44^{high} central memory cells (T_{CM}) or CD62L^{low}CD44^{high} effector T cell subsets [45] among CD4$^+$ and CD8$^+$ T cells (representative in **Figure 4.2 D** for the spleen). Similarly, the mean fluorescence intensity (MFI) of activated or T_{Reg} marker IL2Rα (CD25) [202] and naïve or memory T cell marker IL7Rα (CD127) [203] were comparable between *Got1* wildtype or -deficient CD4$^+$ and CD8$^+$ T cells, respectively (representative in **Figure 4.2 E** for the spleen).

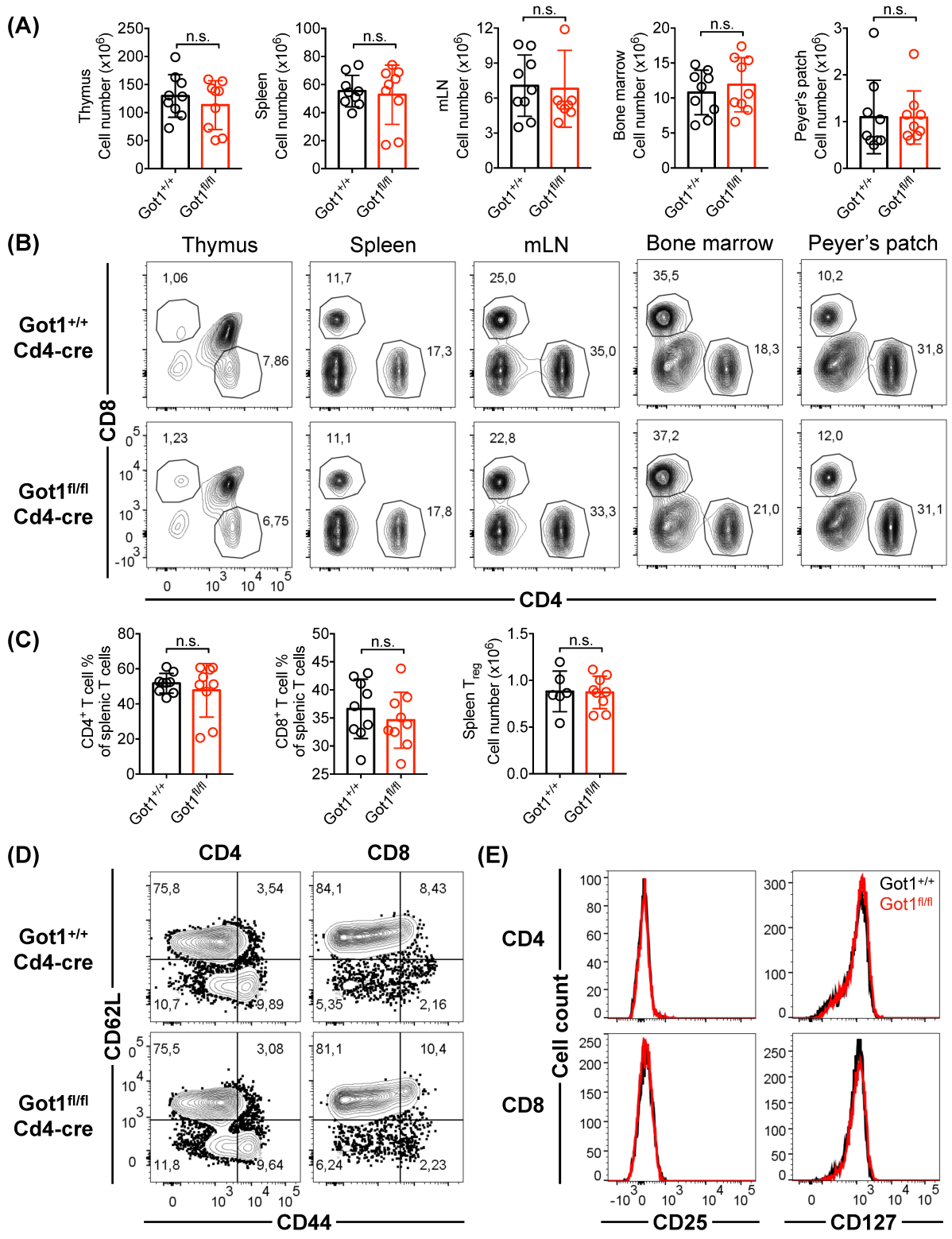

Figure 4.2: Immune characterization of naïve wildtype and Got1-deficient mice. *A: Absolute cell numbers in thymus, spleen, mLN, bone marrow and Peyer's patch (± SD). B: Representative flow cytometry analysis of the distribution of CD4⁺ and CD8⁺ T cells in the respective organs. C: Percentages of CD4⁺ and CD8⁺ T cells among all lymphocytes in the spleen and number of splenic T_{Reg} cells. D: Representative flow cytometry analysis of CD62L and CD44 in splenic CD4⁺ and CD8⁺ T cells. E: Representative MFI of CD25 and CD127 in splenic CD4⁺ and CD8⁺ T cells. Data shown from 3 experiments with 9 pairs of mice in total. n.s. = p>0.05. P values were calculated using two-tailed unpaired Student's t-tests.*

Although the inhibition of GOT1 was previously reported to increase the differentiation of T_{Reg} [188], we did not observe changes in T_{Reg} percentages among $CD4^+$ T cells and found equal expression of FOXP3 (representative in **Figure 4.2 C** for the spleen) in *Got1*-deficient cells.

To learn about the kinetics and signals that contribute to the protein expression of GOT1, we first performed experiments *in vitro*.

4.3. GOT1 expression correlates with TCR stimulation *in vitro*

To investigate the stimuli that contribute to the upregulation of GOT1 in T cells, *in vitro* stimulated cells were analyzed by Western blot. In a pilot test, wildtype P14 $CD8^+$ T cells were stimulated with the cognate peptide gp33 in the presence of IL-2 for 1-3 days. We compared the GOT1 protein levels to naïve cells and $Got1^{flox/flox}Cd4\text{-}cre^+$ cells, which were stimulated under the same conditions (**Figure 4.3 A**). Furthermore, after 3 days, the stimulating peptide was washed out from the culture and the cells were treated with IL-15 to induce memory cell formation (d3+1). GOT1 protein was weakly expressed in naïve P14 cells and was found to be upregulated after 3 days of activation (**Figure 4.3 B** and **C**). After the stimulating peptide was removed, GOT1 expression was reduced to basal levels, indicating that IL-15 treatment did not sustain GOT1 expression. In *Got1*-deficient T cells, protein levels were strongly reduced. We compared the expression kinetics to the phosphorylation of S6 as a readout for distal TCR signaling after mTOR activation [92]. S6 phosphorylation peaked 1 day after stimulation and was reduced after 3 days of activation.

It should be noted that the lower molecular weight band that is visible below the GOT1-derived signal in **Figure 4.3 B** and subsequent Western blots resulted from residual pS6 signal after stripping of the membrane. The delayed but similar expression profile of GOT1 compared to pS6 indicated antigen dependent TCR stimulation as necessary signal for transcription. Thus, in a follow up experiment we evaluated the contributions of TCR signaling to GOT1 transcription.

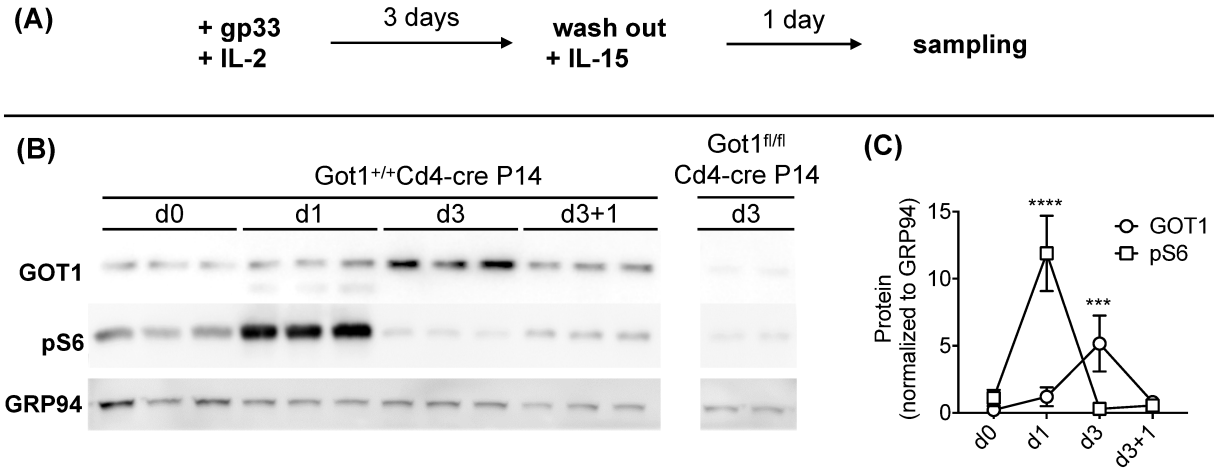

Figure 4.3: GOT1 expression in CD8⁺ T cells requires antigenic stimulation. *A: Schematic representation of the in vitro treatment. P14 T cells were in vitro stimulated with gp33 and IL-2 and harvested after 1 or 3 days. 3 day activated P14 Got1-deficient T cells were used as control. After 3 days, cells were skewed with IL-15 for 1 day. B: Western blot analysis of GOT1 and pS6 in three biological replicates. GRP94 protein levels were used as loading control. C: Quantification of GOT1 and pS6 protein levels (± SD). *** = p<0.001; **** = p<0.0001. P values were calculated by comparing the expression to d0 using two-tailed unpaired Student's t-tests.*

To investigate the relationship between GOT1 expression and TCR engagement, P14 T cells were stimulated with gp33 in the presence of IL-2 with Rapamycin (Rapa) or Cyclosporin A (CsA) for 3 days (**Figure 4.4 A**), to selectively interfere with distinct signaling pathways downstream of the TCR.

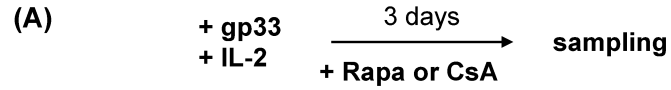

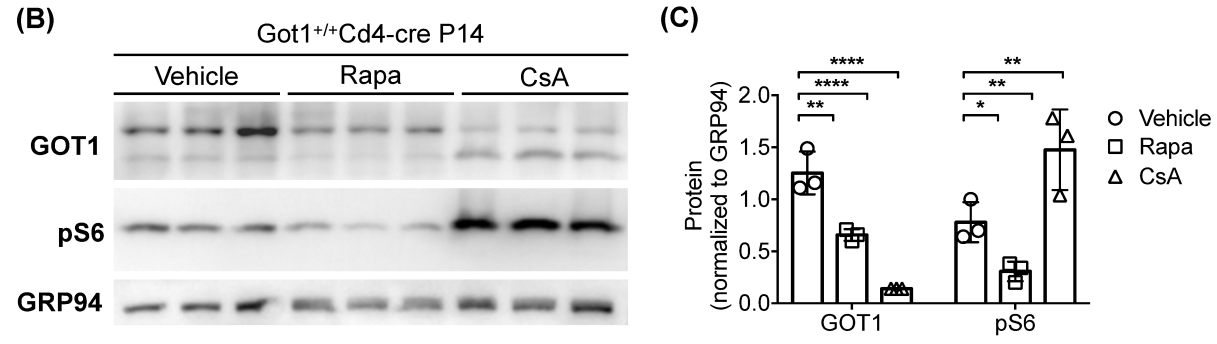

Figure 4.4: GOT1 expression in CD8⁺ T cells requires TCR stimulation. *A: Schematic representation of the in vitro treatment. P14 T cells were in vitro stimulated with gp33, IL-2 and 200 nM Rapa, 5 μM CsA or vehicle for 3 days. B: Western blot analysis of GOT1 and pS6 in three biological replicates. GRP94 protein levels were used as loading control. C: Quantification of GOT1 and pS6 protein levels (± SD). * = p<0.05; ** = p<0.01; **** = p<0.0001. P values were calculated by comparing the expression to vehicle using two-tailed unpaired Student's t-tests.*

Rapa is a negative regulator of the mTOR pathway, and primarily targets mTORC1 [204], while CsA is an inhibitor of the CaN-dependent activation of NFAT [205]. Both treatments significantly decreased the expression of GOT1 compared to vehicle-treated cells (Figure 4.4B and C). This indicated TCR, signaling was indeed necessary for GOT1 upregulation. Similar to GOT1, S6 phosphorylation was significantly decreased in Rapa-treated cells. Interestingly, pS6 signal increased significantly in CsA-treated cells.

Since the preliminary results indicated that GOT1 expression was downstream and dependent on TCR engagement, we investigated if inflammatory stimuli would exacerbate GOT1 expression *in vitro.* P14 T cells were stimulated with gp33 in the presence of IL-2 and treated with type I interferons IFNα+β, type II interferon IFNγ, IL-12 or vehicle for 3 days (**Figure 4.5 A**). However, none of the treatments increased GOT1 or pS6 levels significantly, compared to the control (**Figure 4.5 B** and **C**).

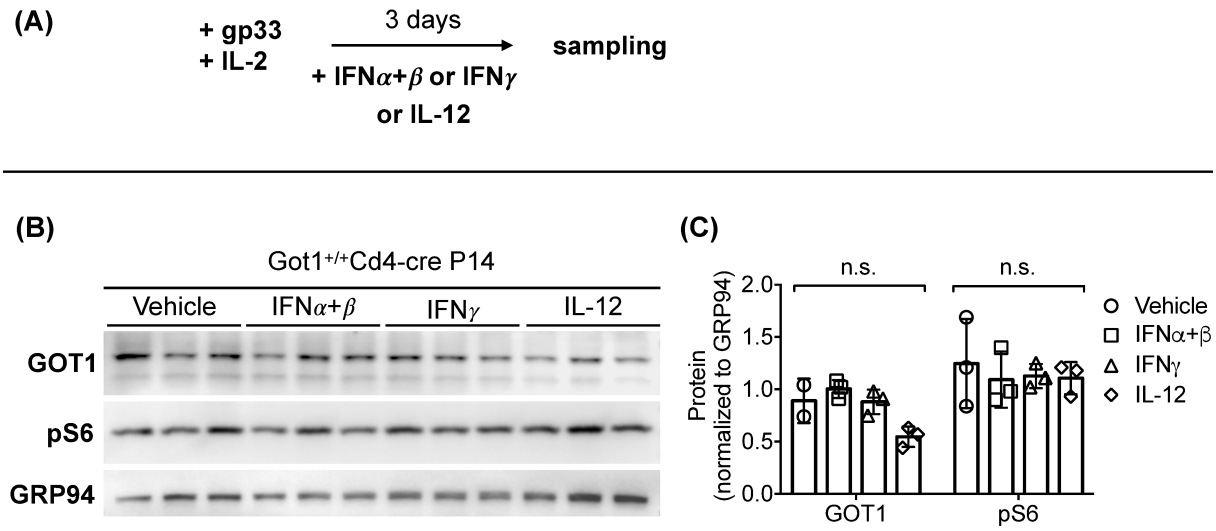

Figure 4.5: GOT1 expression in CD8⁺ T cells is independent of inflammatory stimuli. *A: Schematic representation of the in vitro treatment. P14 T cells were in vitro stimulated with gp33, IL-2 and 10 ng/ml IFNα+β, IFNγ, IL-12 or vehicle for 3 days. B: Western Blot analysis of GOT1 and pS6 in three biological replicates. GRP94 protein levels were used as loading control. C: Quantification of GOT1 and pS6 protein levels (± SD). * = p<0.05; ** = p<0.01; **** = p<0.0001. P values were calculated by comparing the expression to vehicle using two-tailed unpaired Student's t-tests.*

These combined *in vitro* studies indicated, GOT1 expression was dependent on the presence of antigen and increased after T cell activation, but GOT1 expression was independent from inflammatory stimuli or memory-inducing cytokines. Inspired by these results, we investigated the expression of GOT1 in *in vivo* activated T cells.

4.4. GOT1 is expressed in antitumoral T cells in mice and humans

We investigated the upregulation of *Got1* mRNA in TILs from B16 melanoma tumors, expressing the epitopes gp_{33-41} (referred to as B16-gp33, which could be recognized by P14 cells) or the P14-unrelated antigen ovalbumin (referred to as B16-OVA). To check, whether antigen-specificity was relevant for *Got1* expression, naïve or *in vitro* pre-activated P14 T cells were adoptively transferred to mice bearing B16-gp33 and -OVA tumors (**Figure 4.6 A** and **B**). The cells from the tumors were recovered and the expression between naïve, pre-activated, B16-gp33 derived TILs and B16-OVA derived TILs was compared. Naïve T cells expressed very low *Got1* mRNA levels, which were comparable to TILs from B16-OVA cells. In contrast, TILs which recognized their cognate antigen in the B16-gp33 tumors strongly upregulated *Got1* (**Figure 4.6 A**). Pre-activated TILs expressed *Got1*, and similar expression levels were sustained in B16-gp33 TILs. In contrast, *Got1* levels were significantly reduced in cells recovered from B16-OVA tumors. These results indicated, that *Got1* expression was antigen-dependent, also in tumor-reactive T cells.

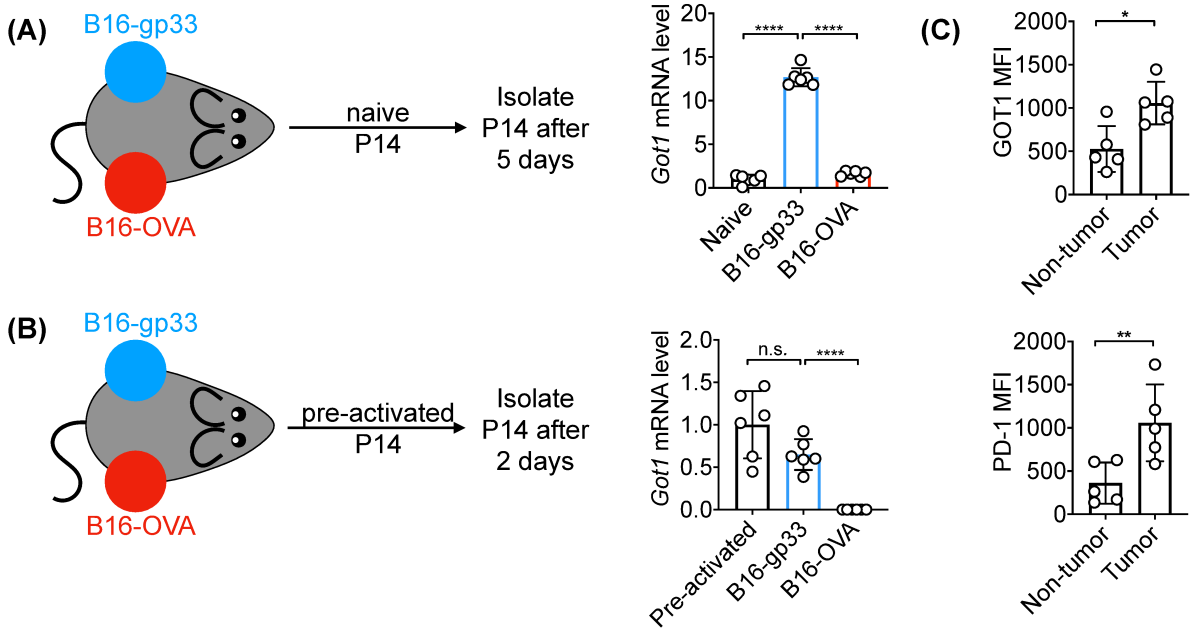

Figure 4.6: Got1 is expressed in antigen-specific TILs. *A: qRT-PCR analysis of TILs recovered from B16-gp33 or -OVA tumors after adoptive transfer of naïve P14 cells (± SD). B: qPCR analysis of TILs recovered from B16-gp33 or -OVA tumors after adoptive transfer of in vitro pre-activated P14 cells (± SD). C: MFI from GOT1 or PD-1 in TILs from human colon cancer tissue or T cells from non-tumor adjacent tissue (± SD). n.s. = p>0.05; * = p<0.05; ** = p<0.01; **** = p<0.0001. P values were calculated using two-tailed unpaired Student's t-tests.*

To investigate if GOT1 expression was also relevant in human diseases, we obtained human colon cancer samples and non-tumor adjacent healthy tissue and recovered the lymphocytes from these tissues. The mean fluorescence intensity (MFI) of GOT1 was significantly increased in TILs compared to T cells from healthy tissue. This increase correlated with the expression

of PD-1, which is known to be upregulated in many human cancers. Therefore, GOT1 was also a marker of activated TILs in humans.

4.5. GOT1 is required for effector cell differentiation, but not for memory formation after acute viral infections

The immune characterization in 4.2 revealed, the absence of GOT1 in T cells did not alter the formation or the activation state of naïve T cell subsets. Therefore, we challenged the mice with different viral infections to induce an acute infection (LCMV Arm), which can be cleared within 8 days, or a chronic (LCMV cl-13) infection, that induced T cell exhaustion.

Surprisingly, the $Got1^{flox/flox}Cd4\text{-}cre^{+}$ mice were able to handle the infections equally to wildtype littermates and did not display obvious phenotypes (data not shown).
To investigate the $CD8^{+}$ T cell intrinsic role of GOT1, and to minimize the potential influence of loss of *Got1* in other T cell subsets, we performed co-adoptive transfer experiments and transferred a 1:1 ratio of naïve P14 wildtype or *Got1*-deficient T cells with mismatched congenic markers (based on the expression of CD45.1 and CD45.2) on wildtype C57BL/6 mice. The mice were challenged with LCMV Arm and sacrificed 8 dpi. The spleens were harvested, and the donor cell phenotypes were investigated by flow cytometry (**Figure 4.7**).
A significant increase in the ratio between wildtype and *Got1*-deficient T cells was observed after infection (**Figure 4.7 B**), indicating a problem with the survival or proliferation of *Got1*-deficient T cells. We profiled the capabilities of wildtype and *Got1*-deficient T cells to form short lived effector cells (SLEC) and memory precursor effector cells (MPEC), based on the expression of CD62L, KLRG1 and CD44 [206]. Both cell types were able to form SLECs and MPECs to a similar extend (**Figure 4.7 C** and **E**). Furthermore, wildtype and *Got1*-deficient T cells expressed similar levels of key transcription factors for T cell differentiation (e.g. T-BET, EOMES or TCF1). The cytokine release of T cells, which were re-stimulated with gp33 in the presence of BFA was investigated and *Got1*-deficient T cells accumulated significantly lower levels of effector molecules TNFα and IFNγ (**Figure 4.7 D** and **E**).

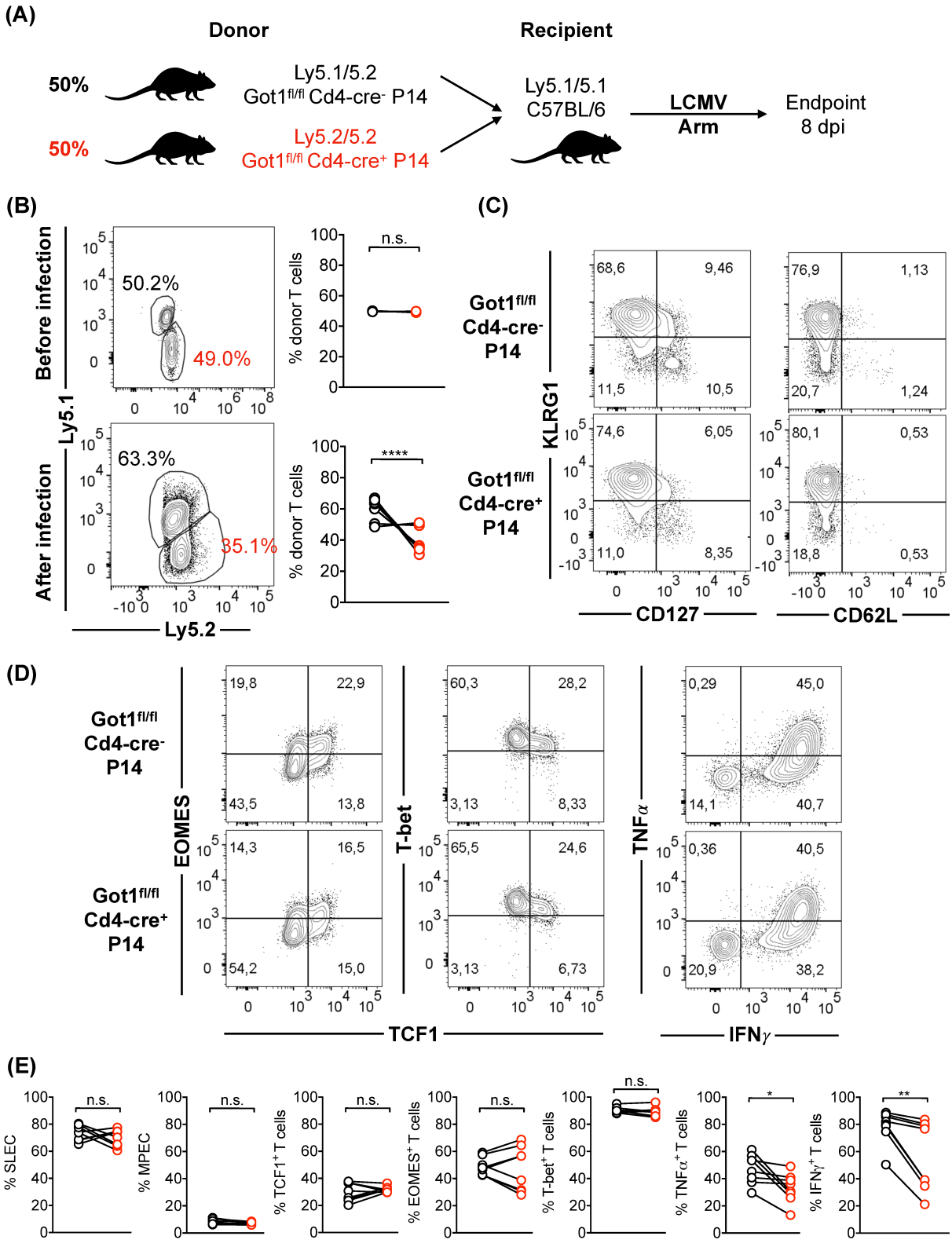

Figure 4.7: Got1 is required for effector cell responses following LCMV Arm infection. *A: Wildtype and Got1-deficient P14 cells (1:1 ratio) were transferred to wildtype mice, infected with LCMV Arm and samples were analyzed 8 dpi. B: Representative FACS plots and quantification of cell ratios before and after viral challenge. C: Representative FACS plots for memory and effector cell markers. D: Representative FACS plots for transcription factors and cytokine secretion. E: Quantification of selected markers in wildtype and Got1-deficient cells. Experiment was performed twice with 8 pairs of mice in total. n.s. = p>0.05; * = p<0.05; ** = p<0.01. P values were calculated by two-tailed paired Student's t-tests.*

These results indicated, GOT1 was dispensable for the differentiation, but indispensable for the maintenance of effector cells during an acute viral infection. Loss of *Got1* correlated with a drastically reduced expression of inflammatory and effector cytokines.

In addition to 8 days after acute Arm infection, a later time point after infection was investigated, when the antigen was already cleared, and the T cells were undergoing memory differentiation (30 dpi). Interestingly, the ratio of wildtype and *Got1*-deficient cells was no longer significantly changed after infection, even though a trend towards lower cell numbers was still visible (**Figure 4.8 B**). Similar to 8 dpi, there was no difference in the expression of effector cell markers and memory formation was not impaired in the absence of GOT1 (**Figure 4.8 C** and **E**). Also, the expression of transcription factors was comparable between wildtype and *Got1*-deficient T cells. However, similar to our previous observations, the loss of GOT1 resulted in significantly reduced expression of effector molecules TNFα and IFNγ (**Figure 4.8 D** and **E**).

Taken together, these results indicated that GOT1 contributed to cell persistence and effector function during viral infections, and its function seemed to be especially relevant as long as the cognate antigen was present. Thus, we were interested in investigating an infection scenario with long term antigen persistence.

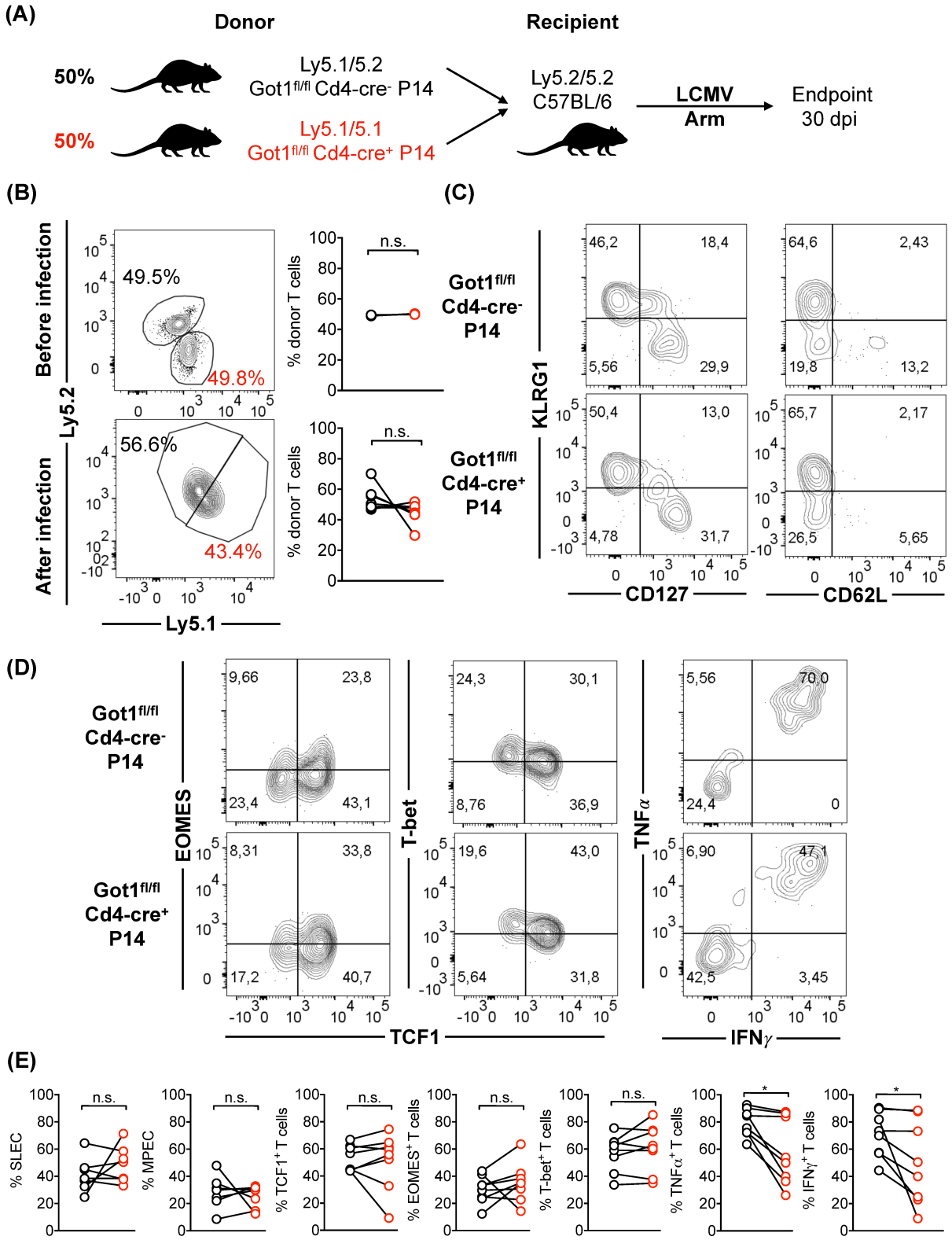

Figure 4.8: Got1 is not required for memory formation following LCMV Arm infection. *A: Wildtype and Got1-deficient P14 cells (1:1 ratio) were transferred on wildtype mice, infected with LCMV Arm and samples were analyzed 30 dpi. B: Representative FACS plots and quantification of cell ratios before and after viral challenge. C: Representative FACS plots for memory and effector cell markers. D: Representative FACS plots for transcription factors and cytokine secretion. E: Quantification of selected markers in wildtype and Got1-deficient cells. Experiment was performed twice with 7 pairs of mice in total. n.s. = p>0.05; * = p<0.05. P values were calculated by two-tailed paired Student's t-tests.*

4.6. GOT1 is required for the persistence of exhausted T cells after chronic viral infections

Inspired by the results obtained from the experiments following an acute viral infection described in 4.4, we compared the T cell response following chronic viral infection, which results in T cell exhaustion, in a similar experimental approach: We transferred a 1:1 ratio of naïve P14 wildtype or *Got1*-deficient T cells with mismatched congenic markers (CD45.1 or CD45.2) on wildtype C57BL/6 mice. We challenged the mice with LCMV cl-13, depleted $CD4^+$ T cells and sacrificed the mice 8 dpi.

Similar to the observations after infection with LCMV Arm, at 8 dpi following LCMV cl-13 infection, the number of *Got1*-deficient T cells was significantly reduced (**Figure 4.9 B**). We investigated the expression of inhibitory receptors PD-1 and TIGIT, as indicators for the development of T cell exhaustion and found a significant decrease of the expression of these inhibitory receptors (**Figure 4.9 C** and **E**). The expression of inhibitory receptors is commonly correlated with reduced effector function. Intriguingly, the observed reduced expression of inhibitory receptors did not improve the expression of effector cytokines. Similar to our previous observations following Arm infections, *Got1*-deficient T cells expressed significantly lower levels of TNFα and IFNγ (**Figure 4.9 D** and **E**) after re-stimulation with gp33 in the presence of BFA.

Surprisingly, a significant reduction of the expression of EOMES and TCF1 was detected (**Figure 4.9 D** and **E**). The combined expression of these transcription factors is associated with a stem cell-like T cell population that mediates the effector response during T cell exhaustion [145, 147]. Conversely to the decreased expression of EOMES, the expression of T-BET was significantly upregulated.

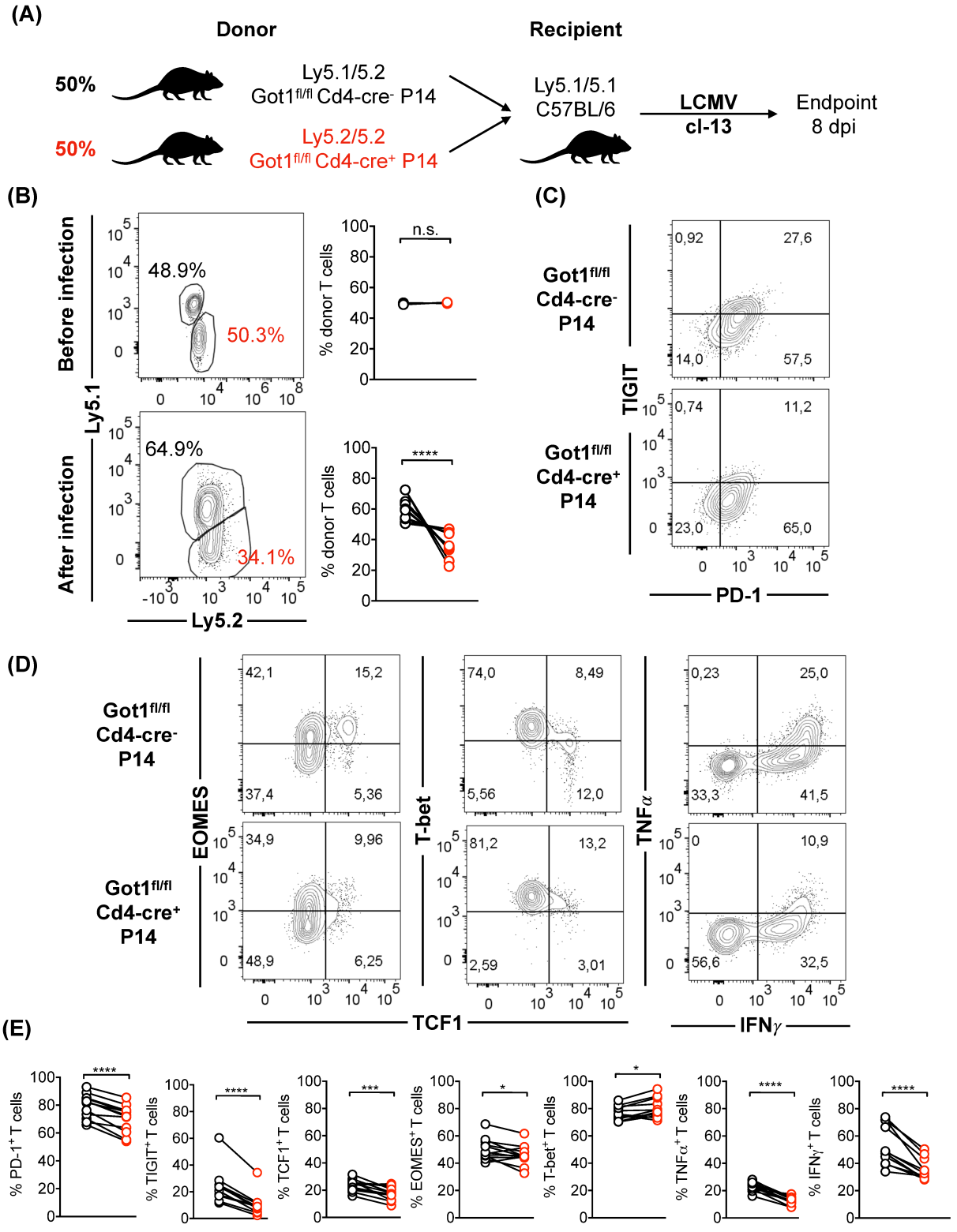

Figure 4.9: Got1 is required for effector cell responses following LCMV cl-13 infection. *A: Wildtype and Got1-deficient P14 cells (1:1 ratio) were transferred on wildtype mice, infected with LCMV cl-13 and samples were analyzed 8 dpi. B: Representative FACS plots and quantification of cell ratios before and after viral challenge. C: Representative FACS plots for inhibitory receptors. D: Representative FACS plots for transcription factors and cytokine secretion. E: Quantification of selected markers in wildtype and Got1-deficient cells. Experiment was performed twice with 12 pairs of mice in total. n.s. = p>0.05; * = p<0.05; *** = p<0.001; **** = p<0.0001. P values were calculated by two-tailed paired Student's t-tests.*

These results indicated, that also after cl-13 infection, GOT1 was required for the maintenance and effector function of the transferred T cells. The dysregulation of transcription factors suggested a decrease in the stem cell-like T cell pool that is required for the long-term residual immune response during a chronic viral infection. Thus, the T cell phenotype was investigated at a later time point after cl-13 infection (21 dpi), when the exhaustion of the adoptively transferred T cells progressed. Compared to 8 dpi, the reduction of cell numbers of *Got1*-deficient T cells after infection was further exacerbated (**Figure 4.10 B**). This was different from the observation at 30 dpi with Arm, and further supported the theory that antigen persistence correlated with the severity of GOT1-associated phenotypes.

Surprisingly, after 21 dpi, cells now expressed similar levels of the exhaustion marker PD-1. TIGIT was still significantly downregulated in *Got1*-deficient cells (**Figure 4.10 C** and **E**). TCF1 expression was significantly decreased in *Got1*-deficient T cells, however EOMES levels were found to be comparable at 21 dpi. T-BET expression was significantly elevated, consistent with our observations after 8 dpi. Still, *Got1*-deficient T cells expressed significantly lower levels of effector cytokines TNFα and IFNγ after re-stimulation (**Figure 4.10 D** and **E**).
Based on the data obtained from the chronic viral infection models, we concluded that GOT1 was required to sustain the pool of long-lived stem cell-like T cells, to mediate the long-term residual immune response during the progression of T cell exhaustion. Furthermore, GOT1 promoted the expression of inhibitory receptors in this context. Surprisingly, the dysregulation of inhibitory receptors was uncoupled from the expression of effector cytokines.

Taking the results from the acute viral infection with Arm into account, we reasoned that GOT1 was required to sustain a $CD8^+$ T cell immune response during acute and chronic viral infection, and absence of GOT1 prevented the accumulation of effector cells and impaired effector function in both investigated infection models.

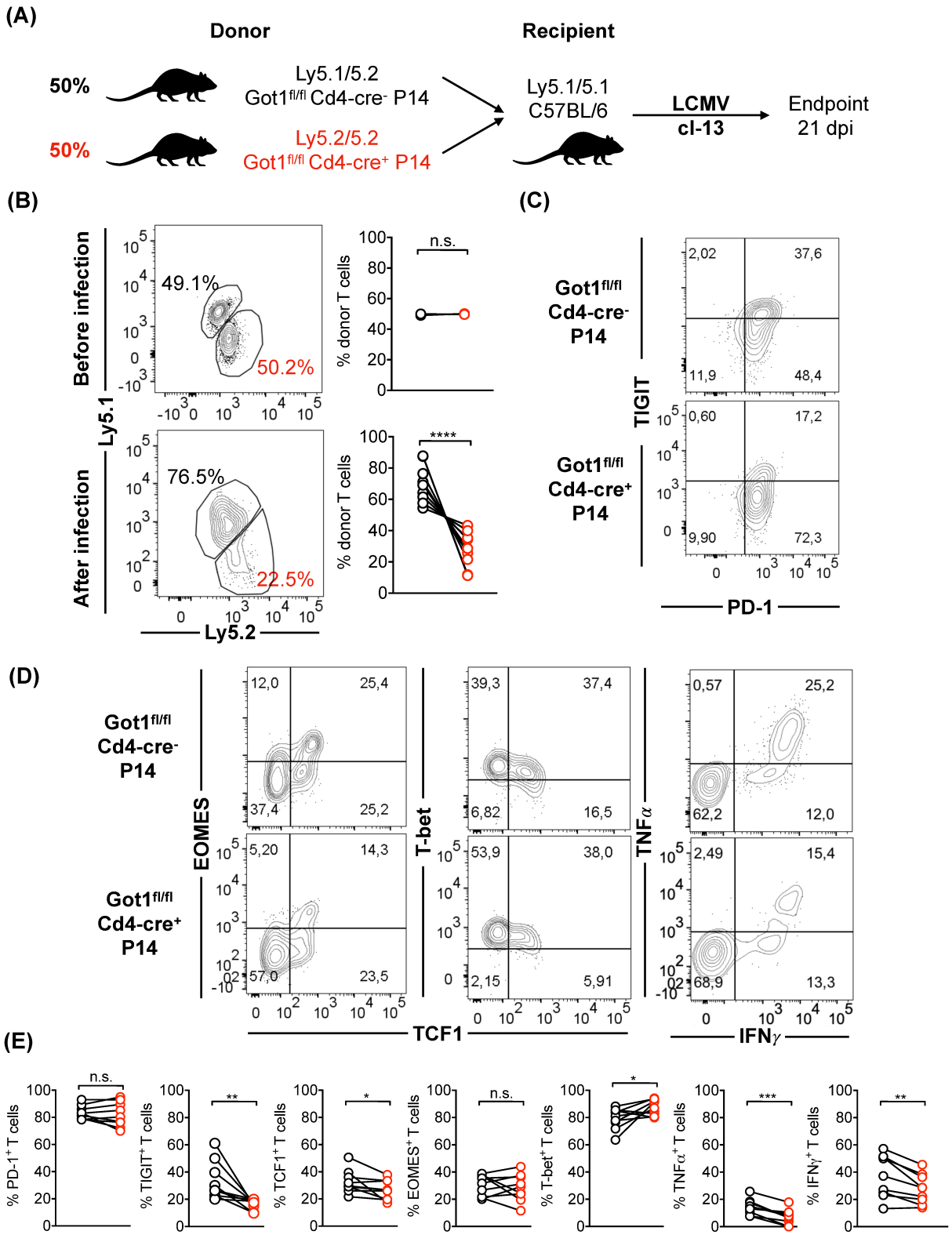

Figure 4.10: Got1 is required for chronic infection with LCMV cl-13. *A: Wildtype and Got1-deficient P14 cells (1:1 ratio) were transferred on wildtype mice, infected with LCMV cl-13 and samples were analyzed 21 dpi. B: Representative FACS plots and quantification of cell ratios before and after viral challenge. C: Representative FACS plots for inhibitory receptors. D: Representative FACS plots for transcription factors and cytokine secretion. E: Quantification of selected markers in wildtype and Got1-deficient cells. Experiment was performed twice with 9 pairs of mice in total. n.s. = p>0.05; * = p<0.05; ** = p<0.01; *** = p<0.001. P values were calculated by two-tailed paired Student's t-tests.*

T cell exhaustion is also frequently observed during tumor progression, and results in loss of effector function and apoptosis of TILs. Thus, T cell exhaustion correlates with a bad prognosis for the patients. Therefore, we expanded the investigation of GOT1 beyond antiviral effector responses and performed adoptive transfer experiments on tumor bearing mice.

4.7. GOT1 is required for antigen-specific anti-tumor T cell responses

We investigated the influence of GOT1 on antitumoral T cell responses in two different melanoma tumor models (B16-gp33 and YUMM-gp33), which both expressed the LCMV antigen gp33. Therefore, the tumor cells could be recognized by P14 T cells. We performed co-adoptive transfer experiments with *in vitro* activated cells on tumor bearing mice, following a similar approach to 4.4. Additionally, we compared the anti-tumor response in single-adoptive transfer experiments, in which wildtype and *Got1*-deficient T cells were separately transferred on tumor bearing mice.

$3x10^5$ wildtype or *Got1*-deficient P14 T cells were transferred on mice which were previously implanted with B16-gp33 tumors, when the tumors were palpable, and the tumor growth was monitored. Mice which received *Got1*-deficient T cells developed bigger tumors compared to mice inoculated with wildtype P14 cells (**Figure 4.11)**, indicating a problem with the antitumoral immune response.

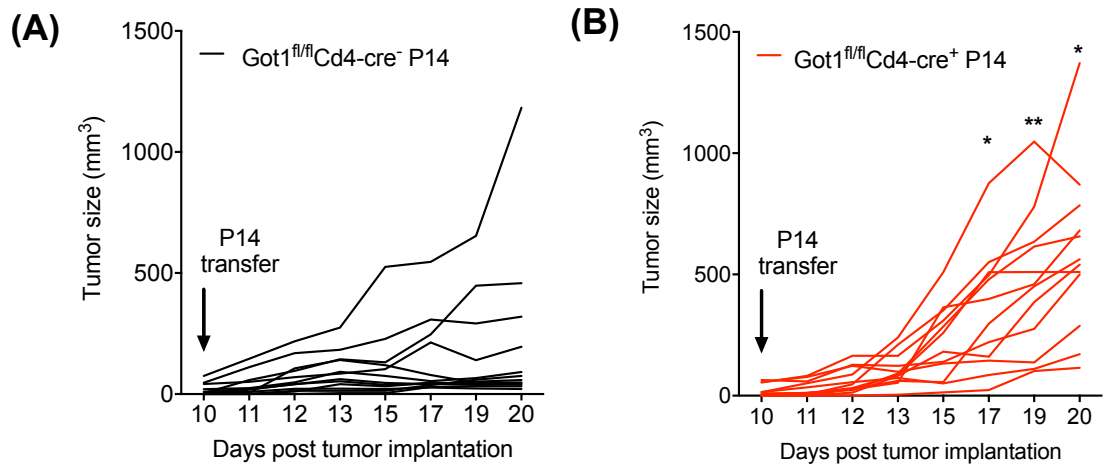

Figure 4.11: Got1 deficiency correlates with tumor growth. *Tumor growth of B16-gp33 melanoma cells after adoptive transfer of in vitro activated wildtype (A) P14 cells or Got1-deficient (B) P14 cells. P14 cell transfer is indicated by an arrow. Experiment was performed twice with 12 pairs of mice. * = p<0.05; ** = p<0.01. P values were calculated by two-tailed unpaired Student's t-tests.*

After purification of the T cells from these mice, we realized that we could only recover very few donor T cells from spleen or tumor respectively. The donor cells were probably rejected over time from the recipient animals during tumor progression. Thus, to investigate the phenotypes of the donor T cells during antitumoral responses, larger numbers ($1x10^6$) of donor cells were transferred to tumor bearing mice, and the mice were sacrificed before the differences of tumor sizes became apparent (ca. 4 days after adoptive transfer, **Figure 4.12 A)**. Furthermore, this strategy allowed to study the T cell intrinsic changes, independently from external influences like hypoxia, due to differences in tumor size (which only became apparent later after adoptive transfer), and we were able to recover sufficient cell numbers for subsequent analysis.

Tumor-associated cytotoxic T cells become exhausted during tumor progression and are characterized by the upregulation of inhibitory surface receptors and the loss of effector functions. Thus, we studied the T cell phenotype of recovered donor cells in the tumor and the spleen respectively, to compare the exhausted TILs to their non-exhausted splenic counterparts. We investigated the exhaustion state, key transcription factors and the ability of the recovered cells to secrete effector cytokines after *in vitro* re-stimulation with the cognate peptide gp33 in the presence of BFA.

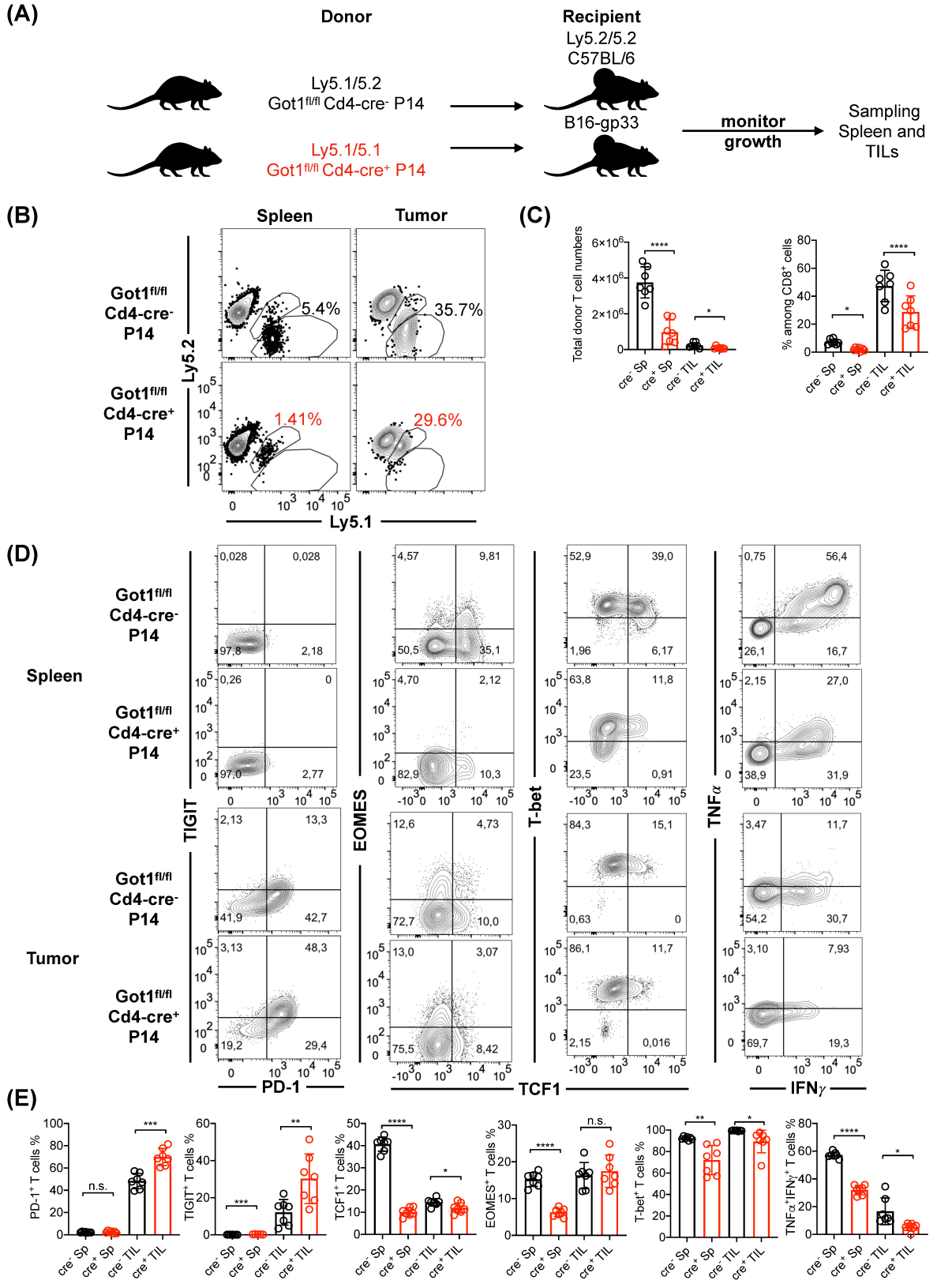

Figure 4.12: Got1 deficiency exacerbated exhaustion of donor TILs in B16-gp33 tumors. *A: Schematic experimental approach of the single transfer. B: Representative FACS blots of wildtype and Got1-deficent donor cells. C: Quantification of wildtype and Got1-deficent donor cells in spleen and TILs. D: Representative FACS blots of inhibitory receptors, transcription factors and cytokines in recovered donor cells. E: Quantification of selected markers. Experiment was performed twice with 6 and 7 pairs of mice; one representative experiment is shown. n.s. = p>0.05; * = p<0.05; ** = p<0.01; *** = p<0.001; **** = p<0.0001. P values were calculated by two-tailed paired Student's t-tests.*

When we investigated the frequencies of donor cells among all infiltrating T cells, we discovered a significant decrease in the abundance on *Got1*-deficient T cells and recovered significantly lower cell numbers in spleen and tumor tissue (**Figure 4.12 B** and **C**). The expression of inhibitory surface receptors was investigated, and a significant increase in the expression of PD-1 and TIGIT in *Got1*-deficient TILs, compared to wildtype TILs, was discovered. TIGIT expression was also significantly increased in splenic *Got1*-deficient T cells (**Figure 4.12 D** and **E**), even though the total expression of TIGIT or PD-1 was much lower compared to TILs, since the splenic T cells were not exhausted. The increased expression of exhaustion markers was a remarkable difference compared to the results we obtained after investigating the exhaustion state during chronic viral infection in 4.6, where loss of *Got1* resulted in the downregulation of inhibitory receptors. The analysis of transcription factor expression revealed a significant loss of TCF1 expression in *Got1*-deficient TILs, which was even more dramatic in the splenic counterparts. EOMES and T-BET protein levels were also significantly decreased in *Got1*-deficient T cells from the spleen, while EOMES levels were unchanged in TILs (**Figure 4.12 D** and **E**). This was again different from previous data obtained after chronic viral infection: even though TCF1 and EOMES levels were decreased after LCMV cl-13 infection, there was an upregulation of T-BET in *Got1*-deficient T cells (4.6). Consistent with previous findings (4.4 and 4.6), after *in vitro* re-stimulation with antigen, *Got1*-deficient cells expressed significantly lower levels of TNFα and IFNγ (**Figure 4.12 D** and **E**) in spleen and tumor. Similar to the expression of inhibitory receptors, splenic (less-exhausted) cells expressed overall higher cytokine levels compared to TILs.

Simultaneously to these single transfer experiments, we performed co-adoptive transfer experiments, and transferred similar numbers of wildtype and *Got1*-deficient T cells together on tumor bearing mice (**Figure 4.13 A**).
The results obtained from the co-adoptive transfer experiments correlated well with the results following the separate cell transfers shown above. A significant decrease in the frequency of *Got1*-deficient T cells in spleen and TILs, compared to wildtype donor cells, was discovered. Even though the absolute numbers of recovered donor cells from the tumors did not reach statistical significance, there was a trend toward lower absolute *Got1*-deficient T cell numbers (**Figure 4.13 B** and **C**).

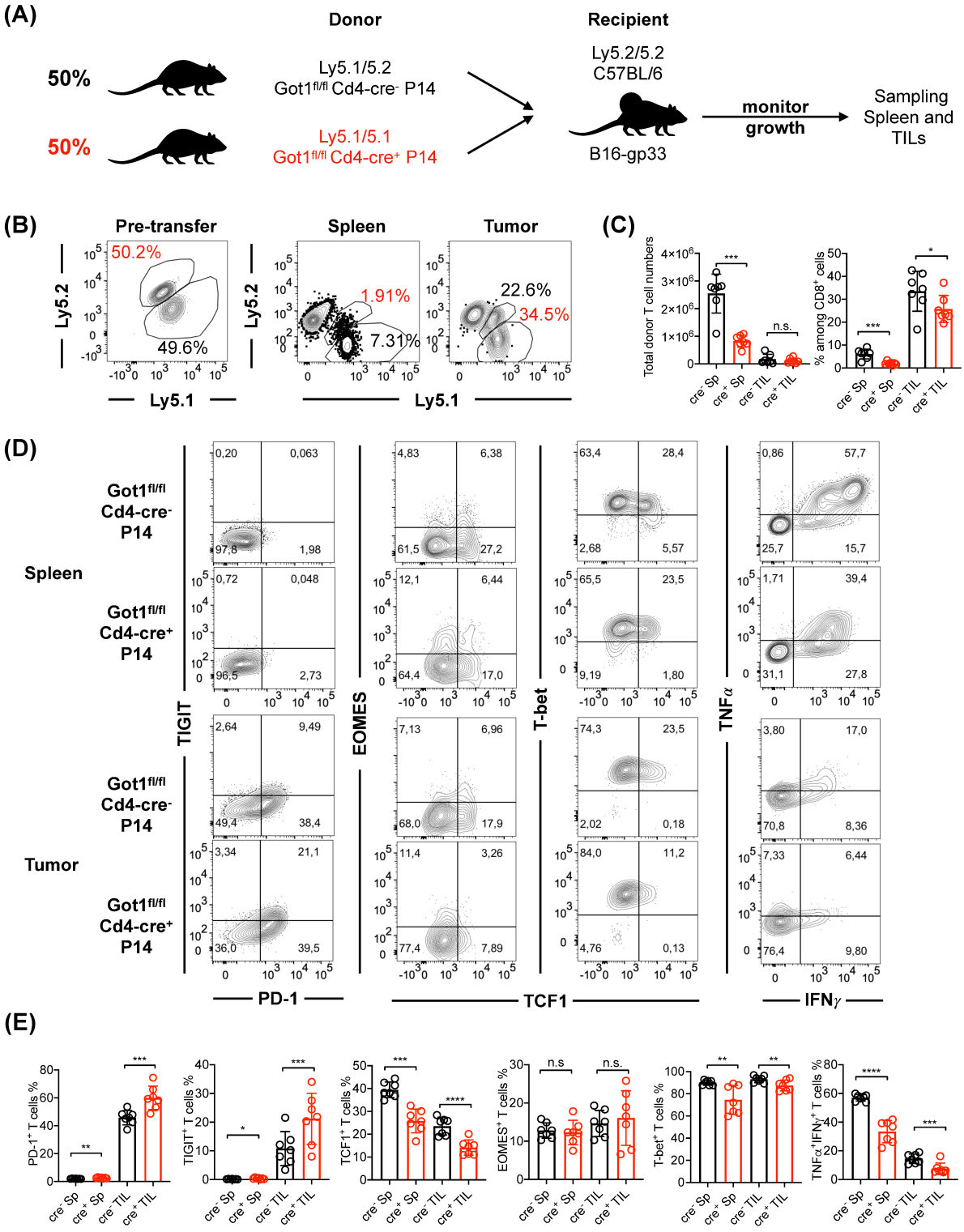

Figure 4.13: Got1-deficiency exacerbated exhaustion of co-transferred donor TILs in B16-gp33 tumors. *A: Schematic experimental approach of the co-transfer. B: Representative FACS blots of wildtype and Got1-deficent donor cells. C: Quantification of wildtype and Got1-deficent donor cells in spleen and TILs. D: Representative FACS blots of inhibitory receptors, transcription factors and cytokines in recovered donor cells. E: Quantification of selected markers. Experiment was performed twice with 6 and 7 pairs of mice; one representative experiment is shown. n.s. = p>0.05; * = p<0.05; ** = p<0.01; *** = p<0.001; **** = p<0.0001. P values were calculated by two-tailed paired Student's t-tests.*

The analysis of the donor T cells concerning exhaustion state and transcription factors (**Figure 4.13 D** and **E**) yielded similar results to what we observed after single transfer experiments: here, *Got1*-deficient T cells expressed significantly higher levels of PD-1 and TIGIT in TILs and splenic T cells. TCF1 and T-BET levels were again significantly decreased in both investigated organs. However, EOMES expression was similar between wildtype and *Got1*-deficient T cells in this experiment. Consistent to our previous findings, the expression of cytotoxic molecules was significantly reduced in *Got1*-deficient T cells from spleen and tumors.
The overall results obtained from adoptive transfer experiments on B16-gp33 tumor-bearing mice revealed a problem of *Got1*-deficient T cells to produce long-term persistent antitumoral T cells with residual effector function and indicated that *Got1*-deficient TILs were more exhausted compared to their wildtype counterparts.

Simultaneous to the B16-gp33 experiments shown above, we performed similar experiments using the YUMM-gp33 tumor model, to confirm that the phenotypes shown above were conserved for antitumoral immune responses.
YUMM-gp33 tumors turned out to be far more aggressive and grew almost twice as fast compared to B16-gp33. YUMM tumors have previously been reported to be immunologically “cold” tumors with limited lymphocyte infiltration [207], which could explain the fast growth kinetics. Therefore, YUMM-gp33 tumor bearing mice were sacrificed shortly after adoptive transfer, and no long-term tumor growth as in **Figure 4.11** could be monitored. However, purified TILs showed similar traits compared to TILs recovered from B16-gp33 tumors.

After single transfer of wildtype or *Got1*-deficient P14 cells (**Figure 4.14 A**), we recovered significantly lower numbers of donor cells from spleen and TILs, and the percentage of *Got1*-deficient cells among all $CD8^+$ T cells was significantly reduced in spleen and tumors (**Figure 4.14 B** and **C**). *Got1*-deficient T cells expressed higher levels of TIGIT (significant in spleen), however there was only a trend towards higher PD-1 levels after single adoptive transfer. TCF1 and EOMES expression in splenic donor cells was strongly reduced, while it was not significantly changed in TILs. T-BET expression was significantly reduced in wildtype and *Got1*-deficient P14 cells from spleen and tumors (**Figure 4.14 D** and **E**). Cytokine secretion (TNFα and IFNγ) was also significantly decreased in *Got1*-deficient splenocytes and TILs.

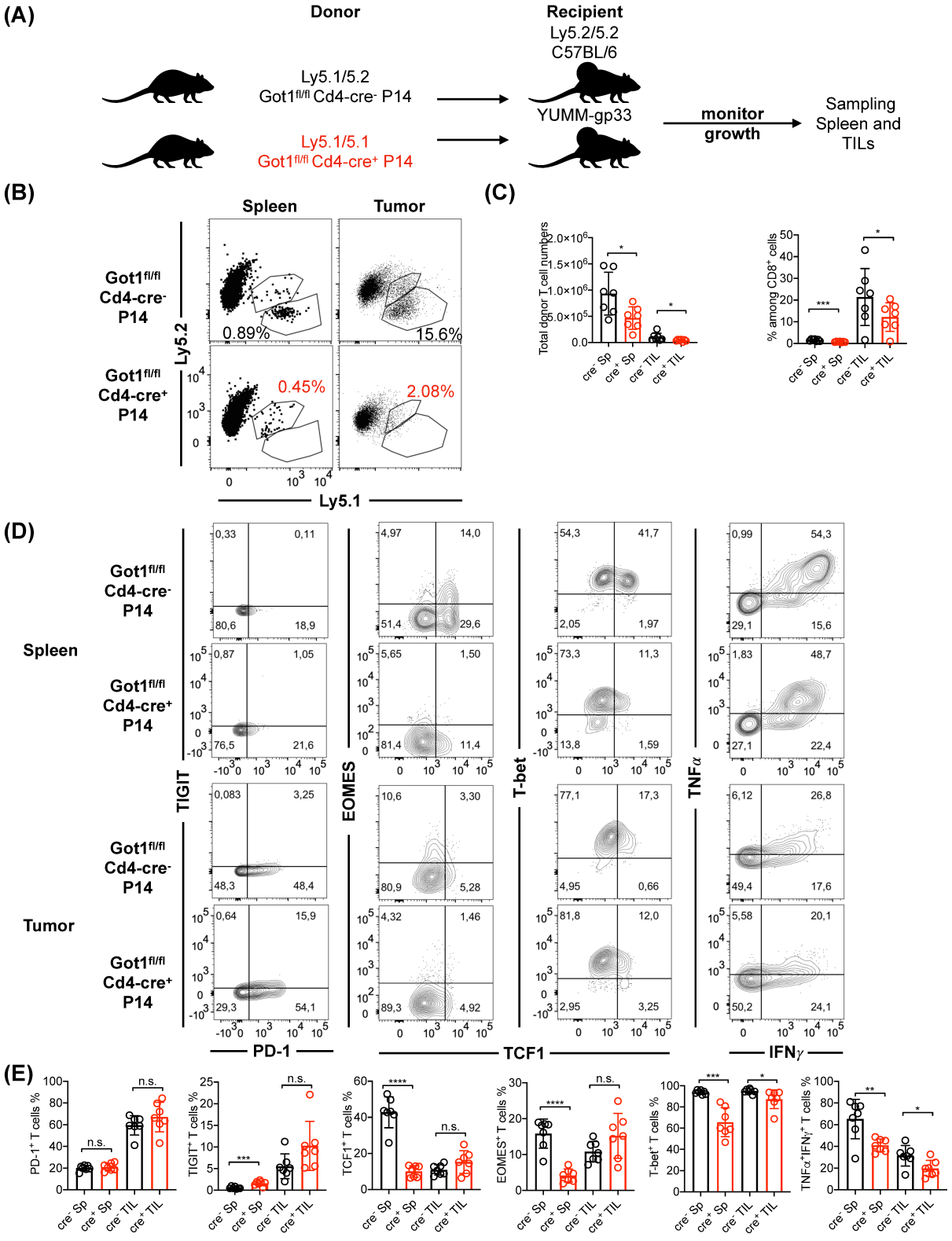

Figure 4.14: Got1-deficiency exacerbated exhaustion of donor TILs in YUMM-gp33 tumors. *A: Schematic experimental approach of the single transfer. B: Representative FACS blots of wildtype and Got1-deficent donor cells. C: Quantification of wildtype and Got1-deficent donor cells in spleen and TILs. D: Representative FACS blots of inhibitory receptors, transcription factors and cytokines in recovered donor cells. E: Quantification of selected markers. Experiment was performed twice with 6 and 7 pairs of mice; one representative experiment is shown. n.s. = p>0.05; * = p<0.05; ** = p<0.01; *** = p<0.001; **** = p<0.0001. P values were calculated by two-tailed paired Student's t-tests.*

Similar results were obtained, when TILs recovered after co-adoptive transfer on YUMM-gp33 bearing mice were investigated. We recovered significantly lower numbers of *Got1*-deficient donor cells in spleen and tumor. In this experiment, PD-1 and TIGIT levels were significantly increased in *Got1*-deficient donor cells from spleen and TILs. Cytokine secretion in splenic *Got1*-deficient T cells was significantly reduced, while in TILs the cytokine expression was not significantly downregulated in this experiment (**Figure 4.15 D** and **E**).

Our experimental results of the antitumoral immune response of *Got1*-deficient T cells after the experiments shown above led to the conclusion, that *Got1*-deficient T cells failed to produce long-term functional antitumoral T cells, which led to enhanced tumor growth. We were wondering about the cell-intrinsic changes of the T cells that led to this loss of effector potential and thus moved on to study metabolic changes caused by deletion of *Got1.* Since it was difficult to obtain enough T cells from tumors for further metabolic analysis, and sorting of the T cell by fluorescent activated cell sorting was previously shown to significantly impact the metabolic status of T cells [208], we decided to purify T cells from the spleens of virally infected mice for our metabolic studies.

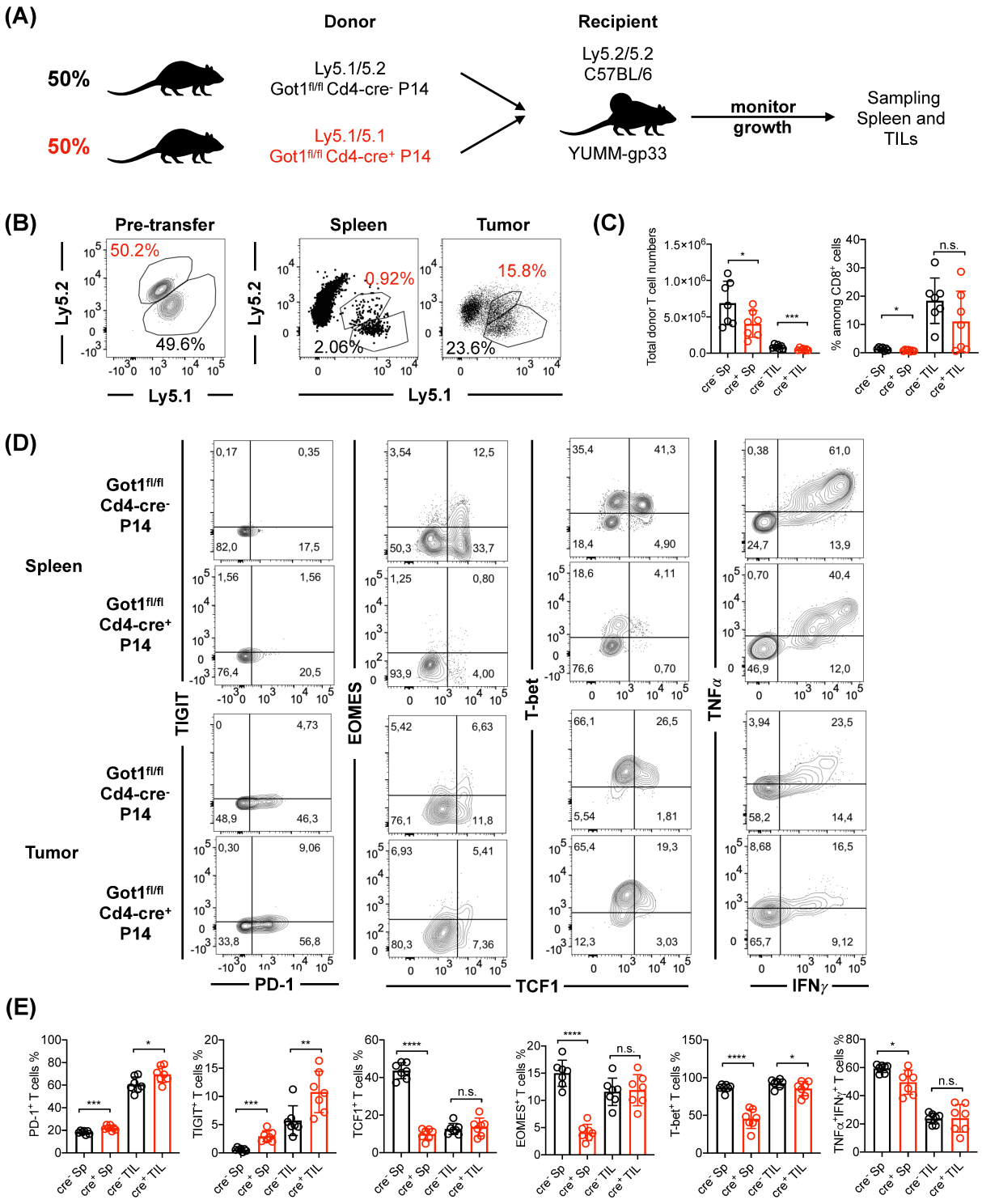

Figure 4.15: Got1-deficiency exacerbated exhaustion of co-transferred donor TILs in YUMM-gp33 tumors. *A: Schematic experimental approach of the co-transfer. B: Representative FACS blots of wildtype and Got1-deficent donor cells. C: Quantification of wildtype and Got1-deficent donor cells in spleen and TILs. D: Representative FACS blots of inhibitory receptors, transcription factors and cytokines in recovered donor cells. E: Quantification of selected markers. Experiment was performed twice with 6 and 7 pairs of mice; one representative experiment is shown. n.s. = p>0.05; * = p<0.05; ** = p<0.01; *** = p<0.001; **** = p<0.0001. P values were calculated by two-tailed paired Student's t-tests.*

4.8. *Got1*-deficient T cells show metabolic defects *in vivo* after viral infection

Since GOT1 and the MAS are converting intermediates of the TCA cycle, we investigated the abundance of TCA cycle metabolites in CD8$^+$ T cells purified with magnetic beads from the spleens of LCMV cl-13 or Arm infected mice. The abundance of organic acids was determined by mass spectrometry (MS) (**Figure 4.16**).

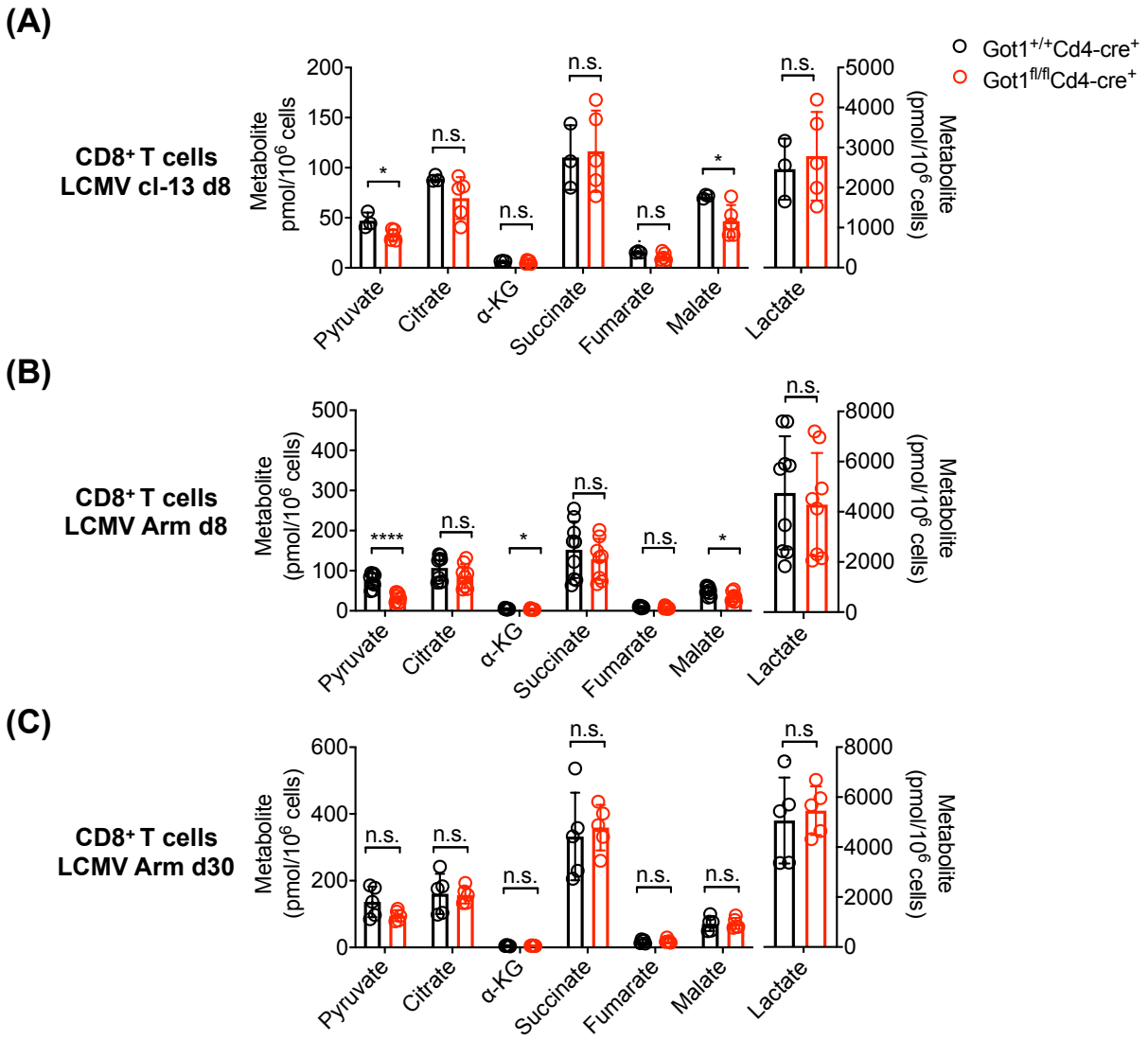

Figure 4.16: MS quantification revealed altered organic acid levels in Got1-deficient CD8$^+$ T cells. *A: Samples obtained from T cells after LCMV cl-13 infection, 8 dpi. B: Samples obtained from T cells after LCMV Arm infection, 8 dpi C: Samples obtained from T cells after LCMV Arm infection, 30 dpi. Accumulated data from 2 experiments with 5-9 mice in total. n.s. = p>0.05; * = p<0.05; **** = p<0.0001. P values were calculated by two-tailed unpaired Student's t-tests.*

After infection with LCMV cl-13 (8 dpi), most TCA cycle metabolites were decreased in *Got1*-deficient T cells and the difference was significant for malate (**Figure 4.16 A**). Also, pyruvate levels were significantly reduced in *Got1*-deficient T cells, while lactate levels were comparable. Pyruvate is the end product of glycolysis and can feed the TCA cycle in form of

acetyl-CoA or, can be converted to OAA to feed the TCA cycle [209]. During aerobic glycolysis, pyruvate is converted into lactate and secreted from the cell.
Similar results were obtained when we investigated infection with LCMV Arm (8 dpi). Again, most TCA cycle metabolites were decreased in *Got1*-deficient T cells and the difference was significant for malate and α-KG (**Figure 4.16 B**). Similar to cl-13 infection, pyruvate levels were significantly reduced in *Got1*-deficient T cells, while lactate levels remained unchanged. Interestingly, the observed changes were lost at 30 dpi (**Figure 4.16 C**), consistent with the loss of most GOT1-associated phenotypes observed at 30 dpi in 4.4.

The reduced abundance of TCA cycle metabolites and TCA anaplerotic sources implicated, that *Got1*-deficient T cells had problems to maintain normal levels of TCA metabolites, resulting in the depletion of TCA intermediates. The ratio of NAD^+ and NADH is an important read-out for the metabolic fitness of cells, and is tightly connected to key metabolic pathways, for example glycolysis and TCA cycle, which consume NAD^+ to produce NADH for OXPHOS. Also, the MAS is involved in the electron transport from NADH into the mitochondria. Thus, we reasoned that an altered TCA composition and defects in the MAS caused by deletion of GOT1 might be accompanied by a change in the ratio of NAD^+ and NADH. Indeed, we observed significantly increased levels of NADH, resulting in a significantly decreased ratio of NAD^+/NADH in *Got1*-deficient T cells (**Figure 4.17)**, that were obtained from the same experiments as **Figure 4.16**. Consistent to previous observations, this change was significant only at 8 dpi, but the ratio was not significantly changed at 30 dpi.

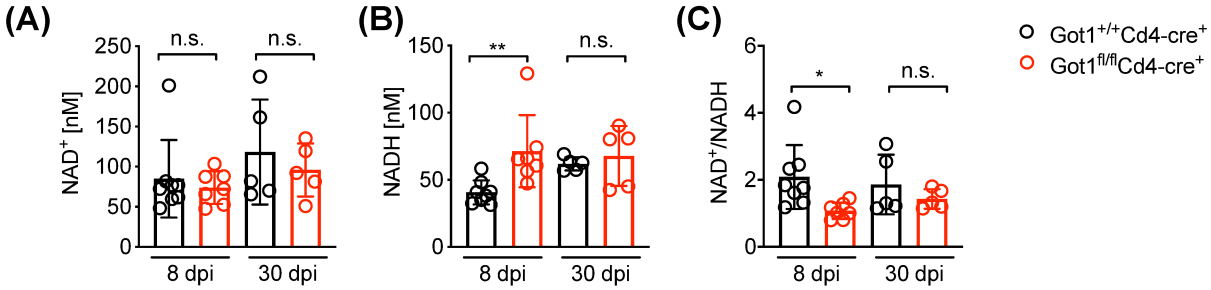

Figure 4.17: Changes of NAD⁺ and NADH levels in wildtype and Got1-deficient CD8⁺ T cells. *A: NAD^+ levels measured in $CD8^+$ T cells after LCMV Arm infection, 8 and 30 dpi. B: NADH levels measured in $CD8^+$ T cells after LCMV Arm infection, 8 and 30 dpi. C: NAD^+/NADH levels calculated from A and B. Accumulated data from 2 experiments with 5-8 mice in total. n.s. = p>0.05; * = p<0.05; ** = p<0.01. P values were calculated by two-tailed unpaired Student's t-tests.*

Inspired by these results and the aforementioned altered TCA cycle profile, we wondered if the loss of *Got1* would influence intracellular nutrient utilization.

4.9. The loss of GOT1 does not impair the utilization of extracellular nutrients

We expected that the loss of GOT1 would impair the T cells to incorporate upstream metabolites that feed into cellular metabolism. Thus, we *in vitro* activated wildtype and *Got1*-deficient T cells and labelled them with metabolites, where all carbons were exchanged with non-radioactive stable carbon-13 isotopes (^{13}C).
The cells were pulsed with D-Glucose-$^{13}C_6$, L-Glutamine-$^{13}C_5$ or Na-Lactate-$^{13}C_3$ and the incorporation of the ^{13}C label into downstream metabolites was followed using MS (**Figure 4.18 A**). Surprisingly, there were no striking differences in the label propagation between both cell types in the described experiments (**Figure 4.18 B**). These findings were counterintuitive, given the observed changes in the abundance of organic acids in *in vivo* activated cells (4.8.).

The shown graphs in **Figure 4.18 B** display the proportion of the label: m+0 reflects the unlabeled metabolite and the increasing integer reflects how many carbon atoms were exchanged for ^{13}C. Both cell types were able to incorporate the tracers to comparable amounts, with only subtle differences. For example, we observed the trend towards increased m+3 label frequency in α-KG from L-Glutamine-$^{13}C_5$, indicating a slightly higher dependency on glutamine to the α-KG pool in the *Got1*-deficient cells. The uptake of glutamine was similar between both cell types, but *Got1*-deficient cells displayed a small but significant ($p<0.05$) drop in the glutamic acid pool and, after a D-Glucose-$^{13}C_6$ pulse, showed a small but significant ($p<0.05$) increase of m+2 glutamine, which may be derived from α-KG (**Figure 4.18 A,** D-Glucose-$^{13}C_6$ flux).
We also profiled the label-integration into other proteinogenic amino acids (**Supplementary Figure 1**) and found no differences between wildtype and *Got1*-deficient T cells.

We reasoned that, at least under the used *in vitro* culture approach, *Got1*-deficient T cells were able to take up and utilize exogenous metabolites similarly to their wildtype counterparts, indicating the overall metabolic flux of the cells was intact. We simultaneously assessed potential influence on the electron transport in the ETC and the coupling between the ETC and OXPHOS for energy production.

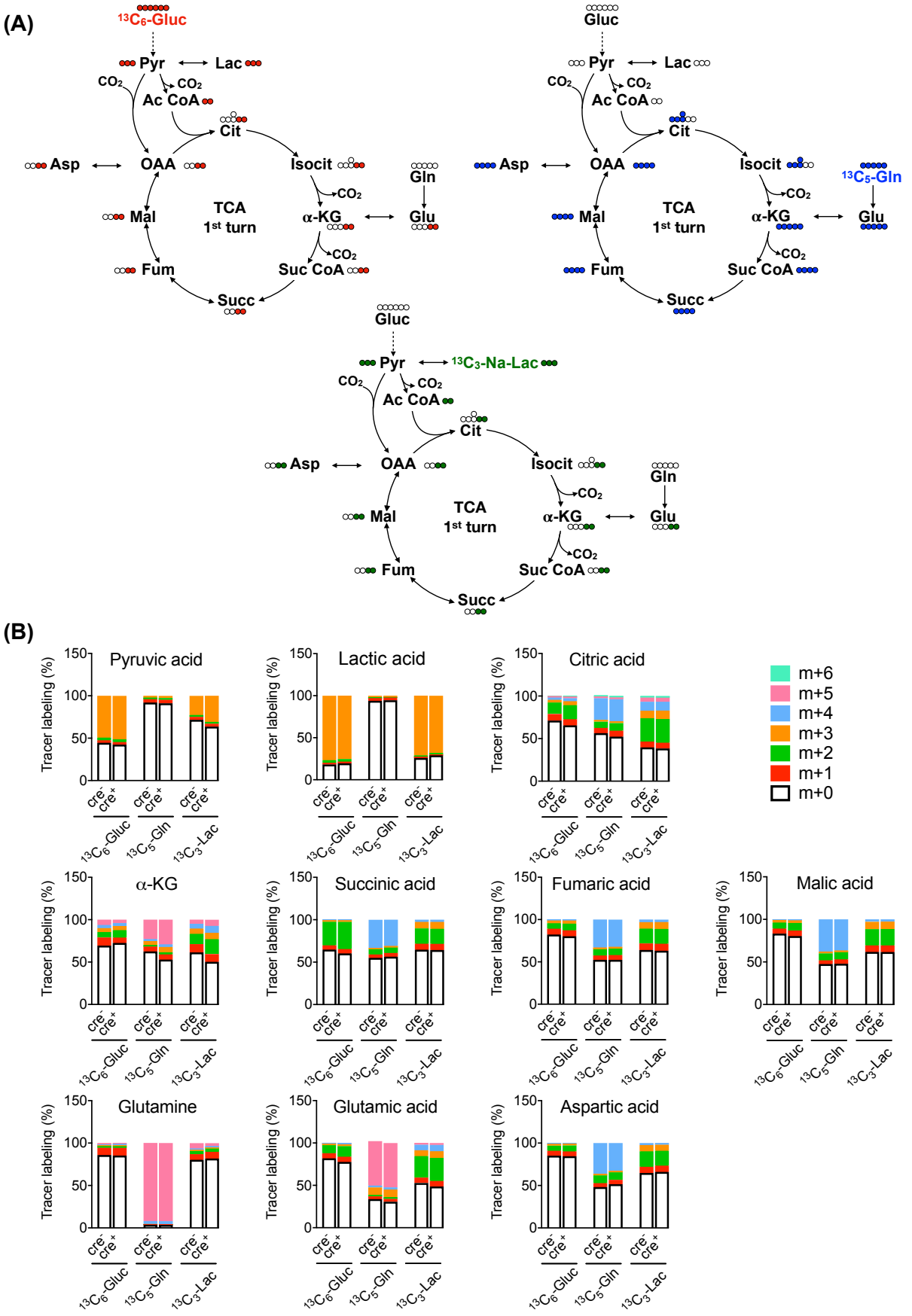

Figure 4.18: Stable isotype labeling of in vitro cultivated wildtype and Got1-deficient P14 cells. *A: Schematic representation of the ^{13}C labeled compounds in downstream metabolites. B: Bar graphs showing the label distribution in TCA cycle metabolites and associated metabolites. Graphs show the mean of three biological replicates.*

4.10. GOT1 does not influence electron flux in the ETC

We wondered if the deficiency of *Got1* impaired electron transport in the ETC, because the MAS is involved in electron shuttling to the mitochondrial matrix. Therefore, we performed electron flow analysis and treated wildtype and *Got1*-deficient T cells activated *in vitro* (similar to 4.9 and the donor cells used for adoptive transfer on tumor bearing mice) with PMP, to permeabilize the plasma membrane, while leaving the mitochondrial membrane intact. This allowed us to study mitochondrial metabolism without prior mitochondrial purification. Electron flow was monitored by measuring the oxygen consumption rate (OCR) in a Seahorse extracellular flux analyzer (**Figure 4.19 A**). In the assay, cells were cultivated in the presence of the mitochondrial uncoupler FCCP together with malate and pyruvate-containing medium, to feed into ETC complex I. The sequential injection of complex I inhibitor rotenone, complex II substrate succinate, complex III inhibitor antimycin A (AA) and complex IV substrates ascorbate and TMPD enabled us to study electron transport between the complexes. However, the electron flow was not significantly influenced by *Got1* deficiency.

We also performed a mitochondrial coupling assay to investigate the coupling between ETC and energy production with a similar experiment as described above, using PMP. In the assay, cells were cultivated in the presence of succinate and rotenone-containing medium, to investigate ETC complex II driven oxygen consumption. We sequentially injected ADP, to investigate the phosphorylating respiration with ADP, oligomycin (OM) to investigate residual respiration after ATP-synthase was blocked, FCCP to investigate maximal electron flow, and complex III inhibitor AA. Similar to the results above, the coupling between the ETC and energy production by OXPHOS were not significantly influenced by *Got1* deficiency (**Figure 4.19 B**), at least not under the used *in vitro* culture approach.

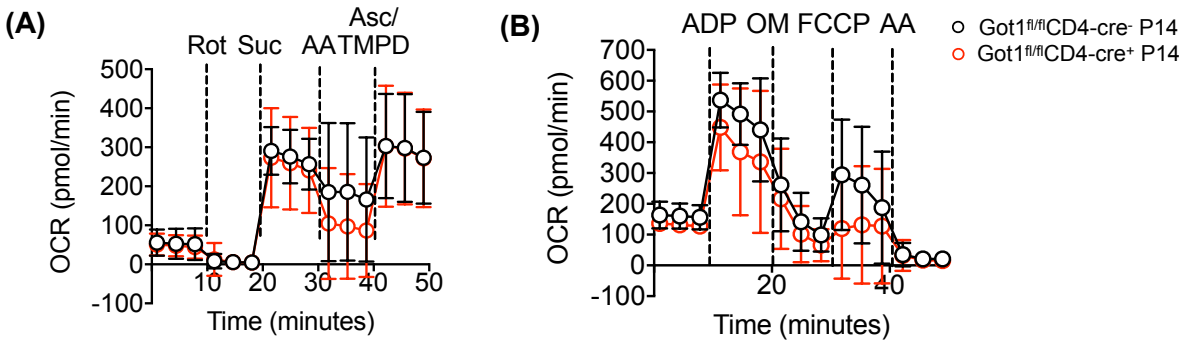

Figure 4.19: Seahorse electron flow (A) and coupling assay (B) showed similar results for in vitro activated wildtype and Got1-deficient T cells. *Results are pooled from 4-5 independent experiments each with one pair of mice. Rot = Rotenone; Suc = Disodium succinate; AA = Antimycin A; Asc = L-ascorbic acid; TMPD = N, N, N', N'-tetramethyl-p-phenylenediamine; ADP = Adenosine 5'-diphosphate OM = Oligomycin; FCCP = Carbonyl cyanide 4-(trifluoromethoxy)phenylhydrazone.*

4.11. GOT1-associated phenotypes correlate with nutrient withdrawal *in vitro*

According to our observations *in vivo*, *Got1*-deficient T cells faced problems to persist during viral infection and cancer development. We searched for a method to re-capitulate the phenotype *in vitro.* When a 1:1 mixture of wildtype and *Got1*-deficient T cells was cultured in the presence of gp33 in complete RPMI, the ratio between both cell types was largely maintained, similar to the observations of similar behavior between wildtype and *Got1*-deficient T cells in 4.9 and 4.10. We reasoned that activated T cells *in vivo,* especially in the TME face nutrient restriction. Therefore, the medium composition was changed to a minimal RPMI without glucose, glutamine and pyruvate with physiological glucose concentrations (6.7 mM) and 10 % dialyzed FBS, where macromolecules below 10 kDa (e.g. small molecules, amino acids) were removed.

We followed the abundance of the cells over a time course of 78 hours after activation and compared the ratio to cells cultivated in complete RPMI (**Figure 4.20 A** and **B**). A reduction of cell numbers in minimal RPMI started between 30-42 hours after activation, while the cell ratio was maintained in complete medium. We furthermore investigated the apoptosis rate of the cells and observed an increase in annexin V (AnxV) and propidium iodide (PI) positive apoptotic cells (**Figure 4.20 C** and **D**), which was exacerbated in minimal RPMI medium conditions.
Because of the previously observed changes in TCA cycle composition and reducing equivalents NAD^+ and NADH, we investigated ΔΨm and mitochondrial integrity by staining with ΔΨm dependent and independent dyes. We observed an accumulation of dysfunctional depolarized mitochondria (positive for Mito™Green, with reduced Mito™DeepRed fluorescence), correlating with the observed cell ratio changes (**Figure 4.21 A** and **C**). We further investigated the ROS levels in the cells, to identify a potential increase in oxidative stress. Indeed, *Got1*-deficient T cells expressed higher levels of ROS compared to wildtype cells (**Figure 4.21 B** and **D**).

Inspired by these results, we assessed potential bioenergetic differences and investigated the ability of the cells to perform OXPHOS and glycolysis in normal conditions and after nutrient restriction.

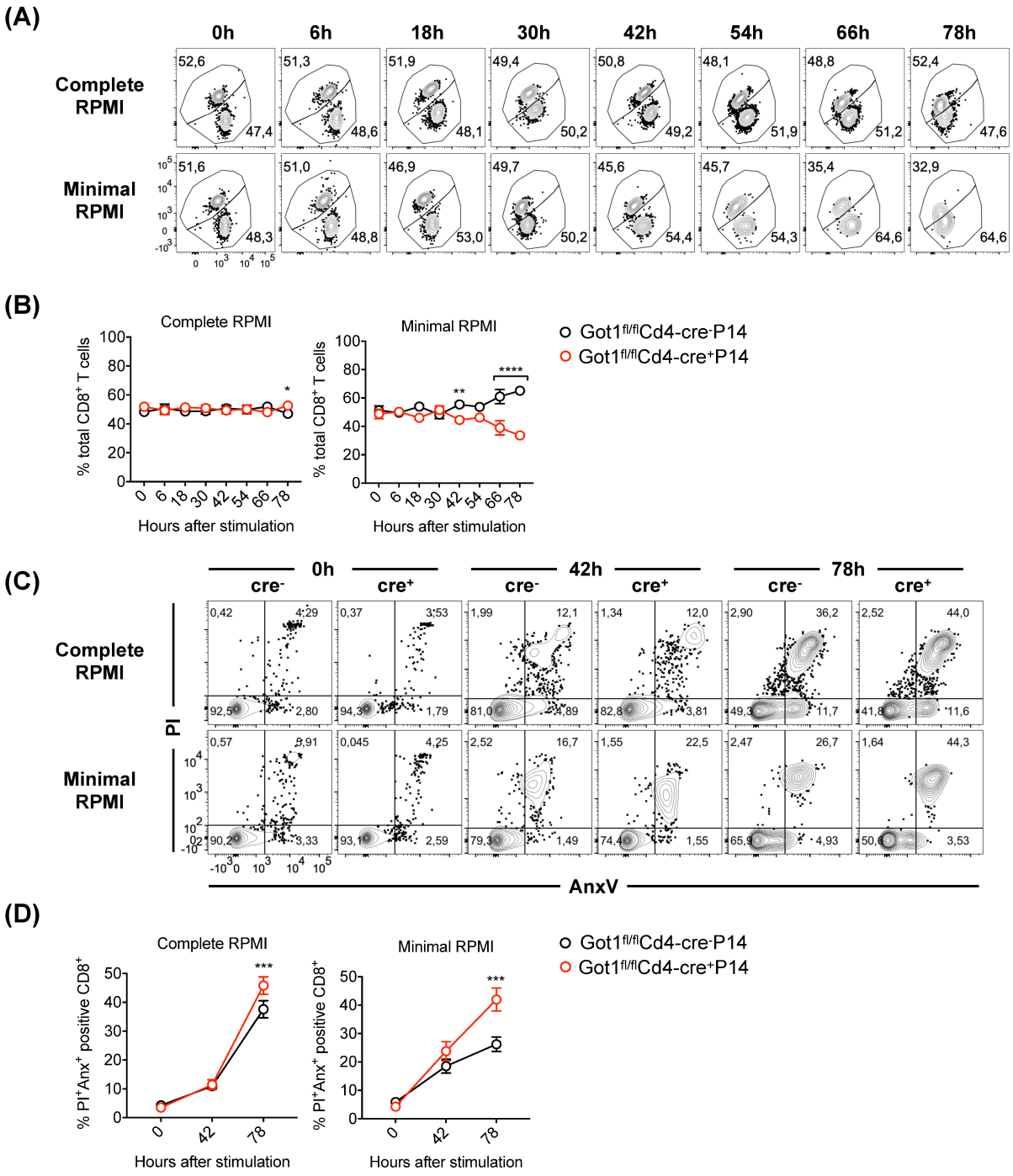

Figure 4.20: Got1 deficiency influences cell persistence and apoptosis after nutrient restriction in vitro. *A: Representative FACS plots of the ratio changes between wildtype and Got1-deficient cells over time in complete and minimal RPMI. B: Quantification of the ratio changes in complete medium and minimal RPMI (± SD). C: Representative FACS plots of PI⁺AnxV⁺ apoptotic cells over time in complete and minimal RPMI. D: Quantification of the apoptotic cells in complete medium and minimal RPMI (± SD). Experiments were performed at least 3 times and representative results are shown. * = p<0.05; ** = p<0.01; *** = p<0.001; **** = p<0.0001. P values were calculated by two-way ANOVA.*

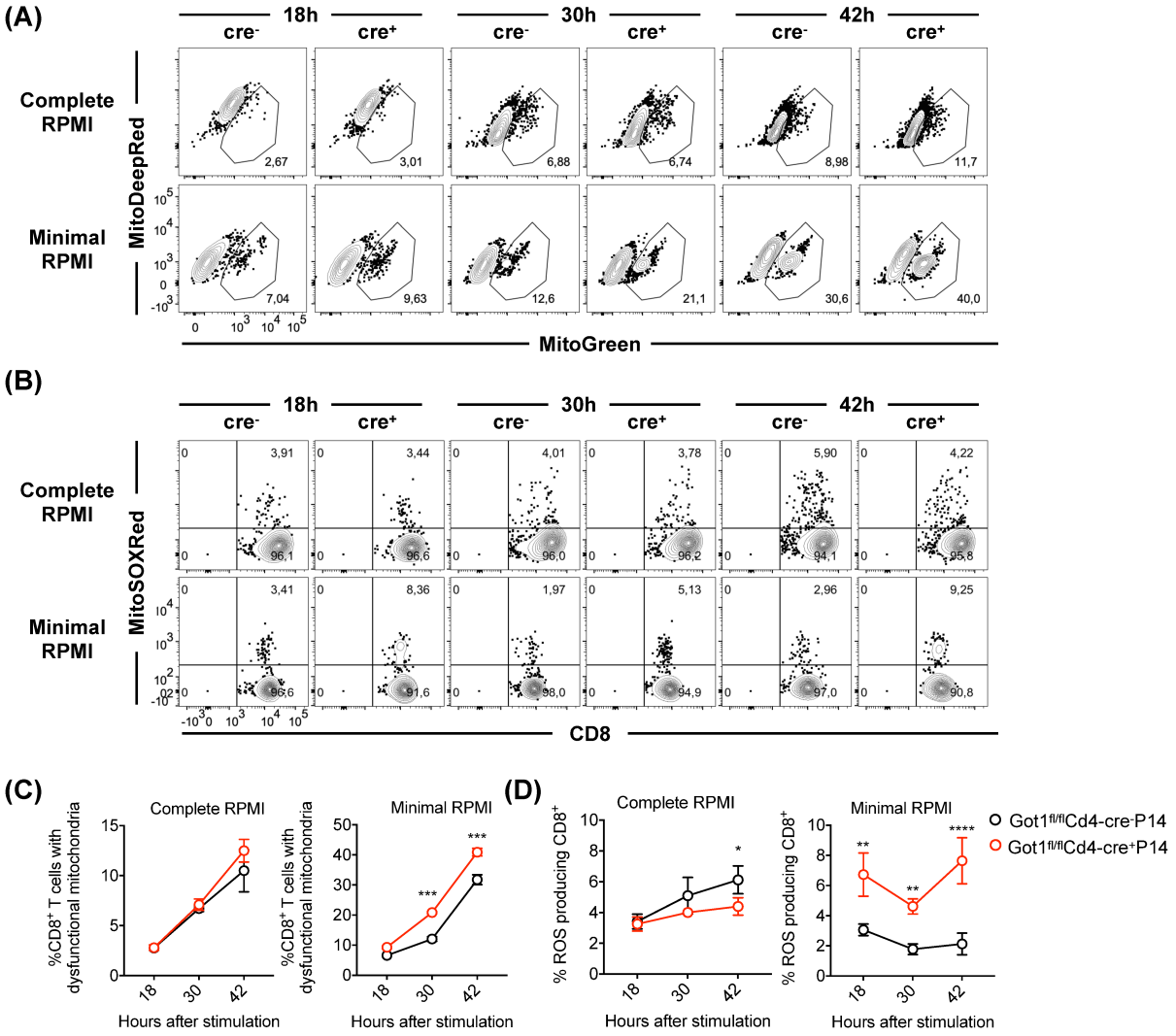

Figure 4.21: Got1 deficiency influences mitochondrial function and ROS after nutrient restriction in vitro. *A: Representative FACS plots of depolarized mitochondria in wildtype and Got1-deficient cells over time in complete and minimal RPMI. B: Representative FACS plots of ROS over time in complete and minimal RPMI.C: Quantification depolarized mitochondria in complete medium and minimal RPMI (± SD). D: Quantification of ROS in complete medium and minimal RPMI (± SD). Experiments were performed at least 3 times and representative results are shown. * = p<0.05; ** = p<0.01; *** = p<0.001; **** = p<0.0001. P values were calculated by two-way ANOVA.*

4.12. Loss of GOT1 correlates with bioenergetic insufficiencies

Wildtype and *Got1*-deficient T cells were activated and cultivated *in vitro* similar to 4.9 and the donor cells used for adoptive transfer on tumor bearing mice, or nutrients were withdrawn overnight, before we investigated the cellular energetic state using the Seahorse extracellular flux analyzer (**Figure 4.22**). *Got1* deficiency did not significantly impact the abilities of the cells to perform glycolysis, as the extracellular acidification rate (ECAR) was comparable between both cell types and cultivation conditions.

A significant decrease in the basal OCR, an indicator for the ability of the cells to perform mitochondrial respiration, was observed. These results indicated, GOT1 was needed to maintain OXPHOS after nutrient restriction.

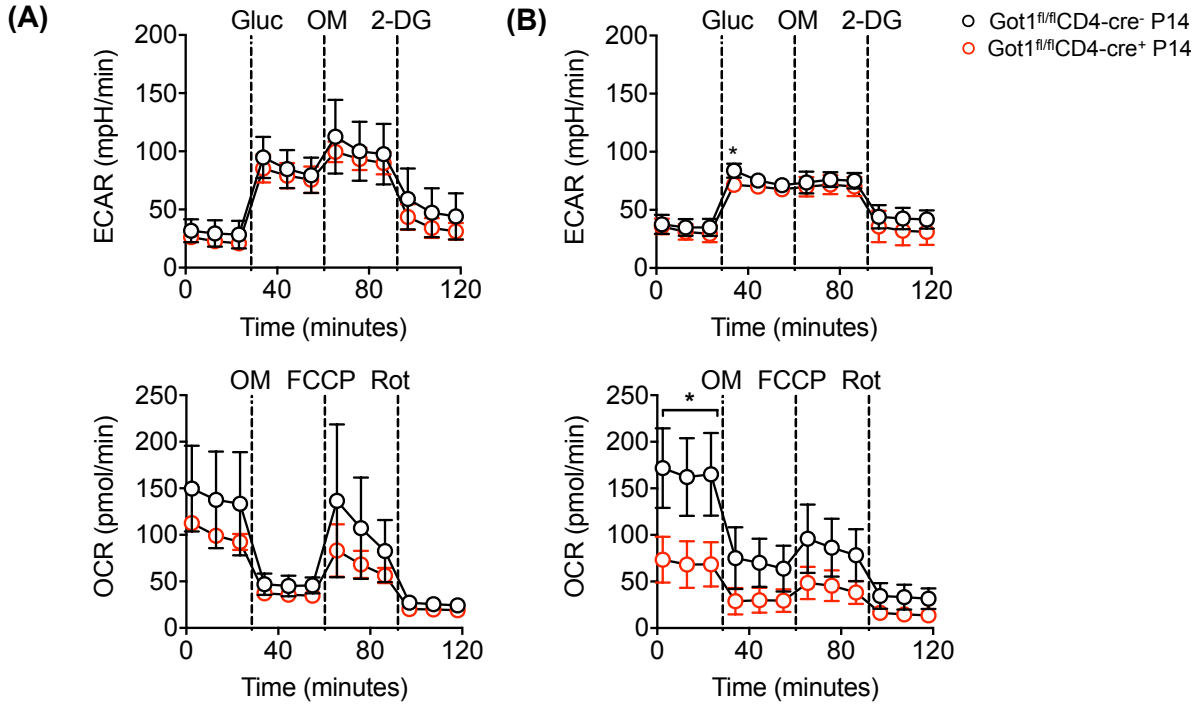

Figure 4.22: GOT1 deficiency affects OCR under nutrient-restricted conditions in vitro. *Seahorse glycolytic and mitochondrial stress test of wildtype and Got1-deficient T cells cultivated in A: complete RPMI or B: under nutrient restriction. Experiments were performed with 3 pairs of mice (± SD). * = p<0.05. P values were calculated by unpaired two-sided t-tests. Gluc = Glucose; OM = Oligomycin; 2-DG = 2-Deoxyglucose; FCCP = Carbonyl cyanide 4-(trifluoromethoxy)phenylhydrazone; Rot = Rotenone.*

4.13. GOT1-associated phenotypes can be rescued *in vitro*

Our previous results indicated that loss of GOT1 increased the dependency on extracellular metabolites. Since we observed changes in the TCA cycle composition, we supplemented back a panel of metabolites associated with the MAS, TCA cycle and glycolysis, to potentially restore the phenotypes observed after *in vitro* co-cultivation in minimal medium (4.11). We furthermore supplemented back antioxidants (e.g. N-acetyl-cysteine (NAC)) and precursors of NAD^+ (nicotinamide riboside (NR)).

Interestingly, the addition of membrane permeable dimethyl α-KG, OAA, pyruvate, NR, NAC, or simply non-dialyzed FBS were able to fully or partially rescue the observed phenotypes (**Figure 4.23**). Especially the ratio of wildtype and *Got1*-deficient T cells improved significantly after addition of the metabolites mentioned above (**Figure 4.23 A** and **B**). Also, elevated glucose levels were able to partially rescue the ratio between both cell types. However, glucose

did not relief the mitochondrial phenotype nor the elevated ROS production, in line with previous result, showing glycolysis was not affected by the loss of GOT1.

Similar to the cell ratios, the ratio of depolarized mitochondrial from wildtype and *Got1*-deficient cells increased to the levels of cells cultivated in complete medium (**Figure 4.23 C** and **D**). Also, ROS production in *Got1*-deficient cells decreased significantly after treatment (**Figure 4.23 E** and **F).** The effect on apoptosis was mixed in these experiments. The ratio of PI^+AnxV^+ expression between wildtype and *Got1*-deficient cells was lower in minimal medium cultivated cells, but not significantly different from complete medium. The addition of all tested metabolites reduced the apoptosis of wildtype and *Got1*-deficient T cells alike, and the changes were the strongest after the addition of α-KG and non-dialyzed FBS, which significantly improved cell survival (**Figure 4.23 G** and **H**).

Elevated levels of aspartic acid, malic acid and glutamic acid (not shown) failed to fully restore the GOT1-associated defects. Interestingly, also sodium lactate was able to partially rescue the observed phenotypes.
Inspired by these results, we reasoned that GOT1 reduced the dependency on exogenous metabolites for metabolic balance and fitness in activated T cells. These results were especially striking for the supplementation of “normal” FBS, pyruvate, OAA and α-KG. Pyruvate and α-KG were shown to be reduced in *Got1*-deficient $CD8^+$ T cells after LCMV infection (**Figure 4.16**), we expected that supplementation of these metabolites could enhance the performance of *Got1*-deficient T cells *in vivo*.

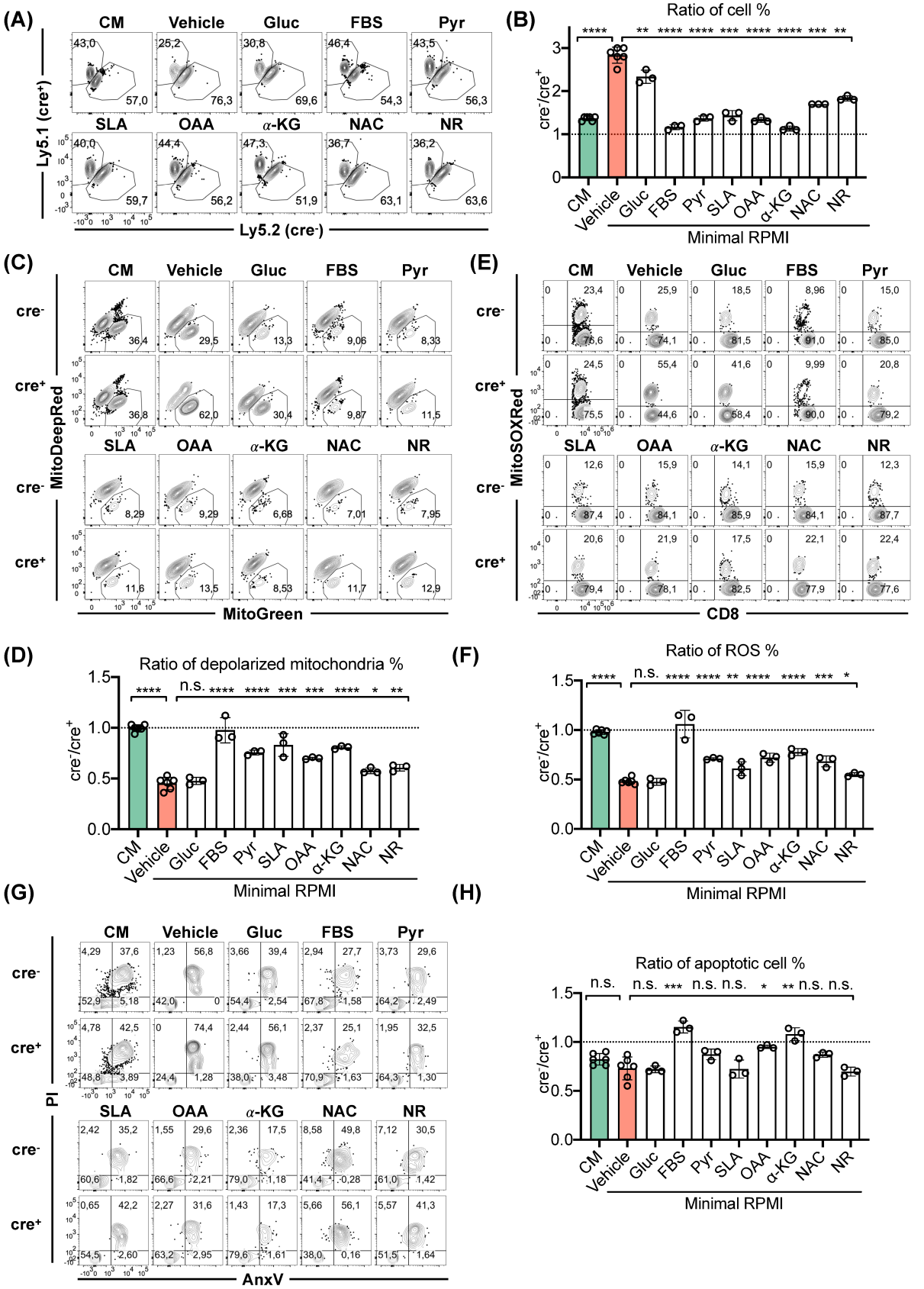

Figure 4.23: GOT1-associated phenotypes can be rescued in vitro. *A: Representative FACS plots of the ratio of wildtype and Got1-deficient T cells after in vitro treatment. B: Ratio of wildtype and Got1-deficient T cell % after in vitro treatment (± SD). C: Representative FACS plots of depolarized mitochondrial after in vitro treatment. D: Ratio of depolarized mitochondria in wildtype and Got1-deficient T cells (± SD). [Legend continues on next page]*

*E: Representative FACS plots of ROS after in vitro treatment. F: Ratio of ROS in wildtype and Got1-deficient T cells (± SD). G: Representative FACS plots of apoptotic cells after in vitro treatment. H: Ratio of apoptotic cells in wildtype and Got1-deficient T cells (± SD). n.s. = p>0.05; * = p<0.05; ** = p<0.01; *** = p<0.001; **** = p<0.0001. P values were calculated by comparison to vehicle (highlighted in red), using unpaired two-sided Student's t-tests. CM = complete RPMI (highlighted in green), Gluc = 11 mM glucose, FBS = non-dialyzed FBS (10 % v/v), Pyr = 10 mM sodium pyruvate, SLA = 1 mM sodium lactate, OAA = 1 mM oxaloacetate, α-KG = 10 mM dimethyl α-KG, NAC = 1 mM N-acetyl-l-cysteine, NR = 1 mM nicotinamide-riboside.*

4.14. Pyruvate and α-KG supplementation restored GOT1-associated phenotypes *in vivo*

Inspired by the *in vitro* rescue of GOT1-associated phenotypes, we studied the result of nutrient supplementation *in vivo.* Because the phenotypes were visible when cells were cultivated under minimal medium conditions, we pre-activated wildtype and *Got1*-deficient T cells in minimal medium for 1 day with gp33 and in presence of a vehicle, 1 mM sodium pyruvate or 10 mM dimethyl α-KG. $3x10^5$ pre-treated cells were transferred to mice bearing B16-gp33 tumors and the tumor growth was followed (**Figure 4.24**). Consistent with our previous observations, the transfer of vehicle-treated *Got1*-deficient T cells led to significantly larger and heavier tumors (**Figure 4.24 B** and **C**). Treatments of *Got1*-deficient T cells with both metabolites were able to significantly reduce the tumor sizes and the tumor weights, compared to vehicle treated cells. This was specific for *Got1*-deficient cells, as the metabolite treatment did not have effects on wildtype T cells.

We profiled the phenotype of the donor T cells by flow cytometry. Consistent with our previous findings, we recovered significantly higher numbers of wildtype donor cells from spleens and tumors, compared to *Got1*-deficient donor cells (**Figure 4.25 A**), when the cells were only treated with vehicle. The pre-treatment with the metabolites significantly increased the recovered *Got1*-deficient donor cell numbers but did not show any influence on recovered wildtype donor cell numbers. In line with previous findings, we found elevated PD-1 expression in vehicle treated *Got1*-deficient TILs (**Figure 4.25 B**). The treatment with pyruvate significantly reduced the PD-1 expression in *Got1*-deficient donor cells, while the treatment with α-KG only showed a trend towards reducing PD-1 levels.

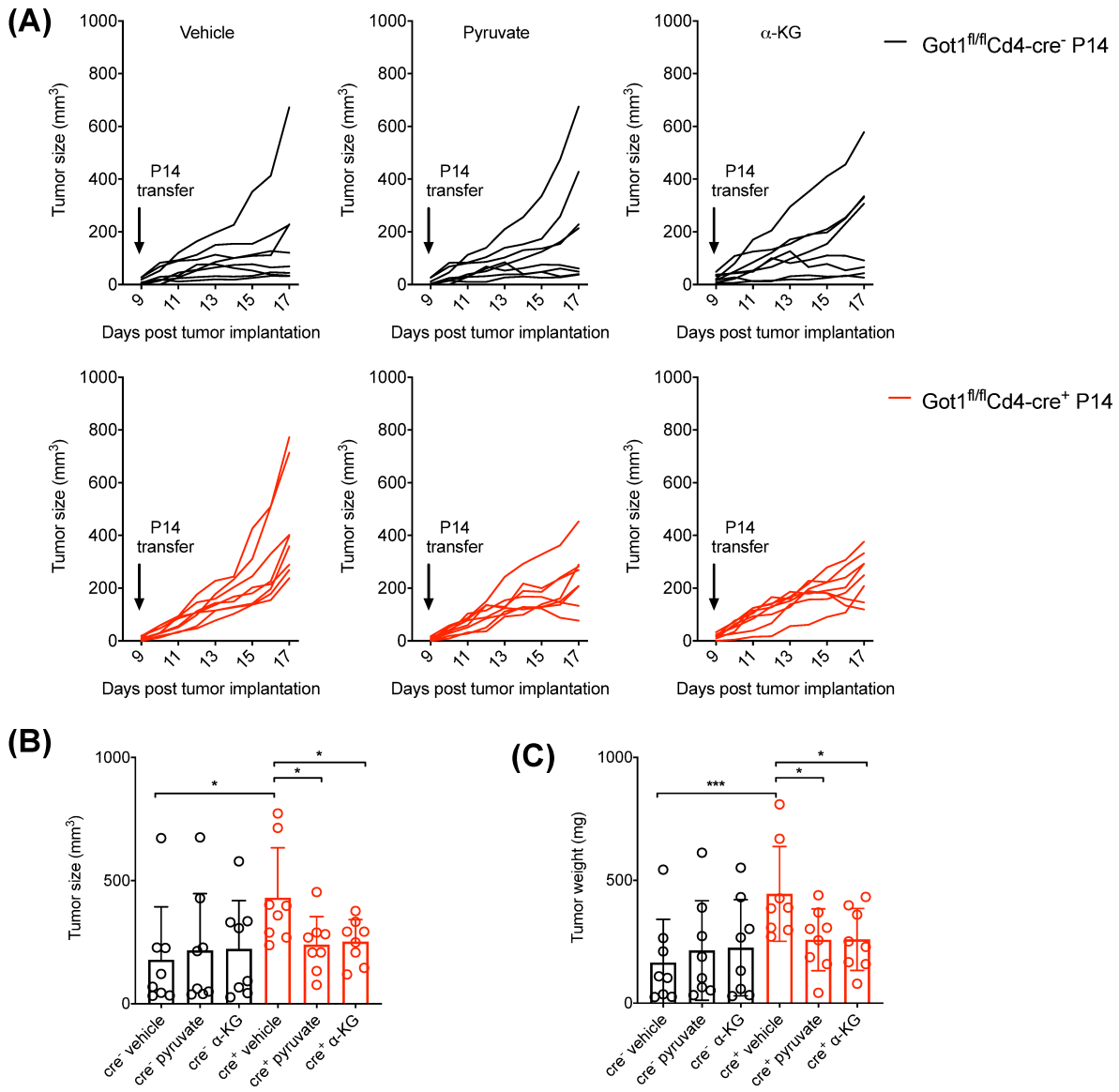

Figure 4.24: Antitumoral function can be improved by pre-treatment of Got1-deficient P14 cells. *A: Spider plots of the tumor growth curves after adoptive transfer of vehicle, sodium pyruvate or dimethyl α-KG pre-treated donor cells. B: Comparison of final tumor sizes between the experiment groups (± SD). C: Comparison of final tumor weights between the experiment groups (± SD). Data from 2 experiments with 8 mice in total. * = p<0.05; *** = p<0.001. P values were calculated by comparison to Got1-deficient vehicle-treated cells, using unpaired two-sided Student's t-tests.*

The cytokine secretion, measured by TNFα and IFNγ, was significantly reduced in vehicle treated *Got1*-deficient donor cells from spleen and tumor (**Figure 4.25 C**). Metabolite treatment did not influence the cytokine production of wildtype cells, but significantly restored cytokine secretion in *Got1*-deficient splenic T cells. Cytokine secretion was also significantly improved in *Got1*-deficient TILs after the treatment with α-KG, while there was a trend towards increased cytokine secretion after pyruvate treatment.

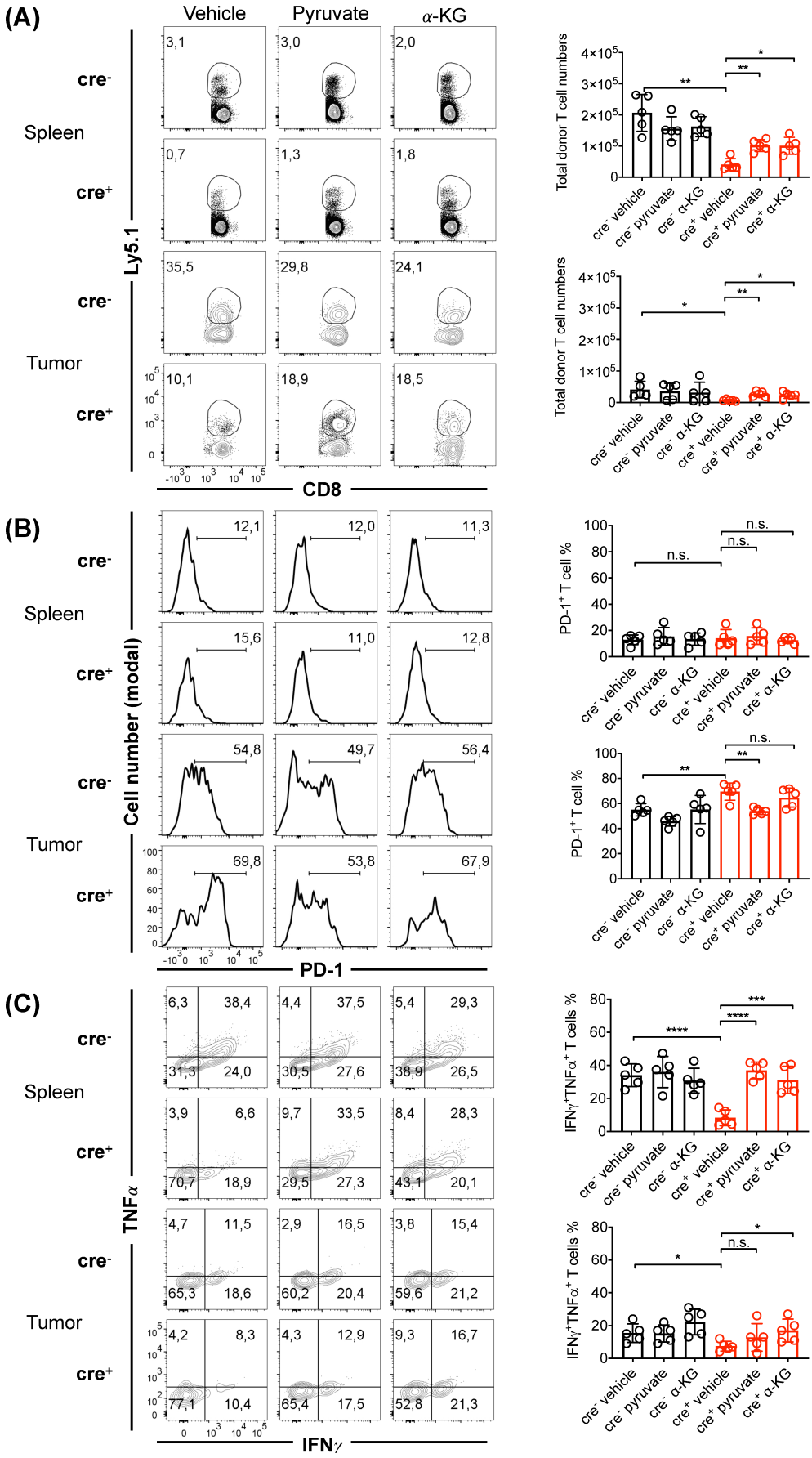

Figure 4.25: Flow cytometry analysis of recovered pre-treated wildtype or Got1-deficient P14 cells from B16-gp33 tumors or spleens. *[Legend continues on next page]*

*A: Analysis of the cell numbers from vehicle, sodium pyruvate or dimethyl α-KG pre-treated recovered donor cells (± SD). B: Analysis of the PD-1 expression from vehicle, sodium pyruvate or dimethyl α-KG pre-treated recovered donor cells (± SD). C: Analysis of the cytokine secretion from vehicle, sodium pyruvate or dimethyl α-KG pre-treated recovered donor cells (± SD). Data from 1 experiment with 5 mice. n.s. = p>0.05; * = p<0.05; ** = p<0.01; *** = p<0.001; **** = p<0.0001. P values were calculated by comparison to vehicle, using unpaired two-sided Student's t-tests.*

This experimental approach showed, the defect of *Got1*-deficient cells could at least be partially restored when exogenous nutrients were supplemented back during cell activation, and supported our theory, that GOT1 was required to desensitize T cells to nutrient deprivation and was required to maintain effector function during chronic antigen stimulation.

5. Discussion

$CD8^+$ T cells mediate powerful immune responses to protect the organism against infectious diseases and from the development of cancer. Immune responses are accompanied by tremendous cell-intrinsic and metabolic changes and can result in T cell exhaustion after chronic stimulation and long-term antigen exposure. Exhausted T cell express inhibitory surface receptors and display a reduced effector potential, resulting in the failure to control the infections or restrain tumor growth. The targeting of negative regulators of T cell function (also referred to as immune checkpoints) with the goal of reversing T cell exhaustion, showed promising clinical success in the treatment of different forms of cancer. The development of immunotherapies is in the spotlight of immune-oncologic research, and there is great interest in novel immunotherapeutic approaches and in the identification and targeting of new immune checkpoints or metabolic checkpoints, to improve existing therapies.

The aim of this thesis was the characterization of the MAS enzyme GOT1 in T cell biology, T cell metabolism, and to study its contribution to mitochondrial health during T cell exhaustion. We identified GOT1 to be important for the cellular NAD^+/NADH redox balance and energy metabolism, to maintain mitochondrial fitness and to protect cells from apoptosis during chronic antigen stimulation. Surprisingly, the effect of GOT1 on the cells became only dramatic after T cell activation, when extracellular nutrients were limited. The absence of GOT1 exacerbated the T cell exhaustion phenotype of melanoma TILs, resulting in impaired antitumoral immune responses and increased tumor burden. During viral infection, loss of GOT1 negatively affected antiviral effector, but not memory responses during acute and chronic LCMV infection. Taken together, GOT1 was identified to desensitize T cells to nutrient availability during chronic stimulation.

5.1. The expression of *Got1* is dependent on TCR stimulation, but delayed compared to TCR-associated pathways

We wanted to understand the cues that induce *Got1* expression. Our *in vitro* observations showed antigen-stimulation was required to induce GOT1, and antigen-withdrawal resulted in rapid downregulation of the protein (**Figure 4.3**). Similar results were obtained *in vivo*. Naïve CTLs transferred to tumor bearing mice with tumors expressing the cognate epitope gp33 or the unrelated antigen OVA, showed profound differences in *Got1* mRNA expression. Adoptive transfer of pre-activated T cells resulted in downregulation of GOT1 in TILs recovered from the OVA-expressing tumors, while GOT1 expression was maintained in gp33-expressing tumors (**Figure 4.6 A** and **B**).

These results indicated that antigen-specific signals were required for *Got1* expression. We found the upregulation of GOT1 was independent from additional pro-inflammatory cytokines (**Figure 4.5**). Interestingly, the expression of GOT1 was delayed compared to classical TCR pathways like mTORC1 (measured by pS6 phosphorylation), which already peaked after 1 day, and GOT1 was found to be upregulated at day 3 after *in vitro* stimulation. *Got1* expression therefore required persistent antigen stimulation. This would explain the transient expression when antigen was available, and why the gene was quickly downregulated after the antigen was removed.

The transcriptional regulation of GOT1 in T cells is unknown. Based on the delayed expression kinetics we observed for GOT1, compared to the rapid induction of direct targets of TCR signaling, for example pS6, we assume that GOT1 is not directly induced by TCR signaling pathways. However, since the expression was sensitive to selective blockage of mTOR or NFAT pathways (**Figure 4.4**), we concluded that the cooperation of TCR downstream signaling cascades were necessary to induce GOT1. In myocytes, PGC1-α is a key transcription factor for metabolic genes and has been implicated in the transcriptional upregulation of GOT1 and mitochondrial genes [210], and PGC1-α dependent regulation of mitochondrial genes improved T cell function of exhausted T cells [157, 158]. Also, c-Myc has been related to the transcriptional regulation of glutaminolysis genes [211]. HIF1-α was shown to act as a tumor suppressor by limiting *Got1* and *Got2* expression in tumor cells [212]. Further investigations are necessary to understand the dominant transcriptional cues that drive and sustain *Got1* expression in T cells.

We observed, GOT1 was also expressed in human TILs from colon carcinoma samples, and its expression correlated with the expression of PD-1 (**Figure 4.6 C**). It should be noted, that PD-1 *in vitro* is strongly upregulated at about day 2 after stimulation [213], indicating a similar expression pattern compared to GOT1.

5.2. *In vitro* and *in vivo* studies of *Got1*-deficient T cells

In the presented work, *Got1*-deficient mouse models were used to study GOT1 in T cells *in vitro* and *in vivo*. We validated the efficiency of the Cd4cre/loxP based T cell specific knockout by Western blot in purified T cells and confirmed that the protein was efficiently deleted in the cells (**Figure 4.1**). In our experiments, we used either $Got1^{+/+}$ mice which lacked the floxed *Got1* allele, or $Cd4cre^{-}$ mice without the cre-recombinase as controls. In a recent study, it was shown that inducible cre-recombinases (ERT2-cre) could affect cell persistence due to toxicity of certain cre drivers [214]. However, the constitutive active Cd4-cre used in this study did not affect cell persistence in the transgenic animals and justified the use of $Cd4\text{-}cre^{-}$ control mice.

Even though GOT1 is a central enzyme in the MAS, *in vitro* cultivated cells behaved comparable to the wildtype counterparts. Differences became only visible, when we stimulated the cells under nutrient restricted conditions, or transferred cells to recipient hosts challenged with viral infections or tumors. Suddenly, the loss of GOT1 resulted in severe metabolic defects in the cells. This is in line with our previous findings, indicating TCR stimulation and cell activation are necessary to stimulate *Got1* transcription. In line with these observations, we observed that naïve cells were not dependent on GOT1 expression and did not show relevant phenotypes during the immune characterization (**Figure 4.2**).

5.3. GOT1 is dispensable in environments of excessive nutrient availability

The MAS enables electron-shuttling across the inner mitochondrial membrane in a NAD^{+}/NADH dependent manner. Since the MAS can therefore be considered as a linker between cytosolic and mitochondrial metabolism, we assumed that GOT1 deficiency would disturb the energy metabolism in the cells.

We discovered that *Got1*-deficient T cells were able to perform glycolysis and OXPHOS to a normal extend, when we investigated *in vitro* activated cells that were cultured in complete medium (**Figure 4.22 A**). Furthermore, we observed that the electron transport between the

single complexes of the ETC was comparable between wildtype and *Got1*-deficient cells. Also, we investigated the coupling between the electron flow and energy production and found no significant differences, even though there were strong variations between the single samples in the assay, caused by unknown sources (reflected by high error bars in **Figure 4.19**). This indicated, *Got1*-deficient T cells were able to maintain mitochondrial metabolism and electron transport through the ETC even in absence of GOT1. Using stable isotype labeling, we showed that *Got1*-deficient T cells were able to metabolize extracellular nutrients (glucose, glutamine and lactate) to a similar extend and had no striking defects in incorporating the supplemented metabolites into downstream metabolic pathways (**Figure 4.18** and **Supplementary Figure 1**).

Several explanations could help to understand, how the interruption of a central metabolic pathway like the MAS could be tolerated by the cells. For example, compensatory pathways could maintain metabolic functions in *Got1*-deficient cells. The MAS is not the only mitochondrial shuttling system. A second prominent example for electron transfer through the mitochondrial membrane is the glycerol-3-phosphate (G3P) shuttle. Similar to the MAS, the G3P shuttle transfers reducing agents through the mitochondrial inner membrane [215]. The G3P shuttle oxidizes NADH to NAD^+ in the cytosol, similar to the MAS. In the mitochondrial matrix, in contrast to MAS, G3P shuttle transfers electrons to FAD^+ to produce its reduced form $FADH_2$. $FADH_2$ is recycled when it transfers electrons to reduce coenzyme Q, which is part of the ETC. We have unpublished RNA sequencing data, demonstrating an increase in the mRNA levels of glycerol-3-phosphate dehydrogenase 2, a key enzyme in the G3P shuttle, in *Got1*-deficient $CD8^+$ T cells after LCMV cl-13 infection. The same dataset also showed increased levels of nicotinamide nucleotide adenylyltransferase 1. This enzyme is part of the NAD^+ salvage pathway [216]. Since GOT1 and the MAS are tightly connected to the levels of NAD^+ and NADH, and we have noticed a decrease in the NAD^+/NADH balance in *Got1*-deficient T cells that will be discussed further below, the upregulation of both pathways could be a sign of compensatory mechanism to maintain NAD^+/NADH redox balance in effector $CD8^+$ T cells.

5.4. GOT1 is required to maintain cellular metabolic fitness during nutrient restriction

It has been appreciated before, that complete cell culture medium is not physiological, and does not recapitulate pathological situations [217, 218]. The impressive impact of GOT1 deficiency in TILs from the investigated melanoma model (discussed further below), supported the hypothesis, that nutrient restriction was a critical factor for *Got1*-associated phenotypes in

T cells. Therefore, we withdrew nutrients *in vitro* by substituting FBS in a minimal base medium by dialyzed FBS, where nutrients below 10 kDa were removed.
Using this cell culture approach, phenotypes were uncovered that might have been veiled by the excessive nutrient availability discussed above. We observed dramatic metabolic defects in *Got1*-deficient cells *in vitro*. Loss of GOT1 impaired OXPHOS and increased the ROS expression in mitochondria. This indicated mitochondrial dysfunction, which was supported by reduced ΔΨm in *Got1*-deficient T cells.

5.4.1. GOT1 mediates redox balance and ROS expression

One difference between the culture condition in complete medium and minimal medium was the absence of 2-mercaptoethanol in the minimal medium culture. The addition of 2-mercaptoethanol is thought to reduce the oxidative stress burden from ROS secretion of proliferating cells in the cell culture [219]. We supplemented back 2-mercaptoethanol in the minimal medium culture and found no improvement of the GOT1-associated phenotypes. This indicated, extracellular ROS were not the major driver of the observed phenotypes.

Cellular ROS production in moderate levels is necessary for T cell activation and effector function, and is correlated to TCR stimulation [220-223]. ROS in intracellular signaling have multiple sources, with one major contribution originating from mitochondrial complexes I and III and by reverse electron transport of these complexes in the ETC [222, 224-226].
Side effect of excessive ROS production in T cells manifest in impaired effector functions [227] and can even lead to AICD [228]. It has also been shown before that a decreased NAD^+/NADH ratio, or the excessive abundance of NADH contributes to excessive ROS production [229-231].

In line with these findings, we measured a decrease of NAD^+/NADH ratio in *Got1*-deficient T cells after *in vivo* stimulation following viral infection with LCMV Arm (**Figure 4.17**).
The altered redox balance is a possible explanation for excessive ROS production in *Got1*-deficient T cells (**Figure 4.21 B** and **C**). Interestingly, enhanced ROS production and disturbances in NAD^+/NADH after depletion of GOT1 have also been observed in pancreatic cancer [232-234]. Furthermore, breast cancer cell lines displayed a reduced NAD^+/NADH after treatment with AOA [235]. This revealed that certain cancer types rely on the GOT1-dependent maintenance of metabolic integrity to support cancer proliferation.
It should be noted that the aforementioned inhibitor AOA is frequently used in the literature to disturb transaminase activity, however AOA is not a GOT1-specific inhibitor, but disturbs the activity of all PLP-dependent [236] enzymes including GOT1, GOT2 and other aminotransferases.

Excessive ROS production can originate also from the loss of reduction or synthesis of detoxifying antioxidants, such as glutathione (GSH). The production and the recycling of intracellular antioxidants is dependent on the redox state and intracellular metabolism [237]. For example, the reduction of oxidized GSH (GSSG) to the reduced form is dependent on the simultaneous oxidation of nicotinamide adenine dinucleotide phosphate (NADPH). NADPH on the other hand is a side product from the pentose phosphate pathway, starting from glucose-6-phosphate [238]. Other intracellular sources of NADPH are generated by malic enzyme 1 during the conversion from malate to pyruvate, or by NADP-dependent isocitrate dehydrogenase 1 during the conversion from isocitrate to α-KG [239]. Using MS, we have observed that all investigated TCA cycle intermediates were decreased in *Got1*-deficient T cells (**Figure 4.16**). The depletion of reaction intermediates that are accompanied by simultaneous reduction of $NADP^+$ could therefore interfere with the antioxidant pool. Although we have yet to measure $NADP^+$/NADPH and GSH/GSSG levels in *Got1*-deficient T cells, it is likely that we will also see an imbalance in these metabolites following GOT1 depletion.
In line with our observations in $CD8^+$ T cells, this hypothesis is also supported by the observation of GOT1 in different cancer cell lines. GOT1 overexpression resulted in decreased ROS levels and improved GSH synthesis, for example by increasing NADPH synthesis following glutaminolysis and the activity of malic enzyme [232, 240, 241].

We supplemented NAC *in vitro* and observed reduction of GOT1-associated phenotypes like ROS production and mitochondrial dysfunction. NAC has direct and indirect antioxidative properties, since it can serve as an oxidant scavenger or be used as precursor for GSH synthesis [242]. Taking the experimental data into account, our results indicate that GOT1 maintains cellular redox balance, antioxidant pool and controlled ROS expression during nutrient restriction.

5.4.2. GOT1 maintains mitochondrial fitness and desensitizes T cells to oxidative stress and apoptosis

The increase in ROS levels was accompanied by increased levels of dysfunctional mitochondria in *Got1*-deficient cells *in vitro* (**Figure 4.21 A** and **C**). The MAS has been related to mitochondrial membrane potential in several studies and cell types, however GOT1 itself has hardly been studied in this context. Usage of AOA impacted redox balance and decreased ΔΨm in neurons and microglia [243, 244]. Our own observations support the theory that GOT1 supports ΔΨm under nutrient deprivation.

Interestingly, in prostaglandin E2 and IL-4 activated macrophages, the relationship of GOT1 and ΔΨm was reciprocal, and induction of *Got1* expression correlated with a decrease in ΔΨm, which initiated the transcription of ΔΨm-dependent genes [245]. This indicates, ΔΨm might be regulated by additional factors and depend on the cell type and stimulation context.

Decreased ΔΨm in T cells was directly linked to mitochondrial dysfunction and impaired oxidative metabolism. The measurement of OCR in nutrient-starved T cells resulted in a significant decrease of basal oxygen consumption in *Got1*-deficient T cells (**Figure 4.22 B**). We assume that the negative effect on OXPHOS was further amplified by the reduction of TCA cycle intermediates we observed after MS analysis. A link between MAS/GOT1 and oxidative metabolism has been reported in pancreatic cells in a low pH environment. It was observed that MAS enzymes including GOT1 were upregulated to increase mitochondrial respiration [232].

Besides OXPHOS, we also assessed glycolysis when GOT1 was depleted, but did not find differences to wildtype cells. Both cell types had similar ECAR values, a readout for the lactate production and secretion during aerobic glycolysis [246]. Furthermore, supplementation of glucose did only partially improve phenotypes associated with *Got1* deficiency. This showed that even though the redox state of the cells was altered, there were still sufficient NAD^+ levels available to maintain glycolytic flux. It has been reported, that loss of GOT1 increased aerobic glycolysis in pancreatic cancer cells [233]. These findings underline that the impact of MAS and GOT1 on glycolysis might be cell type specific.

To the present time, we have investigated electron flow in the ETC, connection between electron flow and energy production and nutrient assimilation of ^{13}C labeled substrates only in cells cultivated under normal cell culture conditions. Repeating these experiments under nutrient restriction will be helpful to gain further insights, which cellular pathways are most depend on GOT1.

We observed decreased abundance of *Got1*-deficient T cells *in vitro* (**Figure 4.20**). This decrease was accompanied by a simultaneous increase in apoptotic *Got1*-deficient cells, and apoptosis rates could be reduced by the *in vitro* supplementation of several metabolites. We suspect that the combined decrease of metabolic and mitochondrial fitness might have induced apoptosis in *Got1*-deficient cells. In accordance, studies using AOA treatment also increased the apoptosis rates of neurons and microglia [243, 244].

However, increase in apoptosis is not the only potential explanation for the decreased wildtype/*Got1*-deficient cell ratio *in vitro* and *in vivo.* These differences could also be the result of inhibited T cell proliferation. This theory was supported by the observation that glutamine-deprivation resulted in impaired proliferation and ROS imbalance in $CD4^+$ T cells [247]. Our

minimal medium conditions were indeed glutamine deficient. We added back glutamine to the culture and observed mixed results. Even tough glutamine supplementation elevated the cell numbers and decreased the apoptosis rates of the cells, this affect was not specific for *Got1*-deficicent T cells, but observed in wildtype cells as well, and the ratio between both cell types was not reproducibly restored (data not shown). We also labeled the *in vitro* cultivated cells with cell tracer violet, to observe the proliferation rates in both cell subsets (data not shown). Unfortunately, we were not able to detect proliferation peaks in the flow cytometry analysis, which are used to quantify the proliferation capacity of the cells. Thus, we cannot fully exclude, that the observed phenotypes might additionally be the result of impaired cell proliferation. It would for example be interesting to label the cells *in vivo* with bromdesoxyuridin, or to label the cells with cell tracer violet before the adoptive transfer, to investigate the proliferative potential after adoptive transfer *in vivo*.

5.4.3. GOT1 desensitizes T cells to extracellular nutrient availability

When we supplemented back a panel of metabolites, we observed a complete or partial rescue of the GOT1-associated phenotypes described above (**Figure 4.23**). Potent rescue was achieved after the addition of pyruvate, α-KG and OAA. Since we also detected pyruvate and α-KG as being reduced in the MS analysis of viral infected *Got1*-deficient T cells, we reasoned that these metabolites were important to maintain cellular metabolic fitness in the absence of GOT1. Unfortunately, we were not able to determine the levels of OAA in *Got1*-deficient T cells, due to limitations in the sensitivity of the MS measurements and commercially available kits.

Pyruvate is the end-product of glycolysis and can either be converted to lactate by lactate dehydrogenase [248], feed in the TCA in form of acetyl-coA or replenish TCA cycle by anaplerotic reactions as OAA through the activity of pyruvate carboxylase. All three reactions could have beneficial outcome for the *Got1*-deficient cells.
The reaction by lactate dehydrogenase is accompanied by the oxidation of NADH to NAD^+. This could help to restore the NAD^+/NADH ratio in *Got1*-deficient T cells, and normalize associated phenotypes, e.g. mitochondrial fitness and ROS levels and will be discussed further below. Also, the conversion of pyruvate into acetyl-coA could replenish the TCA cycle. The conversion from pyruvate to acetyl-coA is mediated by pyruvate dehydrogenase, but is accompanied by the reduction of NAD^+ to NADH [249]. This makes it less likely to be favorable to rescue GOT1-associated phenotypes. Pyruvate carboxylase converts pyruvate to OAA in an ATP-dependent reaction [250], to replenish the TCA cycle. Since we have observed a rescue effect also after the supplementation of OAA, it is likely that replenishment of the TCA cycle is a key feature to restore cellular health during the depletion of GOT1. Indeed, it was

also observed in pancreatic cancer cells, that OAA could correct GOT1-associated phenotypes [233, 251]. It should be noted that GOT1-derived OAA supported NADPH synthesis in pancreatic cancer cells and improved cancer cell fitness [241], and this mechanism might be of importance in T cells as well.

Based on earlier publications, it was suggested that GOT1 plays a pivotal role to support aspartate synthesis to support proliferation by providing amino acids and building blocks for subsequent nucleotide synthesis [190]. A separate study showed that respiration was essential for aspartate synthesis, and cells with respirational defects were auxotroph for pyruvate, which acted as electron acceptor to recycle NAD^+ by the action of lactate dehydrogenase [252]. This indicates, the loss of GOT1 could have reduced cellular aspartate and nucleotide synthesis, and therefore impacted proliferation. We were not able to measure the aspartate levels in *Got1*-deficient cells. However, we supplemented back the protonated form of aspartate (aspartic acid) and did not observe a relevant improvement of GOT1-associated defects (data not shown). This suggests, aspartate synthesis was not the main role of the GOT1 and the MAS in T cells. We could further investigate this, by supplementing back nucleotides in the cell culture.
Furthermore, the cited papers implied, the addition of exogenous pyruvate would enable the recycling of NAD^+ through the mechanism mentioned above. We have not measured the lactate or lactic acid secretion of *Got1*-deficient cells; however, we did not observe significant intracellular changes of lactate in our MS analysis (**Figure 4.16**). Furthermore, we observed no differences in the ECAR levels of *Got1*-deficient cells in minimal or complete medium, indicating similar lactate secretion. These findings do not support the role of pyruvate as an electron acceptor in *Got1*-deficient T cells. To investigate this assumption further, it would for example be interesting to measure, if pyruvate supplementation was sufficient to restore the NAD^+/NADH balance, and to investigate if the ECAR of *Got1*-deficient cells would increase upon an exogenous pyruvate pulse, which would reveal if pyruvate would be primary turned into lactate. Also, a pulse with $^{13}C_3$-pyruvate could help to understand the fate of pyruvate in *Got1*-deficient cells.

Potent rescue of Got1-deficient T cells was also achieved after supplementation with OAA. Besides the activity of pyruvate carboxylase, OAA can be formed from malate by malate dehydrogenase [253] in the TCA cycle, using NAD^+. Also, malate can be oxidized to OAA by succinate dehydrogenase, an enzyme of TCA cycle and complex II of the ETC, when succinate in not available [254-256]. OAA could therefore feed the TCA cycle, but could also be used in subsequent metabolic pathways, for example the synthesis of amino acids or to restore NADPH balance. It has also been appreciated, that phosphoenolpyruvate is a key metabolite

to sustain NFAT signaling in TILs [257]. It can be converted from OAA by phosphoenolpyruvate carboxykinase 1 to support the tumoricidal activity of TILs, elucidating another potential contribution of OAA to T cell function.

We also observed a potent rescue of *Got1*-dependent phenotypes after the addition of α-KG. This metabolite is a key component in the TCA cycle, and can directly be formed by transamination in the MAS, but also by alanine amino transferases, using pyruvate and glutamate in a reversible transamination reaction [258]. Also, isocitrate dehydrogenase in the TCA cycle and glutamate dehydrogenase can produce α-KG in an anaplerotic reaction [259]. Both reactions are NAD^+ dependent. The dependency of *Got1*-deficient T cells on exogenous α-KG, OAA and pyruvate indicated that *Got1*-deficient T cells were sensitive to the restriction of metabolites that directly or indirectly fed the TCA cycle. Therefore, one major role of GOT1 in T cells seem to be maintenance of TCA balance, and the integrity of the TCA cycle. Since most of the aforementioned reactions to replenish the TCA cycle are NAD^+ dependent, it was logical that the addition of the NAD^+ precursor NR rescued GOT1-associated phenotypes as well. Furthermore, this underlined the observation of reduced NAD^+/NADH ratio after GOT1-depletion. It would worthwhile to investigate, whether the addition of other TCA components that were not significantly changed in the MS profiling, for example succinate or fumarate, would contribute to rescue *Got1* deficiency as well. This would help to understand if the replenishment of TCA intermediates is a key feature of GOT1.

We have also observed that sodium lactate was able to partially rescue *Got1* deficiency. Lactate can be converted to pyruvate by the reverse reaction from lactate dehydrogenase, using NAD^+ as cofactor. It is possible that the need for pyruvate triggered lactate assimilation in the *Got1*-deficient cells, when no alternative metabolites were available. This finding was really surprising, given the negative impact of lactate and lactic acid on $CD8^+$ T cell function reported elsewhere [260].

Potential rescue *in vitro* was also met by supplementing non-dialyzed FBS. We could not determine the exact metabolite composition of FBS, but based on our results, we assume that it contains traces of pyruvate, OAA, α-KG and additional metabolites, and the presence of these substances reversed GOT1-mediated phenotypes. In line with this hypothesis, even though the exact composition of FBS is not known and highly batch-dependent, it has been observed before that pyruvate could substitute for FBS in hepatocyte and fibroblast cell cultures to ensure cell survival [261, 262]. Moreover, substitution of pyruvate, OAA or α-KG could all promote growth of isolated carcinosarcoma cells, grown in the presence of dialyzed FBS [263].

5.5. GOT1 maintains T cell effector functions and antagonizes T cell exhaustion

From the presented *in vitro* results, we learned that GOT1 affected the metabolic balance in deficient T cells. These intracellular changes had direct impact on antiviral and antitumoral effector responses and the development of T cell exhaustion.

5.5.1. GOT1 is required for effector but not memory T cell formation

We studied the role of GOT1 during T cell effector functions using LCMV infection models. The experimental co-adoptive transfer approach allowed us to study the $CD8^+$ T cell intrinsic roles of GOT1 by transfer of antigen-specific wildtype and deficient T cells to the same host. This strategy corrected for potential genetic variabilities of the host, the viral load and the inflammatory milieu and is commonly used to study T-cell intrinsic responses [264].

At 8 dpi, both used viral infection models (LCMV Arm and cl-13) induce similar antiviral responses regarding the frequency of effector cells and the expression of effector and memory markers [139]. However, while at 8-10 dpi during Arm infection, the antigen is already cleared and the cells start to undergo contraction, viremia is maintained in cl-13 infections. Still, this early timepoint allowed us to compare effector responses before memory or exhaustion of the cells developed.
Indeed, we observed overlapping phenotypes in both viral infection models (**Figure 4.7** and **Figure 4.9**). Wildtype cells outcompeted the *Got1*-deficient T cells already 8 days after viral infection, independently of the viral strain, and exhibited greater effector potential. This indicated a need of functional GOT1 for mounting effector responses, independent from the disease model. Based on our *in vitro* observations, showing that *Got1*-deficient T cells had increased levels of apoptotic cells, we reasoned that the altered donor cell ratios could be a result of decreased viability or decreased proliferation of *Got1*-deficient T cells *in vivo.*

It should be noted that even though the observed phenotypes were similar, the impact was greater in *Got1*-deficient T cells after LCMV cl-13 infection, indicating the severity of GOT1-associated phenotypes correlated with the presence of antigen, similar to our *in vitro* analysis. Another possible explanation for the exacerbated phenotypes in *Got1*-deficient T cells might be the enhanced dependency on the help by $CD4^+$ T cells. In LCMV cl-13 infection, we depleted $CD4^+$ T cells by injection of anti-CD4 antibodies, to exacerbate exhaustion and prevent the mice from viral clearance, which is routinely done in this infection model [265].

At 8 dpi, we did not observe differences in transcription factor expression in *Got1*-deficient T cells after LCMV Arm expression. Transcription factors were altered during LCMV cl-13 infection, and the potential results are discussed below.

Following GOT1-associated phenotypes to 30 dpi after LCMV Arm infection, we discovered that memory formation was independent of GOT1 (**Figure 4.8**). After a contraction phase, the amount of residual donor cells was not significantly different between wildtype and *Got1*-deficient cells and the expression of memory markers (for example IL-7Rα) was comparable in both cell types. This complemented our hypothesis, that antigen persistence correlates with the severity of phenotypes caused by the loss of GOT1. Furthermore, we hypothesized that GOT1 was especially important during nutrient restriction, and we did not expect the cells to be nutrient restricted during memory formation.
Still, a significant decrease in effector cytokine secretion was maintained during *in vitro* recall with the cognate antigen gp33. The loss of cytokine expression was a fundamental phenotype and observed in all investigated disease models, including tumor models. This cumulative evidence showed that GOT1 might be essential to mediate cytokine expression. An explanation for this could be altered posttranscriptional and epigenetic regulation due to the altered use of metabolic enzymes and an overall altered metabolic profile. For example, *Ifng* mRNA has an ARE-element, which can be bound by GAPDH during cell quiescence to suppress transcription. After increased metabolic demands, GAPDH releases the mRNA to enable glycolysis and *Ifng* transcription [266, 267]. A similar relationship between GAPDH and *Tnfa* mRNA was observed in monocytes [268]. Also, a LDHA-dependent increase of gene acetylation has been shown to promote *Ifng* transcription [269].

5.5.2. GOT1 antagonizes T cell exhaustion

T cell exhaustion is accompanied by severe metabolic and mitochondrial alterations, such as loss of ΔΨm and aberrant expression of ROS in T cells during chronic viral infections and in TILs [157, 158, 270-272].

We compared the role of GOT1 in T cell exhaustion following a chronic viral infection (LCMV cl-13) and in melanoma tumors and found overlapping but also complementary phenotypes.
We followed the progression of exhaustion induced by LCMV cl-13 and sampled at 8 dpi and 21 dpi. At 8 dpi, T cells are not yet defined as exhausted, even though they express inhibitory receptors like TIGIT and PD-1, which were shown to be rapidly upregulated after TCR stimulation, and can be interpreted as activation markers at this stage [273]. We observed that already after 8 dpi *Got1*-deficient cells reduced the expression of inhibitory receptors TIGIT and PD-1, which indicated a decreased stimulation of the cells. Furthermore, we observed a

reciprocal expression of T-BET and PD-1 in *Got1*-deficient T cells. This observation could be explained by a report showing that T-BET can suppress PD-1 transcription [274]. Also, T-BET was long believed to be the key transcription factor of IFNγ, which would oppose the observed reduction of IFNγ expression. However, it was acknowledged, that T-BET is required for lineage commitment and IFNγ expression in T_H1 cells, while T-BET deficient $CD8^+$ cells could express IFNγ independent from T-BET [275]. Therefore, the observed reduction of effector cytokines was probably uncoupled from the expression of T-BET and inhibitory receptors.
A decrease of TCF1 and EOMES in *Got1*-deficient cells was detected at 8 dpi following LCMV cl-13 infection. The co-expression of these markers defines a small subset of stem cell-like T cells, that are required to maintain residual effector functions during the progression of exhaustion [145, 147]. This early defect of the stem cell-like T cell pool could explain the exacerbated phenotype we observed following LCMV cl-13 to 21 dpi, when T cell exhaustion was established, which was visible for example by a severe decrease of total IFNγ expression. We observed a severe depletion of *Got1*-deficient T cells, indicating the cells could not be maintained during chronic antigen presence. This could result from the lack of $TCF1^+EOMES^+$ non-exhausted stem cell-like precursors, which were already reduced at 8 dpi. The observation was supported by a maintained reduced TCF1 expression at 21 dpi (**Figure 4.10**).
TIGIT was still significantly reduced at 21 dpi in *Got1*-deficient cells. This finding was surprising, given the inhibitory role of TIGIT during exhaustion. Decreased TIGIT expression would indicate a less-exhausted phenotype, but we observed that the residual cytokine secretion of the cells was still lower compared to the wildtype counterparts. We concluded that TIGIT expression was independent from cytokine secretion in this context. Interestingly, even though a high T-BET expression was maintained at 21 dpi, PD-1 was no longer downregulated upon GOT1 deletion. We cannot fully explain this seemingly contradictory results. PD-1 expression could be delayed and therefore only highly expressed at the later timepoint in *Got1*-deficent cells. Another possibility would be selective pressure upon high PD-1 expressing cells, resulting in reduced viability in the absence of GOT1.

We have shown in our *in vitro* studies, that GOT1-associated phenotypes correlated with nutrient depletion. It is not clear whether the metabolite levels during chronic viral infections decrease. The tremendous expansion of immune cells during the T cell expansion phase of viral infections might lead to a transient nutrient depletion and competition for nutrients among the immune cell subsets [276]. Also, as mentioned before, *in vitro* cultivation in complete medium does not recapitulate the physiological environment, and proliferating T cells from LCMV infected mice could already be starved in physiological nutrient conditions, comparted to the rich complete medium, and therefore show GOT1-associated defects.

Using syngeneic melanoma tumor models that expressed the gp33 antigen to be recognized by the adoptively transferred donor cells, we observed a more severe exhaustion in *Got1*-deficient TILs. First, it should be noted that overall similar phenotypes in YUMM-gp33 and B16-gp33 tumors were observed, revealing the GOT1-associated phenotypes were stable for antigen-dependent anti-tumor immune responses (**Figure 4.12** to **Figure 4.15**). Similar to LCMV cl-13 and LCMV Arm responses, we observed a decrease in cell numbers and cytokine secretion in *Got1*-deficient T cells. The reduction of cell frequency and effector potential resulted in enhanced tumor progression after adoptive transfer of *Got1*-deficient cells (**Figure 4.11**). As discussed above, this indicated a universal role of GOT1 for cytokine expression and in maintenance of effector T cells.
We recovered significantly less *Got1*-deficient donor cells in spleen and tumor. On first glance, this was surprising, given the T cells from the spleen showed decreased inhibitory receptor expression and sustained effector cytokine secretion, indicating the spleen residing cells were not exhausted and probably also less activated, and therefore less dependent on GOT1. We reasoned that, because of the failed cell persistence of *Got1*-deficient cells in the tumors, splenic T cells served as a reservoir that was rapidly depleted to refill the TIL pool in the tumor. We observed also a severe decrease of TCF1 and EOMES expressing *Got1*-deficient cells in the spleen, indicating a loss of the stem cell-like T cell compartment. This could further explain the low cell numbers in spleen and tumor, as the stem cell-like T cells give rise to effector cells.

In contrast to our observation in the LCMV cl-13 model, inhibitory receptor expression was strongly enhanced in *Got1*-deficient TILs, indicating a more advanced exhaustion state of the cells. These results are seemingly contradictory and could be explained by disease model-specific effects: LCMV cl-13 results in a systemic infection throughout the whole body and therefore affects all antigen specific T cells. In contrast, tumors mainly impact infiltrating cells in the TME. We observed that GOT1 expression correlated positively with PD-1 in human colon cancer cells. This correlation indicates that cells expressing high levels of inhibitory receptors are also more dependent on GOT1 to maintain their metabolic fitness and long-term persistence. Thus, inhibitory receptor positive cells lacking GOT1 are more sensitive to the above-mentioned phenotypes and apoptosis. As mentioned before, we have observed a large pool of inhibitory receptor negative wildtype donor cells in the spleen of tumor bearing mice, that were almost completely depleted in *Got1*-deficient cells. The depletion could have originated from recruitment of the cells to the tumors. Following LCMV cl-13 infection, we observed only a small fraction of inhibitory receptor negative wildtype cells, indicating only a small fraction of cells was not activated and could serve as reservoir. Therefore, in the LCMV cl-13 model, *Got1*-deficient mice had problems to sustain inhibitory receptor positive cells. This could explain the reciprocal inhibitory receptor expression we observed in the different models.

Furthermore, the TME is known to be severely nutrient depleted, and also resides many other immune cells and immunosuppressive cells [277] that might have affected GOT1-associated phenotypes additionally.

It was remarkable, that supplementation of pyruvate and α-KG alleviated GOT1 dependent phenotypes in TILs after adoptive transfer, increased TIL cell numbers, effector function and reduced inhibitory receptor expression (**Figure 4.24** and **Figure 4.25**). This supported the meaning of these metabolites for T cell function when GOT1 was absent and underlined the role of GOT1 in TIL effector function and metabolite homeostasis. However, it is unclear to this point, how the transient exposure during the initial T cell priming could enhance T cell function even after adoptive transfer, when cells were facing the nutrient restricted TME. It is possible, GOT1 was needed to establish an early transcriptional or epigenetic profile to enable full effector potential of the cells. In line with this theory is the observation, that GOT1 was required for the accumulation of 2-hydroxyglutarate, which suppressed T_{Reg} proliferation by hypermethylation of the *Foxp3* locus [188]. A transcriptional or epigenetic analysis of the primed and pre-treated cells or recovered TILs could help to answer this question.

If we combine the observed experimental results and take the *in vitro* observations into account, the *in vivo* results of *Got1*-deficient T cells supported the theory, that GOT1 was required to initiate and maintain effector responses during chronic antigenic stimuli by providing T cells with enhanced metabolic stability and for decreasing the dependency on extracellular nutrients.

5.6. Conclusion

The presented thesis characterized the MAS enzyme GOT1 in antiviral and antitumoral T cell responses. GOT1 was shown to be expressed in T cells after antigen specific TCR stimulation. It was required for the effector, but not memory differentiation following acute antiviral infection. During the development of T cell exhaustion induced by chronic viral infection and in a melanoma model, GOT1 was shown to be required for the maintenance of effector responses and cytokine secretion. GOT1 supported the maintenance of a stem cell-like T cell compartment to sustain long term residual immune responses during chronic antigen stimulation. GOT1 correlated with the expression of inhibitory receptors in human tumor samples, and we postulate that inhibitory receptor expressing cells are more dependent on the expression of GOT1. Based on the presented data, we assume that GOT1 antagonizes T cell exhaustion and desensitizes T cells to nutrient restriction, as summarized in **Figure 5.1**. Nutrient restriction combined with GOT1 deficiency resulted in excessive ROS production,

depleted TCA cycle metabolites, reduced ΔΨm, decreased the NAD^+/NADH ratio and led to reduced OXPHOS levels, but did not affect glycolysis. The associated phenotypes resulted in apoptosis and might have impacted cellular proliferation. A panel of TCA cycle intermediates, NAD^+ precursor or antioxidants corrected or partially corrected GOT1 deficiency and had positive outcome on tumor size and TIL effector functions after adoptive transfer, although the exact mechanism of action is not fully clear to this time.

These findings underline the importance of metabolism and mitochondrial function for T cell effector responses and T cell exhaustion. Our presented data shed light on GOT1-associated defects, but to this time it is not clear, how GOT1 could regulate the expression of inhibitory receptors, effector cytokines or transcription factors. It should be noted, GOT1 might influence additional key epigenetic molecules and cofactors, apart from 2-hydroxyglutarate. Interestingly most GOT1-associated molecules investigated in this study, for example NAD^+, α-KG, ROS and acetyl-CoA (which can be derived from pyruvate) are metabolites that can be used as cofactors for chromatin remodeling enzymes [278, 279]. Therefore, GOT1 could be required to maintain epigenetic effector T cell signatures. The altered regulation of effector cytokine expression and inhibitory receptors could therefore be a result of altered transcriptional activation and gene accessibility. It would certainly be interesting to assess the potential effect on GOT1 deficiency on the epigenome.

Initially, we expected that GOT1, due to its correlation to PD-1 expression, would promote T cell exhaustion and could therefore serve as a druggable metabolic checkpoint. However, our results indicate that GOT1 protects T cells from apoptosis during prolonged antigen exposure and nutrient limitations, therefore supporting metabolic health even under difficult nutrient environments, for example the TME. Several studies discussed above use the small molecule inhibitor AOA to target the MAS by inhibiting GOT1 and its isozyme GOT2 in tumor cells, since for example pancreatic cancer cells were shown to depend on MAS function for proliferation and growth. The aim of these studies was to sensitize these tumors to chemotherapies, by disrupting their metabolic fitness. Our results show, that GOT1 and MAS inhibition could have a severe impact on the survival and effector function of CTLs, especially during antitumor responses. As mentioned before, GOT1 inhibition was also shown to differentiate pathogenic T_H17 cells back to T_{Reg}. An accumulation of T_{Reg} in the TME could further exacerbate TIL dysfunction and therefore would impair anti-tumor T cell responses even more. Therefore, a clinical application of these inhibitors would have to be closely monitored for potential immune-related side effects, to prevent that tumors would benefit from the resulting impaired TIL function. On the other hand, GOT1 might therefore be a suitable target to dampen immune responses during the development of autoimmune diseases. Then, the supplementation of

AOA would not only increase the suppressive potential of T_{Reg}, but also impact the autoreactive T cells directly.

In this work, we have focused on the investigation of GOT1 in $CD8^+$ cells. Since $CD4^+$ T cells also expressed GOT1 (**Figure 4.1**), and some GOT1-associated phenotypes have been suggested in T_{Reg} (see 1.4.1) it would be interesting to investigate, if GOT1 impacts the metabolic integrity and effector function of $CD4^+$ T cells as well. We have started to investigate the role of GOT1 in the $CD4^+$ T cell compartment by analyzing the organic acid composition analogous to 4.8, and found that in $CD4^+$ T cells were also significantly depleted in pyruvate (**Supplementary Figure 2**). Thus, we might observe overlapping phenotypes in both T cell compartments, and it would be exciting to study GOT1 in other T cell and immune cell subsets in the future.

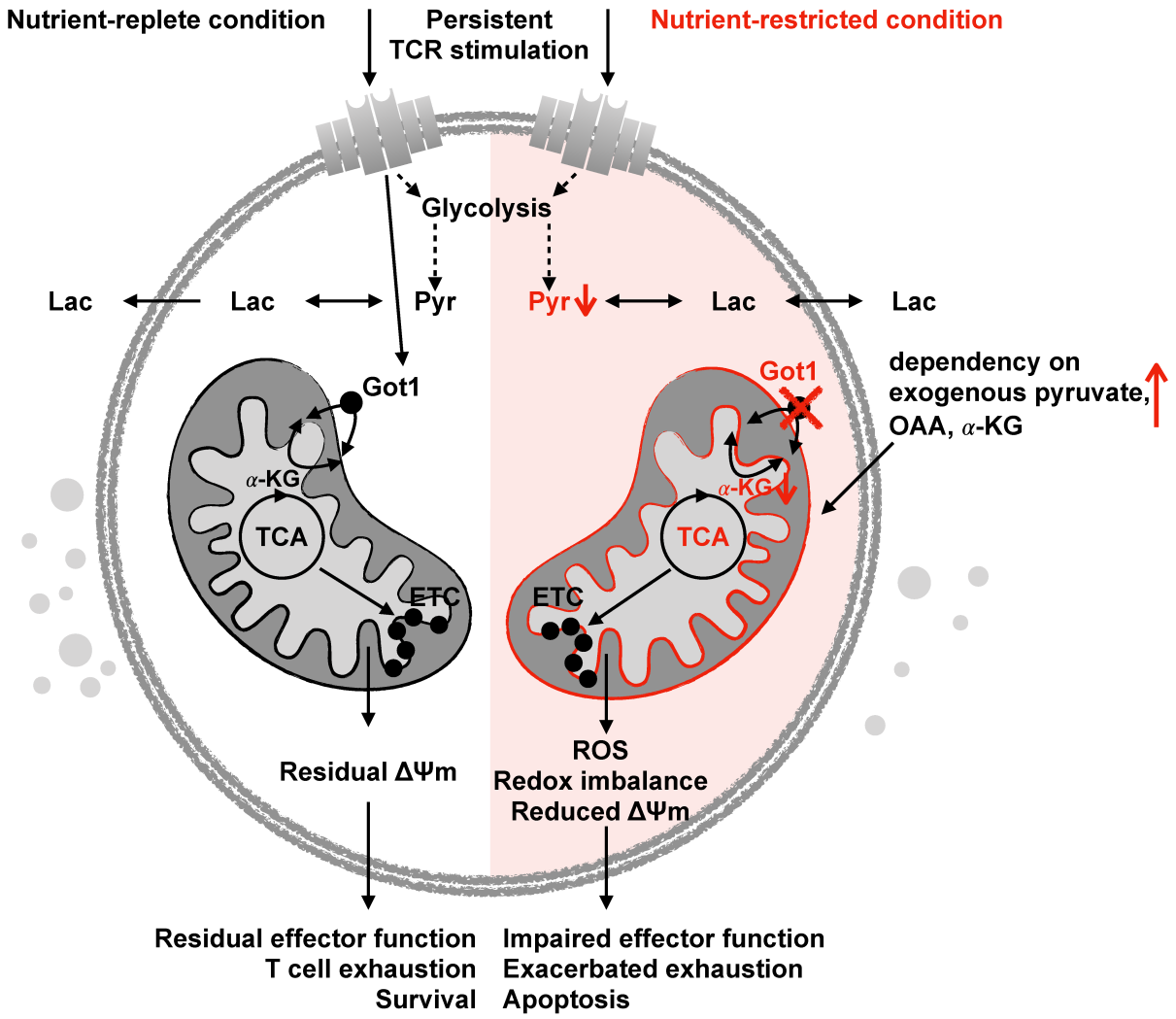

Figure 5.1: GOT1 maintains metabolic fitness to antagonize T cell exhaustion. *In a low nutrient environment, the deficiency of GOT1 results in mitochondrial dysfunction by increased ROS and redox stress, and increases the dependency on extracellular availability of pyruvate, OAA, α-KG and others. As a result, GOT1 deficiency leads to impaired effector function, exacerbated T cell exhaustion and apoptosis.*

References

1. Janeway, C.A., Jr., *The immune system evolved to discriminate infectious nonself from noninfectious self.* Immunol Today, 1992. **13**(1): p. 11-6.
2. Travis, J., *Origins. On the origin of the immune system.* Science, 2009. **324**(5927): p. 580-2.
3. Jones, J.D. and J.L. Dangl, *The plant immune system.* Nature, 2006. **444**(7117): p. 323-9.
4. Kenneth Murphy, P.T., and Mark Walport, *Janeway's Immunobiology, 7th Edition.* 2009.
5. White, S.H., W.C. Wimley, and M.E. Selsted, *Structure, function, and membrane integration of defensins.* Curr Opin Struct Biol, 1995. **5**(4): p. 521-7.
6. Sarma, J.V. and P.A. Ward, *The complement system.* Cell Tissue Res, 2011. **343**(1): p. 227-35.
7. Akira, S., S. Uematsu, and O. Takeuchi, *Pathogen recognition and innate immunity.* Cell, 2006. **124**(4): p. 783-801.
8. El-Zayat, S.R., H. Sibaii, and F.A. Mannaa, *Toll-like receptors activation, signaling, and targeting: an overview.* Bulletin of the National Research Centre, 2019. **43**(1): p. 187.
9. Franchi, L., et al., *Function of Nod-like receptors in microbial recognition and host defense.* Immunol Rev, 2009. **227**(1): p. 106-28.
10. Janeway, C.A., Jr. and R. Medzhitov, *Innate immune recognition.* Annu Rev Immunol, 2002. **20**: p. 197-216.
11. Lanier, L.L., *NK cell receptors.* Annu Rev Immunol, 1998. **16**: p. 359-93.
12. Bennett, M.S., J.L. Round, and D.T. Leung, *Innate-like lymphocytes in intestinal infections.* Curr Opin Infect Dis, 2015. **28**(5): p. 457-63.
13. Osmond, D.G., *B cell development in the bone marrow.* Semin Immunol, 1990. **2**(3): p. 173-80.
14. Koch, U. and F. Radtke, *Mechanisms of T cell development and transformation.* Annu Rev Cell Dev Biol, 2011. **27**: p. 539-62.
15. Miller, J.F., *Immunological function of the thymus.* Lancet, 1961. **2**(7205): p. 748-9.
16. LeBien, T.W. and T.F. Tedder, *B lymphocytes: how they develop and function.* Blood, 2008. **112**(5): p. 1570-80.
17. Martensson, I.L., et al., *The pre-B cell receptor checkpoint.* FEBS Lett, 2010. **584**(12): p. 2572-9.
18. Klein, L., et al., *Positive and negative selection of the T cell repertoire: what thymocytes see (and don't see).* Nat Rev Immunol, 2014. **14**(6): p. 377-91.
19. Starr, T.K., S.C. Jameson, and K.A. Hogquist, *Positive and negative selection of T cells.* Annu Rev Immunol, 2003. **21**: p. 139-76.
20. Friess, M.D., K. Pluhackova, and R.A. Bockmann, *Structural Model of the mIgM B-Cell Receptor Transmembrane Domain From Self-Association Molecular Dynamics Simulations.* Front Immunol, 2018. **9**: p. 2947.
21. Tonegawa, S., et al., *Evidence for somatic generation of antibody diversity.* Proc Natl Acad Sci U S A, 1974. **71**(10): p. 4027-31.
22. Cooper, M.D. and M.N. Alder, *The evolution of adaptive immune systems.* Cell, 2006. **124**(4): p. 815-22.
23. Suan, D., C. Sundling, and R. Brink, *Plasma cell and memory B cell differentiation from the germinal center.* Curr Opin Immunol, 2017. **45**: p. 97-102.

24. Medzhitov, R. and C.A. Janeway, Jr., *Innate immunity: impact on the adaptive immune response.* Curr Opin Immunol, 1997. **9**(1): p. 4-9.
25. Wieczorek, M., et al., *Major Histocompatibility Complex (MHC) Class I and MHC Class II Proteins: Conformational Plasticity in Antigen Presentation.* Front Immunol, 2017. **8**: p. 292.
26. Leahy, D.J., *A structural view of CD4 and CD8.* FASEB J, 1995. **9**(1): p. 17-25.
27. Golubovskaya, V. and L. Wu, *Different Subsets of T Cells, Memory, Effector Functions, and CAR-T Immunotherapy.* Cancers (Basel), 2016. **8**(3).
28. Zhu, J. and W.E. Paul, *CD4 T cells: fates, functions, and faults.* Blood, 2008. **112**(5): p. 1557-69.
29. Zambrano-Zaragoza, J.F., et al., *Th17 cells in autoimmune and infectious diseases.* Int J Inflam, 2014. **2014**: p. 651503.
30. Fontenot, J.D., M.A. Gavin, and A.Y. Rudensky, *Foxp3 programs the development and function of CD4+CD25+ regulatory T cells.* Nat Immunol, 2003. **4**(4): p. 330-6.
31. Vignali, D.A., L.W. Collison, and C.J. Workman, *How regulatory T cells work.* Nat Rev Immunol, 2008. **8**(7): p. 523-32.
32. Chattopadhyay, S., N.G. Chakraborty, and B. Mukherji, *Regulatory T cells and tumor immunity.* Cancer Immunol Immunother, 2005. **54**(12): p. 1153-61.
33. Osinska, I., K. Popko, and U. Demkow, *Perforin: an important player in immune response.* Cent Eur J Immunol, 2014. **39**(1): p. 109-15.
34. Afonina, I.S., S.P. Cullen, and S.J. Martin, *Cytotoxic and non-cytotoxic roles of the CTL/NK protease granzyme B.* Immunol Rev, 2010. **235**(1): p. 105-16.
35. Schoenborn, J.R. and C.B. Wilson, *Regulation of interferon-gamma during innate and adaptive immune responses.* Adv Immunol, 2007. **96**: p. 41-101.
36. Badovinac, V.P. and J.T. Harty, *Intracellular staining for TNF and IFN-gamma detects different frequencies of antigen-specific CD8(+) T cells.* J Immunol Methods, 2000. **238**(1-2): p. 107-17.
37. Lalvani, A., et al., *Rapid effector function in CD8+ memory T cells.* J Exp Med, 1997. **186**(6): p. 859-65.
38. Veiga-Fernandes, H., et al., *Response of naive and memory CD8+ T cells to antigen stimulation in vivo.* Nat Immunol, 2000. **1**(1): p. 47-53.
39. Russ, B.E., et al., *T cell immunity as a tool for studying epigenetic regulation of cellular differentiation.* Front Genet, 2013. **4**: p. 218.
40. Kaech, S.M., E.J. Wherry, and R. Ahmed, *Effector and memory T-cell differentiation: implications for vaccine development.* Nat Rev Immunol, 2002. **2**(4): p. 251-62.
41. Gray, J.I., L.M. Westerhof, and M.K.L. MacLeod, *The roles of resident, central and effector memory CD4 T-cells in protective immunity following infection or vaccination.* Immunology, 2018.
42. Mackay, L.K., et al., *The developmental pathway for CD103(+)CD8+ tissue-resident memory T cells of skin.* Nat Immunol, 2013. **14**(12): p. 1294-301.
43. Surh, C.D. and J. Sprent, *Homeostasis of naive and memory T cells.* Immunity, 2008. **29**(6): p. 848-62.
44. Cui, G., et al., *IL-7-Induced Glycerol Transport and TAG Synthesis Promotes Memory CD8+ T Cell Longevity.* Cell, 2015. **161**(4): p. 750-61.
45. Sallusto, F., J. Geginat, and A. Lanzavecchia, *Central memory and effector memory T cell subsets: function, generation, and maintenance.* Annu Rev Immunol, 2004. **22**: p. 745-63.

46. Schenkel, J.M. and D. Masopust, *Tissue-resident memory T cells.* Immunity, 2014. **41**(6): p. 886-97.
47. Liu, Y., C. Ma, and N. Zhang, *Tissue-Specific Control of Tissue-Resident Memory T Cells.* Crit Rev Immunol, 2018. **38**(2): p. 79-103.
48. Kumar, B.V., et al., *Human Tissue-Resident Memory T Cells Are Defined by Core Transcriptional and Functional Signatures in Lymphoid and Mucosal Sites.* Cell Rep, 2017. **20**(12): p. 2921-2934.
49. Virgin, H.W., E.J. Wherry, and R. Ahmed, *Redefining chronic viral infection.* Cell, 2009. **138**(1): p. 30-50.
50. Blumberg, R.S., et al., *Structure of the T-cell antigen receptor: evidence for two CD3 epsilon subunits in the T-cell receptor-CD3 complex.* Proc Natl Acad Sci U S A, 1990. **87**(18): p. 7220-4.
51. Clevers, H., et al., *The T cell receptor/CD3 complex: a dynamic protein ensemble.* Annu Rev Immunol, 1988. **6**: p. 629-62.
52. Reth, M., *Antigen receptor tail clue.* Nature, 1989. **338**(6214): p. 383-4.
53. Letourneur, F. and R.D. Klausner, *Activation of T cells by a tyrosine kinase activation domain in the cytoplasmic tail of CD3 epsilon.* Science, 1992. **255**(5040): p. 79-82.
54. Engelman, D.M., *Electrostatic fasteners hold the T cell receptor-CD3 complex together.* Mol Cell, 2003. **11**(1): p. 5-6.
55. Curtsinger, J.M. and M.F. Mescher, *Inflammatory cytokines as a third signal for T cell activation.* Curr Opin Immunol, 2010. **22**(3): p. 333-40.
56. Curtsinger, J.M., et al., *Inflammatory cytokines provide a third signal for activation of naive CD4+ and CD8+ T cells.* J Immunol, 1999. **162**(6): p. 3256-62.
57. Arenas-Ramirez, N., J. Woytschak, and O. Boyman, *Interleukin-2: Biology, Design and Application.* Trends Immunol, 2015. **36**(12): p. 763-777.
58. Weiss, A. and D.R. Littman, *Signal transduction by lymphocyte antigen receptors.* Cell, 1994. **76**(2): p. 263-74.
59. Iwashima, M., et al., *Sequential interactions of the TCR with two distinct cytoplasmic tyrosine kinases.* Science, 1994. **263**(5150): p. 1136-9.
60. van Oers, N.S. and A. Weiss, *The Syk/ZAP-70 protein tyrosine kinase connection to antigen receptor signalling processes.* Semin Immunol, 1995. **7**(4): p. 227-36.
61. Clements, J.L., et al., *Integration of T cell receptor-dependent signaling pathways by adapter proteins.* Annu Rev Immunol, 1999. **17**: p. 89-108.
62. Cockcroft, S. and G.M. Thomas, *Inositol-lipid-specific phospholipase C isoenzymes and their differential regulation by receptors.* Biochem J, 1992. **288 (Pt 1)**: p. 1-14.
63. Crabtree, G.R., *Generic signals and specific outcomes: signaling through Ca2+, calcineurin, and NF-AT.* Cell, 1999. **96**(5): p. 611-4.
64. Ebinu, J.O., et al., *RasGRP links T-cell receptor signaling to Ras.* Blood, 2000. **95**(10): p. 3199-203.
65. Foletta, V.C., D.H. Segal, and D.R. Cohen, *Transcriptional regulation in the immune system: all roads lead to AP-1.* J Leukoc Biol, 1998. **63**(2): p. 139-52.
66. Isakov, N. and A. Altman, *Protein kinase C(theta) in T cell activation.* Annu Rev Immunol, 2002. **20**: p. 761-94.
67. August, A. and B. Dupont, *Activation of src family kinase lck following CD28 crosslinking in the Jurkat leukemic cell line.* Biochem Biophys Res Commun, 1994. **199**(3): p. 1466-73.
68. August, A. and B. Dupont, *CD28 of T lymphocytes associates with phosphatidylinositol 3-kinase.* Int Immunol, 1994. **6**(5): p. 769-74.

69. Waickman, A.T. and J.D. Powell, *mTOR, metabolism, and the regulation of T-cell differentiation and function.* Immunol Rev, 2012. **249**(1): p. 43-58.
70. Wang, X., et al., *Regulation of PKC-theta function by phosphorylation in T cell receptor signaling.* Front Immunol, 2012. **3**: p. 197.
71. Schneider, H., et al., *T cell antigen CD28 binds to the GRB-2/SOS complex, regulators of p21ras.* Eur J Immunol, 1995. **25**(4): p. 1044-50.
72. Harding, F.A., et al., *CD28-mediated signalling co-stimulates murine T cells and prevents induction of anergy in T-cell clones.* Nature, 1992. **356**(6370): p. 607-9.
73. Powell, J.D., et al., *Molecular regulation of interleukin-2 expression by CD28 co-stimulation and anergy.* Immunol Rev, 1998. **165**: p. 287-300.
74. Quinn, K.M., et al., *The clock is ticking: the impact of ageing on T cell metabolism.* Clin Transl Immunology, 2019. **8**(11): p. e01091.
75. MacIver, N.J., R.D. Michalek, and J.C. Rathmell, *Metabolic regulation of T lymphocytes.* Annu Rev Immunol, 2013. **31**: p. 259-83.
76. De Boer, R.J., et al., *Recruitment times, proliferation, and apoptosis rates during the CD8(+) T-cell response to lymphocytic choriomeningitis virus.* J Virol, 2001. **75**(22): p. 10663-9.
77. Menk, A.V., et al., *Early TCR Signaling Induces Rapid Aerobic Glycolysis Enabling Distinct Acute T Cell Effector Functions.* Cell Rep, 2018. **22**(6): p. 1509-1521.
78. Warburg, O., *On the origin of cancer cells.* Science, 1956. **123**(3191): p. 309-14.
79. O'Sullivan, D., et al., *Memory CD8(+) T cells use cell-intrinsic lipolysis to support the metabolic programming necessary for development.* Immunity, 2014. **41**(1): p. 75-88.
80. Carr, E.L., et al., *Glutamine uptake and metabolism are coordinately regulated by ERK/MAPK during T lymphocyte activation.* J Immunol, 2010. **185**(2): p. 1037-44.
81. Zhang, L.J. and P. Romero, *Metabolic Control of CD8(+) T Cell Fate Decisions and Antitumor Immunity.* Trends in Molecular Medicine, 2018. **24**(1): p. 30-48.
82. Mills, E.L., B. Kelly, and L.A.J. O'Neill, *Mitochondria are the powerhouses of immunity.* Nature Immunology, 2017. **18**(5): p. 488-498.
83. Ma, E.H., et al., *Metabolic Profiling Using Stable Isotope Tracing Reveals Distinct Patterns of Glucose Utilization by Physiologically Activated CD8(+) T Cells.* Immunity, 2019. **51**(5): p. 856-+.
84. Pan, Y., et al., *Survival of tissue-resident memory T cells requires exogenous lipid uptake and metabolism.* Nature, 2017. **543**(7644): p. 252-256.
85. van der Windt, G.J., et al., *Mitochondrial respiratory capacity is a critical regulator of CD8+ T cell memory development.* Immunity, 2012. **36**(1): p. 68-78.
86. van der Windt, G.J., et al., *CD8 memory T cells have a bioenergetic advantage that underlies their rapid recall ability.* Proc Natl Acad Sci U S A, 2013. **110**(35): p. 14336-41.
87. Gubser, P.M., et al., *Rapid effector function of memory CD8+ T cells requires an immediate-early glycolytic switch.* Nat Immunol, 2013. **14**(10): p. 1064-72.
88. van der Windt, G.J.W., et al., *CD8 memory T cells have a bioenergetic advantage that underlies their rapid recall ability.* Proceedings of the National Academy of Sciences of the United States of America, 2013. **110**(35): p. 14336-14341.
89. Wang, R., et al., *The transcription factor Myc controls metabolic reprogramming upon T lymphocyte activation.* Immunity, 2011. **35**(6): p. 871-82.
90. Inoki, K., et al., *TSC2 is phosphorylated and inhibited by Akt and suppresses mTOR signalling.* Nat Cell Biol, 2002. **4**(9): p. 648-57.
91. Schalm, S.S., et al., *TOS motif-mediated raptor binding regulates 4E-BP1 multisite phosphorylation and function.* Curr Biol, 2003. **13**(10): p. 797-806.

92. Saxton, R.A. and D.M. Sabatini, *mTOR Signaling in Growth, Metabolism, and Disease.* Cell, 2017. **168**(6): p. 960-976.
93. O'Neill, L.A. and D.G. Hardie, *Metabolism of inflammation limited by AMPK and pseudo-starvation.* Nature, 2013. **493**(7432): p. 346-55.
94. McLane, L.M., M.S. Abdel-Hakeem, and E.J. Wherry, *CD8 T Cell Exhaustion During Chronic Viral Infection and Cancer.* Annu Rev Immunol, 2019. **37**: p. 457-495.
95. Blank, C.U., et al., *Defining 'T cell exhaustion'.* Nat Rev Immunol, 2019. **19**(11): p. 665-674.
96. Zajac, A.J., et al., *Viral immune evasion due to persistence of activated T cells without effector function.* J Exp Med, 1998. **188**(12): p. 2205-13.
97. Moskophidis, D., et al., *Virus persistence in acutely infected immunocompetent mice by exhaustion of antiviral cytotoxic effector T cells.* Nature, 1993. **362**(6422): p. 758-61.
98. Doherty, P.C., *Immune exhaustion: driving virus-specific CD8+ T cells to death.* Trends Microbiol, 1993. **1**(6): p. 207-9.
99. Lechner, F., et al., *Analysis of successful immune responses in persons infected with hepatitis C virus.* J Exp Med, 2000. **191**(9): p. 1499-512.
100. Gruener, N.H., et al., *Sustained dysfunction of antiviral CD8+ T lymphocytes after infection with hepatitis C virus.* J Virol, 2001. **75**(12): p. 5550-8.
101. Ye, B., et al., *T-cell exhaustion in chronic hepatitis B infection: current knowledge and clinical significance.* Cell Death Dis, 2015. **6**: p. e1694.
102. Goepfert, P.A., et al., *A significant number of human immunodeficiency virus epitope-specific cytotoxic T lymphocytes detected by tetramer binding do not produce gamma interferon.* J Virol, 2000. **74**(21): p. 10249-55.
103. Shankar, P., et al., *Impaired function of circulating HIV-specific CD8(+) T cells in chronic human immunodeficiency virus infection.* Blood, 2000. **96**(9): p. 3094-101.
104. Kostense, S., et al., *High viral burden in the presence of major HIV-specific CD8(+) T cell expansions: evidence for impaired CTL effector function.* Eur J Immunol, 2001. **31**(3): p. 677-86.
105. Day, C.L., et al., *PD-1 expression on HIV-specific T cells is associated with T-cell exhaustion and disease progression.* Nature, 2006. **443**(7109): p. 350-4.
106. Trautmann, L., et al., *Upregulation of PD-1 expression on HIV-specific CD8+ T cells leads to reversible immune dysfunction.* Nat Med, 2006. **12**(10): p. 1198-202.
107. Mumprecht, S., et al., *Programmed death 1 signaling on chronic myeloid leukemia-specific T cells results in T-cell exhaustion and disease progression.* Blood, 2009. **114**(8): p. 1528-36.
108. Schietinger, A., et al., *Tumor-Specific T Cell Dysfunction Is a Dynamic Antigen-Driven Differentiation Program Initiated Early during Tumorigenesis.* Immunity, 2016. **45**(2): p. 389-401.
109. Baitsch, L., et al., *Exhaustion of tumor-specific CD8(+) T cells in metastases from melanoma patients.* J Clin Invest, 2011. **121**(6): p. 2350-60.
110. Lee, P.P., et al., *Characterization of circulating T cells specific for tumor-associated antigens in melanoma patients.* Nat Med, 1999. **5**(6): p. 677-85.
111. Ahmadzadeh, M., et al., *Tumor antigen-specific CD8 T cells infiltrating the tumor express high levels of PD-1 and are functionally impaired.* Blood, 2009. **114**(8): p. 1537-44.

112. Fourcade, J., et al., *Upregulation of Tim-3 and PD-1 expression is associated with tumor antigen-specific CD8+ T cell dysfunction in melanoma patients.* J Exp Med, 2010. **207**(10): p. 2175-86.
113. Gandhi, M.K., et al., *Expression of LAG-3 by tumor-infiltrating lymphocytes is coincident with the suppression of latent membrane antigen-specific CD8+ T-cell function in Hodgkin lymphoma patients.* Blood, 2006. **108**(7): p. 2280-9.
114. Zhang, Y., et al., *Programmed death-1 upregulation is correlated with dysfunction of tumor-infiltrating CD8+ T lymphocytes in human non-small cell lung cancer.* Cell Mol Immunol, 2010. **7**(5): p. 389-95.
115. Crawford, A., et al., *Molecular and transcriptional basis of CD4(+) T cell dysfunction during chronic infection.* Immunity, 2014. **40**(2): p. 289-302.
116. Fuller, M.J. and A.J. Zajac, *Ablation of CD8 and CD4 T cell responses by high viral loads.* J Immunol, 2003. **170**(1): p. 477-86.
117. Wherry, E.J., et al., *Viral persistence alters CD8 T-cell immunodominance and tissue distribution and results in distinct stages of functional impairment.* J Virol, 2003. **77**(8): p. 4911-27.
118. Brunet, J.F., et al., *A new member of the immunoglobulin superfamily--CTLA-4.* Nature, 1987. **328**(6127): p. 267-70.
119. Tivol, E.A., et al., *Loss of CTLA-4 leads to massive lymphoproliferation and fatal multiorgan tissue destruction, revealing a critical negative regulatory role of CTLA-4.* Immunity, 1995. **3**(5): p. 541-7.
120. Waterhouse, P., et al., *Lymphoproliferative disorders with early lethality in mice deficient in Ctla-4.* Science, 1995. **270**(5238): p. 985-8.
121. Collins, A.V., et al., *The interaction properties of costimulatory molecules revisited.* Immunity, 2002. **17**(2): p. 201-10.
122. Lee, K.M., et al., *Molecular basis of T cell inactivation by CTLA-4.* Science, 1998. **282**(5397): p. 2263-6.
123. Rowshanravan, B., N. Halliday, and D.M. Sansom, *CTLA-4: a moving target in immunotherapy.* Blood, 2018. **131**(1): p. 58-67.
124. Qureshi, O.S., et al., *Trans-endocytosis of CD80 and CD86: a molecular basis for the cell-extrinsic function of CTLA-4.* Science, 2011. **332**(6029): p. 600-3.
125. Parry, R.V., et al., *CTLA-4 and PD-1 receptors inhibit T-cell activation by distinct mechanisms.* Mol Cell Biol, 2005. **25**(21): p. 9543-53.
126. Ishida, Y., et al., *Induced expression of PD-1, a novel member of the immunoglobulin gene superfamily, upon programmed cell death.* EMBO J, 1992. **11**(11): p. 3887-95.
127. Bardhan, K., T. Anagnostou, and V.A. Boussiotis, *The PD1:PD-L1/2 Pathway from Discovery to Clinical Implementation.* Front Immunol, 2016. **7**: p. 550.
128. Freeman, G.J., et al., *Engagement of the PD-1 immunoinhibitory receptor by a novel B7 family member leads to negative regulation of lymphocyte activation.* J Exp Med, 2000. **192**(7): p. 1027-34.
129. Ishida, M., et al., *Differential expression of PD-L1 and PD-L2, ligands for an inhibitory receptor PD-1, in the cells of lymphohematopoietic tissues.* Immunol Lett, 2002. **84**(1): p. 57-62.
130. Latchman, Y., et al., *PD-L2 is a second ligand for PD-1 and inhibits T cell activation.* Nat Immunol, 2001. **2**(3): p. 261-8.
131. Nishimura, H., et al., *Development of lupus-like autoimmune diseases by disruption of the PD-1 gene encoding an ITIM motif-carrying immunoreceptor.* Immunity, 1999. **11**(2): p. 141-51.

132. Nishimura, H., et al., *Autoimmune dilated cardiomyopathy in PD-1 receptor-deficient mice.* Science, 2001. **291**(5502): p. 319-22.
133. Ahn, E., et al., *Role of PD-1 during effector CD8 T cell differentiation.* Proc Natl Acad Sci U S A, 2018. **115**(18): p. 4749-4754.
134. Staron, M.M., et al., *The transcription factor FoxO1 sustains expression of the inhibitory receptor PD-1 and survival of antiviral CD8(+) T cells during chronic infection.* Immunity, 2014. **41**(5): p. 802-14.
135. Arasanz, H., et al., *PD1 signal transduction pathways in T cells.* Oncotarget, 2017. **8**(31): p. 51936-51945.
136. Hui, E., et al., *T cell costimulatory receptor CD28 is a primary target for PD-1-mediated inhibition.* Science, 2017. **355**(6332): p. 1428-1433.
137. Patsoukis, N., et al., *PD-1 increases PTEN phosphatase activity while decreasing PTEN protein stability by inhibiting casein kinase 2.* Mol Cell Biol, 2013. **33**(16): p. 3091-8.
138. Karwacz, K., et al., *PD-L1 co-stimulation contributes to ligand-induced T cell receptor down-modulation on CD8+ T cells.* EMBO Mol Med, 2011. **3**(10): p. 581-92.
139. Blackburn, S.D., et al., *Coregulation of CD8+ T cell exhaustion by multiple inhibitory receptors during chronic viral infection.* Nat Immunol, 2009. **10**(1): p. 29-37.
140. Harjunpaa, H. and C. Guillerey, *TIGIT as an emerging immune checkpoint.* Clinical and Experimental Immunology, 2019.
141. Goldberg, M.V. and C.G. Drake, *LAG-3 in Cancer Immunotherapy.* Curr Top Microbiol Immunol, 2011. **344**: p. 269-78.
142. Das, M., C. Zhu, and V.K. Kuchroo, *Tim-3 and its role in regulating anti-tumor immunity.* Immunol Rev, 2017. **276**(1): p. 97-111.
143. Agresta, L., K.H.N. Hoebe, and E.M. Janssen, *The Emerging Role of CD244 Signaling in Immune Cells of the Tumor Microenvironment.* Front Immunol, 2018. **9**: p. 2809.
144. Wherry, E.J., et al., *Antigen-independent memory CD8 T cells do not develop during chronic viral infection.* Proc Natl Acad Sci U S A, 2004. **101**(45): p. 16004-9.
145. Utzschneider, D.T., et al., *T Cell Factor 1-Expressing Memory-like CD8(+) T Cells Sustain the Immune Response to Chronic Viral Infections.* Immunity, 2016. **45**(2): p. 415-27.
146. He, R., et al., *Follicular CXCR5- expressing CD8(+) T cells curtail chronic viral infection.* Nature, 2016. **537**(7620): p. 412-428.
147. Im, S.J., et al., *Defining CD8+ T cells that provide the proliferative burst after PD-1 therapy.* Nature, 2016. **537**(7620): p. 417-421.
148. Yao, C., et al., *Single-cell RNA-seq reveals TOX as a key regulator of CD8(+) T cell persistence in chronic infection.* Nat Immunol, 2019. **20**(7): p. 890-901.
149. Alfei, F., et al., *TOX reinforces the phenotype and longevity of exhausted T cells in chronic viral infection.* Nature, 2019. **571**(7764): p. 265-269.
150. Scott, A.C., et al., *TOX is a critical regulator of tumour-specific T cell differentiation.* Nature, 2019. **571**(7764): p. 270-274.
151. Khan, O., et al., *TOX transcriptionally and epigenetically programs CD8(+) T cell exhaustion.* Nature, 2019. **571**(7764): p. 211-218.
152. Wang, X., et al., *TOX promotes the exhaustion of antitumor CD8(+) T cells by preventing PD1 degradation in hepatocellular carcinoma.* J Hepatol, 2019. **71**(4): p. 731-741.
153. Seo, H., et al., *TOX and TOX2 transcription factors cooperate with NR4A transcription factors to impose CD8(+) T cell exhaustion.* Proc Natl Acad Sci U S A, 2019. **116**(25): p. 12410-12415.
154. Pallett, L.J., N. Schmidt, and A. Schurich, *T cell metabolism in chronic viral infection.* Clin Exp Immunol, 2019. **197**(2): p. 143-152.

155. Patsoukis, N., et al., *PD-1 alters T-cell metabolic reprogramming by inhibiting glycolysis and promoting lipolysis and fatty acid oxidation.* Nat Commun, 2015. **6**: p. 6692.
156. Delgoffe, G.M. and J.D. Powell, *Feeding an army: The metabolism of T cells in activation, anergy, and exhaustion.* Mol Immunol, 2015. **68**(2 Pt C): p. 492-6.
157. Bengsch, B., et al., *Bioenergetic Insufficiencies Due to Metabolic Alterations Regulated by the Inhibitory Receptor PD-1 Are an Early Driver of CD8(+) T Cell Exhaustion.* Immunity, 2016. **45**(2): p. 358-73.
158. Scharping, N.E., et al., *The Tumor Microenvironment Represses T Cell Mitochondrial Biogenesis to Drive Intratumoral T Cell Metabolic Insufficiency and Dysfunction.* Immunity, 2016. **45**(2): p. 374-88.
159. Sen, D.R., et al., *The epigenetic landscape of T cell exhaustion.* Science, 2016. **354**(6316): p. 1165-1169.
160. Youngblood, B., et al., *Chronic Virus Infection Enforces Demethylation of the Locus that Encodes PD-1 in Antigen-Specific CD8(+) T Cells.* Immunity, 2011. **35**(3): p. 400-412.
161. Pauken, K.E. and E.J. Wherry, *Overcoming T cell exhaustion in infection and cancer.* Trends Immunol, 2015. **36**(4): p. 265-76.
162. Zarour, H.M., *Reversing T-cell Dysfunction and Exhaustion in Cancer.* Clin Cancer Res, 2016. **22**(8): p. 1856-64.
163. Vajdic, C.M. and M.T. van Leeuwen, *Cancer incidence and risk factors after solid organ transplantation.* Int J Cancer, 2009. **125**(8): p. 1747-54.
164. Pages, F., et al., *Immune infiltration in human tumors: a prognostic factor that should not be ignored.* Oncogene, 2010. **29**(8): p. 1093-102.
165. Hanahan, D. and R.A. Weinberg, *Hallmarks of cancer: the next generation.* Cell, 2011. **144**(5): p. 646-74.
166. Munn, D.H. and V. Bronte, *Immune suppressive mechanisms in the tumor microenvironment.* Curr Opin Immunol, 2016. **39**: p. 1-6.
167. Leach, D.R., M.F. Krummel, and J.P. Allison, *Enhancement of antitumor immunity by CTLA-4 blockade.* Science, 1996. **271**(5256): p. 1734-6.
168. Huang, A.C., et al., *T-cell invigoration to tumour burden ratio associated with anti-PD-1 response.* Nature, 2017. **545**(7652): p. 60-65.
169. Snyder, A., et al., *Genetic basis for clinical response to CTLA-4 blockade in melanoma.* N Engl J Med, 2014. **371**(23): p. 2189-2199.
170. Johnson, D.B., C. Peng, and J.A. Sosman, *Nivolumab in melanoma: latest evidence and clinical potential.* Ther Adv Med Oncol, 2015. **7**(2): p. 97-106.
171. Patel, S.P. and R. Kurzrock, *PD-L1 Expression as a Predictive Biomarker in Cancer Immunotherapy.* Mol Cancer Ther, 2015. **14**(4): p. 847-56.
172. Gong, J., et al., *Development of PD-1 and PD-L1 inhibitors as a form of cancer immunotherapy: a comprehensive review of registration trials and future considerations.* J Immunother Cancer, 2018. **6**(1): p. 8.
173. Seidel, J.A., A. Otsuka, and K. Kabashima, *Anti-PD-1 and Anti-CTLA-4 Therapies in Cancer: Mechanisms of Action, Efficacy, and Limitations.* Front Oncol, 2018. **8**: p. 86.
174. Rotte, A., *Combination of CTLA-4 and PD-1 blockers for treatment of cancer.* J Exp Clin Cancer Res, 2019. **38**(1): p. 255.
175. Wykes, M.N. and S.R. Lewin, *Immune checkpoint blockade in infectious diseases.* Nat Rev Immunol, 2018. **18**(2): p. 91-104.
176. Chew, G.M., et al., *TIGIT Marks Exhausted T Cells, Correlates with Disease Progression, and Serves as a Target for Immune Restoration in HIV and SIV Infection.* PLoS Pathog, 2016. **12**(1): p. e1005349.

177. Fromentin, R., et al., *PD-1 blockade potentiates HIV latency reversal ex vivo in CD4(+) T cells from ART-suppressed individuals.* Nat Commun, 2019. **10**(1): p. 814.
178. Zhang, E., et al., *The expression of PD-1 ligands and their involvement in regulation of T cell functions in acute and chronic woodchuck hepatitis virus infection.* PLoS One, 2011. **6**(10): p. e26196.
179. Koksal, A.S., et al., *HBV-related acute hepatitis due to immune checkpoint inhibitors in a patient with malignant melanoma.* Ann Oncol, 2017. **28**(12): p. 3103-3104.
180. Zong, L., et al., *Breakdown of adaptive immunotolerance induces hepatocellular carcinoma in HBsAg-tg mice.* Nat Commun, 2019. **10**(1): p. 221.
181. LaNoue, K.F. and A.C. Schoolwerth, *Metabolite transport in mitochondria.* Annu Rev Biochem, 1979. **48**: p. 871-922.
182. Sluse, F.E., M. Ranson, and C. Liebecq, *Mechanism of the exchanges catalysed by the oxoglutarate translocatory of rat-heart mitochondria. Kinetics of the exchange reactions between 2-oxoglutarate, malate and malonate.* Eur J Biochem, 1972. **25**(2): p. 207-17.
183. LaNoue, K.F. and J.R. Williamson, *Interrelationships between malate-aspartate shuttle and citric acid cycle in rat heart mitochondria.* Metabolism, 1971. **20**(2): p. 119-40.
184. LaNoue, K.F. and M.E. Tischler, *Electrogenic characteristics of the mitochondrial glutamate-aspartate antiporter.* J Biol Chem, 1974. **249**(23): p. 7522-8.
185. LaNoue, K.F., A.J. Meijer, and A. Brouwer, *Evidence for electrogenic aspartate transport in rat liver mitochondria.* Arch Biochem Biophys, 1974. **161**(2): p. 544-50.
186. Jiang, X., H. Chang, and Y. Zhou, *Expression, purification and preliminary crystallographic studies of human glutamate oxaloacetate transaminase 1 (GOT1).* Protein Expr Purif, 2015. **113**: p. 102-6.
187. Sun, L., et al., *Particulate matter of 2.5 mum or less in diameter disturbs the balance of TH17/regulatory T cells by targeting glutamate oxaloacetate transaminase 1 and hypoxia-inducible factor 1alpha in an asthma model.* J Allergy Clin Immunol, 2020. **145**(1): p. 402-414.
188. Xu, T., et al., *Metabolic control of TH17 and induced Treg cell balance by an epigenetic mechanism.* Nature, 2017. **548**(7666): p. 228-233.
189. Zhang, X., J. Liu, and X. Cao, *Metabolic control of T-cell immunity via epigenetic mechanisms.* Cell Mol Immunol, 2018. **15**(3): p. 203-205.
190. Birsoy, K., et al., *An Essential Role of the Mitochondrial Electron Transport Chain in Cell Proliferation Is to Enable Aspartate Synthesis.* Cell, 2015. **162**(3): p. 540-51.
191. Dutko, F.J. and M.B.A. Oldstone, *Genomic and Biological Variation among Commonly Used Lymphocytic Choriomeningitis Virus-Strains.* Journal of General Virology, 1983. **64**(Aug): p. 1689-1698.
192. Ahmed, R., et al., *Selection of genetic variants of lymphocytic choriomeningitis virus in spleens of persistently infected mice. Role in suppression of cytotoxic T lymphocyte response and viral persistence.* J Exp Med, 1984. **160**(2): p. 521-40.
193. Lee, P.P., et al., *A Critical Role for Dnmt1 and DNA Methylation in T Cell Development, Function, and Survival.* Immunity, 2001. **15**(5): p. 763-774.
194. Sawada, S., et al., *A lineage-specific transcriptional silencer regulates CD4 gene expression during T lymphocyte development.* Cell, 1994. **77**(6): p. 917-929.
195. Pircher, H., et al., *Tolerance induction in double specific T-cell receptor transgenic mice varies with antigen.* Nature, 1989. **342**: p. 559.
196. Dagley, M.J. and M.J. McConville, *DExSI: a new tool for the rapid quantitation of 13C-labelled metabolites detected by GC-MS.* Bioinformatics, 2018. **34**(11): p. 1957-1958.

197. Uran, S., et al., *Quantification of 13C pyruvate and 13C lactate in dog blood by reversed-phase liquid chromatography-electrospray ionization mass spectrometry after derivatization with 3-nitrophenylhydrazine.* J Pharm Biomed Anal, 2007. **44**(4): p. 947-54.
198. Lee, P.P., et al., *A critical role for Dnmt1 and DNA methylation in T cell development, function, and survival.* Immunity, 2001. **15**(5): p. 763-74.
199. Sawada, S., et al., *A lineage-specific transcriptional silencer regulates CD4 gene expression during T lymphocyte development.* Cell, 1994. **77**(6): p. 917-29.
200. Pircher, H., et al., *Tolerance induction in double specific T-cell receptor transgenic mice varies with antigen.* Nature, 1989. **342**(6249): p. 559-61.
201. IMPC. Available from: https://www.mousephenotype.org/data/genes/MGI:95791.
202. Malek, T.R., *The biology of interleukin-2.* Annu Rev Immunol, 2008. **26**: p. 453-79.
203. Huster, K.M., et al., *Selective expression of IL-7 receptor on memory T cells identifies early CD40L-dependent generation of distinct CD8+ memory T cell subsets.* Proc Natl Acad Sci U S A, 2004. **101**(15): p. 5610-5.
204. Ballou, L.M. and R.Z. Lin, *Rapamycin and mTOR kinase inhibitors.* J Chem Biol, 2008. **1**(1-4): p. 27-36.
205. Schreiber, S.L. and G.R. Crabtree, *The mechanism of action of cyclosporin A and FK506.* Immunol Today, 1992. **13**(4): p. 136-42.
206. Joshi, N.S., et al., *Inflammation directs memory precursor and short-lived effector CD8(+) T cell fates via the graded expression of T-bet transcription factor.* Immunity, 2007. **27**(2): p. 281-95.
207. Meeth, K., et al., *The YUMM lines: a series of congenic mouse melanoma cell lines with defined genetic alterations.* Pigment Cell Melanoma Res, 2016. **29**(5): p. 590-7.
208. Llufrio, E.M., et al., *Metabolite Concentrations Are Unstable during Cell Sorting.* Faseb Journal, 2018. **32**(1).
209. Jitrapakdee, S., A. Vidal-Puig, and J.C. Wallace, *Anaplerotic roles of pyruvate carboxylase in mammalian tissues.* Cellular and Molecular Life Sciences, 2006. **63**(7-8): p. 843-854.
210. Koves, T.R., et al., *Peroxisome proliferator-activated receptor-gamma co-activator 1alpha-mediated metabolic remodeling of skeletal myocytes mimics exercise training and reverses lipid-induced mitochondrial inefficiency.* J Biol Chem, 2005. **280**(39): p. 33588-98.
211. Wise, D.R., et al., *Myc regulates a transcriptional program that stimulates mitochondrial glutaminolysis and leads to glutamine addiction.* Proceedings of the National Academy of Sciences of the United States of America, 2008. **105**(48): p. 18782-18787.
212. Melendez-Rodriguez, F., et al., *HIF1 alpha Suppresses Tumor Cell Proliferation through Inhibition of Aspartate Biosynthesis.* Cell Reports, 2019. **26**(9): p. 2257-+.
213. Vigano, S., et al., *CD160-Associated CD8 T-Cell Functional Impairment Is Independent of PD-1 Expression.* Plos Pathogens, 2014. **10**(9).
214. Kurachi, M., et al., *Hidden Caveat of Inducible Cre Recombinase.* Immunity, 2019. **51**(4): p. 591-592.
215. Shen, W., et al., *Involvement of a glycerol-3-phosphate dehydrogenase in modulating the NADH/NAD+ ratio provides evidence of a mitochondrial glycerol-3-phosphate shuttle in Arabidopsis.* Plant Cell, 2006. **18**(2): p. 422-41.

216. Schweiger, M., et al., *Characterization of recombinant human nicotinamide mononucleotide adenylyl transferase (NMNAT), a nuclear enzyme essential for NAD synthesis.* FEBS Lett, 2001. **492**(1-2): p. 95-100.
217. Gullino, P.M., S.H. Clark, and F.H. Grantham, *The Interstitial Fluid of Solid Tumors.* Cancer Res, 1964. **24**: p. 780-94.
218. McKee, T.J. and S.V. Komarova, *Is it time to reinvent basic cell culture medium?* Am J Physiol Cell Physiol, 2017. **312**(5): p. C624-C626.
219. Takahashi, M., et al., *Promoting effect of beta-mercaptoethanol on in vitro development under oxidative stress and cystine uptake of bovine embryos.* Biol Reprod, 2002. **66**(3): p. 562-7.
220. Devadas, S., et al., *Discrete generation of superoxide and hydrogen peroxide by T cell receptor stimulation: selective regulation of mitogen-activated protein kinase activation and fas ligand expression.* J Exp Med, 2002. **195**(1): p. 59-70.
221. Jackson, S.H., et al., *T cells express a phagocyte-type NADPH oxidase that is activated after T cell receptor stimulation.* Nat Immunol, 2004. **5**(8): p. 818-27.
222. Yi, J.S., et al., *Electron transport complex I is required for CD8+ T cell function.* J Immunol, 2006. **177**(2): p. 852-62.
223. Klein Geltink, R.I., D. O'Sullivan, and E.L. Pearce, *Caught in the cROSsfire: GSH Controls T Cell Metabolic Reprogramming.* Immunity, 2017. **46**(4): p. 525-527.
224. Sena, L.A., et al., *Mitochondria are required for antigen-specific T cell activation through reactive oxygen species signaling.* Immunity, 2013. **38**(2): p. 225-36.
225. Zhao, R.Z., et al., *Mitochondrial electron transport chain, ROS generation and uncoupling (Review).* Int J Mol Med, 2019. **44**(1): p. 3-15.
226. Scialo, F., D.J. Fernandez-Ayala, and A. Sanz, *Role of Mitochondrial Reverse Electron Transport in ROS Signaling: Potential Roles in Health and Disease.* Front Physiol, 2017. **8**: p. 428.
227. Mak, T.W., et al., *Glutathione Primes T Cell Metabolism for Inflammation.* Immunity, 2017. **46**(4): p. 675-689.
228. Gulow, K., et al., *HIV-1 trans-activator of transcription substitutes for oxidative signaling in activation-induced T cell death.* J Immunol, 2005. **174**(9): p. 5249-60.
229. Zhu, Y., et al., *Exogenous NAD(+) decreases oxidative stress and protects H2O2-treated RPE cells against necrotic death through the up-regulation of autophagy.* Sci Rep, 2016. **6**: p. 26322.
230. Kareyeva, A.V., V.G. Grivennikova, and A.D. Vinogradov, *Mitochondrial hydrogen peroxide production as determined by the pyridine nucleotide pool and its redox state.* Biochim Biophys Acta, 2012. **1817**(10): p. 1879-85.
231. Vinogradov, A.D. and V.G. Grivennikova, *Oxidation of NADH and ROS production by respiratory complex I.* Biochim Biophys Acta, 2016. **1857**(7): p. 863-71.
232. Abrego, J., et al., *GOT1-mediated anaplerotic glutamine metabolism regulates chronic acidosis stress in pancreatic cancer cells.* Cancer Lett, 2017. **400**: p. 37-46.
233. Zhou, X., et al., *Inhibition of glutamate oxaloacetate transaminase 1 in cancer cell lines results in altered metabolism with increased dependency of glucose.* BMC Cancer, 2018. **18**(1): p. 559.
234. Nelson, B.S., et al., *Tissue of origin dictates GOT1 dependence and confers synthetic lethality to radiotherapy.* Cancer Metab, 2020. **8**: p. 1.
235. Thornburg, J.M., et al., *Targeting aspartate aminotransferase in breast cancer.* Breast Cancer Res, 2008. **10**(5): p. R84.

236. Beeler, T. and J.E. Churchich, *Reactivity of the phosphopyridoxal groups of cystathionase.* J Biol Chem, 1976. **251**(17): p. 5267-71.
237. Lu, S.C., *Glutathione synthesis.* Biochim Biophys Acta, 2013. **1830**(5): p. 3143-53.
238. Wamelink, M.M., E.A. Struys, and C. Jakobs, *The biochemistry, metabolism and inherited defects of the pentose phosphate pathway: a review.* J Inherit Metab Dis, 2008. **31**(6): p. 703-17.
239. Cairns, R.A., I.S. Harris, and T.W. Mak, *Regulation of cancer cell metabolism.* Nat Rev Cancer, 2011. **11**(2): p. 85-95.
240. Matschke, J., et al., *Targeted Inhibition of Glutamine-Dependent Glutathione Metabolism Overcomes Death Resistance Induced by Chronic Cycling Hypoxia.* Antioxid Redox Signal, 2016. **25**(2): p. 89-107.
241. Son, J., et al., *Glutamine supports pancreatic cancer growth through a KRAS-regulated metabolic pathway.* Nature, 2013. **496**(7443): p. 101-+.
242. Aldini, G., et al., *N-Acetylcysteine as an antioxidant and disulphide breaking agent: the reasons why.* Free Radic Res, 2018. **52**(7): p. 751-762.
243. Chen, H., et al., *Malate-Aspartate Shuttle Inhibitor Aminooxyacetate Acid Induces Apoptosis and Impairs Energy Metabolism of Both Resting Microglia and LPS-Activated Microglia.* Neurochem Res, 2015. **40**(6): p. 1311-8.
244. Kauppinen, R.A., T.S. Sihra, and D.G. Nicholls, *Aminooxyacetic acid inhibits the malate-aspartate shuttle in isolated nerve terminals and prevents the mitochondria from utilizing glycolytic substrates.* Biochim Biophys Acta, 1987. **930**(2): p. 173-8.
245. Sanin, D.E., et al., *Mitochondrial Membrane Potential Regulates Nuclear Gene Expression in Macrophages Exposed to Prostaglandin E2.* Immunity, 2018. **49**(6): p. 1021-1033 e6.
246. Legmann, R., et al., *Analysis of glycolytic flux as a rapid screen to identify low lactate producing CHO cell lines with desirable monoclonal antibody yield and glycan profile.* BMC Proc, 2011. **5 Suppl 8**: p. P94.
247. Johnson, M.O., et al., *Distinct Regulation of Th17 and Th1 Cell Differentiation by Glutaminase-Dependent Metabolism.* Cell, 2018. **175**(7): p. 1780-1795 e19.
248. Holbrook, J.J. and H. Gutfreund, *Approaches to the study of enzyme mechanisms lactate dehydrogenase.* FEBS Lett, 1973. **31**(2): p. 157-169.
249. Behal, R.H., et al., *Regulation of the pyruvate dehydrogenase multienzyme complex.* Annu Rev Nutr, 1993. **13**: p. 497-520.
250. Jitrapakdee, S., et al., *Structure, mechanism and regulation of pyruvate carboxylase.* Biochem J, 2008. **413**(3): p. 369-87.
251. Yoshida, T., et al., *A covalent small molecule inhibitor of glutamate-oxaloacetate transaminase 1 impairs pancreatic cancer growth.* Biochem Biophys Res Commun, 2020. **522**(3): p. 633-638.
252. Sullivan, L.B., et al., *Supporting Aspartate Biosynthesis Is an Essential Function of Respiration in Proliferating Cells.* Cell, 2015. **162**(3): p. 552-63.
253. Minarik, P., et al., *Malate dehydrogenases--structure and function.* Gen Physiol Biophys, 2002. **21**(3): p. 257-65.
254. Hederstedt, L. and L. Rutberg, *Succinate dehydrogenase--a comparative review.* Microbiol Rev, 1981. **45**(4): p. 542-55.
255. Vinogradov, A.D., et al., *Regulation of succinate dehydrogenase and tautomerization of oxaloacetate.* Adv Enzyme Regul, 1989. **28**: p. 271-80.

256. Panchenko, M.V. and A.D. Vinogradov, *Direct demonstration of enol-oxaloacetate as an immediate product of malate oxidation by the mammalian succinate dehydrogenase.* FEBS Lett, 1991. **286**(1-2): p. 76-8.
257. Ho, P.C., et al., *Phosphoenolpyruvate Is a Metabolic Checkpoint of Anti-tumor T Cell Responses.* Cell, 2015. **162**(6): p. 1217-28.
258. Kendziorek, M., A. Paszkowski, and B. Zagdanska, *Biochemical characterization and kinetic properties of alanine aminotransferase homologues partially purified from wheat (Triticum aestivum L.).* Phytochemistry, 2012. **82**: p. 7-14.
259. McKenna, M.C. and G.C. Ferreira, *Enzyme Complexes Important for the Glutamate-Glutamine Cycle.* Adv Neurobiol, 2016. **13**: p. 59-98.
260. Haas, R., et al., *Lactate Regulates Metabolic and Pro-inflammatory Circuits in Control of T Cell Migration and Effector Functions.* PLoS Biol, 2015. **13**(7): p. e1002202.
261. Kaoru Hasegawa, M.K., *A high concentration of pyruvate is essential for survival and DNA synthesis in primary cultures of adult rat hepatocytes in a serum-free medium.* Biomedical Research, 1981. **2**(2): p. 217-221.
262. Elmore, E. and M. Swift, *Growth of human skin fibroblasts in dialyzed fetal bovine serum.* In Vitro, 1977. **13**(12): p. 837-42.
263. Neuman, R.E. and C.T. Mc, *Growth-promoting properties of pyruvate oxal-acetate, and alpha-ketoglutarate for isolated Walker carcinosarcoma 256 cells.* Proc Soc Exp Biol Med, 1958. **98**(2): p. 303-6.
264. Odorizzi, P.M., et al., *Genetic absence of PD-1 promotes accumulation of terminally differentiated exhausted CD8+ T cells.* J Exp Med, 2015. **212**(7): p. 1125-37.
265. Matloubian, M., R.J. Concepcion, and R. Ahmed, *CD4+ T cells are required to sustain CD8+ cytotoxic T-cell responses during chronic viral infection.* J Virol, 1994. **68**(12): p. 8056-63.
266. Garcin, E.D., *GAPDH as a model non-canonical AU-rich RNA binding protein.* Semin Cell Dev Biol, 2019. **86**: p. 162-173.
267. Chang, C.H., et al., *Posttranscriptional control of T cell effector function by aerobic glycolysis.* Cell, 2013. **153**(6): p. 1239-51.
268. Millet, P., et al., *GAPDH Binding to TNF-alpha mRNA Contributes to Posttranscriptional Repression in Monocytes: A Novel Mechanism of Communication between Inflammation and Metabolism.* J Immunol, 2016. **196**(6): p. 2541-51.
269. Peng, M., et al., *Aerobic glycolysis promotes T helper 1 cell differentiation through an epigenetic mechanism.* Science, 2016. **354**(6311): p. 481-484.
270. Ogando, J., et al., *PD-1 signaling affects cristae morphology and leads to mitochondrial dysfunction in human CD8(+) T lymphocytes.* J Immunother Cancer, 2019. **7**(1): p. 151.
271. Thommen, D.S., et al., *A transcriptionally and functionally distinct PD-1(+) CD8(+) T cell pool with predictive potential in non-small-cell lung cancer treated with PD-1 blockade.* Nat Med, 2018. **24**(7): p. 994-1004.
272. Schurich, A., et al., *Distinct Metabolic Requirements of Exhausted and Functional Virus-Specific CD8 T Cells in the Same Host.* Cell Rep, 2016. **16**(5): p. 1243-1252.
273. Joller, N., et al., *Cutting edge: TIGIT has T cell-intrinsic inhibitory functions.* J Immunol, 2011. **186**(3): p. 1338-42.
274. Kao, C., et al., *Transcription factor T-bet represses expression of the inhibitory receptor PD-1 and sustains virus-specific CD8+ T cell responses during chronic infection.* Nat Immunol, 2011. **12**(7): p. 663-71.
275. Szabo, S.J., et al., *Distinct effects of T-bet in TH1 lineage commitment and IFN-gamma production in CD4 and CD8 T cells.* Science, 2002. **295**(5553): p. 338-42.

276. McKinney, E.F. and K.G.C. Smith, *Metabolic exhaustion in infection, cancer and autoimmunity.* Nat Immunol, 2018. **19**(3): p. 213-221.
277. Hirata, E. and E. Sahai, *Tumor Microenvironment and Differential Responses to Therapy.* Cold Spring Harbor Perspectives in Medicine, 2017. **7**(7).
278. Geltink, R.I.K., R.L. Kyle, and E.L. Pearce, *Unraveling the Complex Interplay Between T Cell Metabolism and Function.* Annual Review of Immunology, Vol 36, 2018. **36**: p. 461-488.
279. Mohammed, S.A., et al., *Epigenetic Control of Mitochondrial Function in the Vasculature.* Frontiers in Cardiovascular Medicine, 2020. **7**.

Supplementary figures

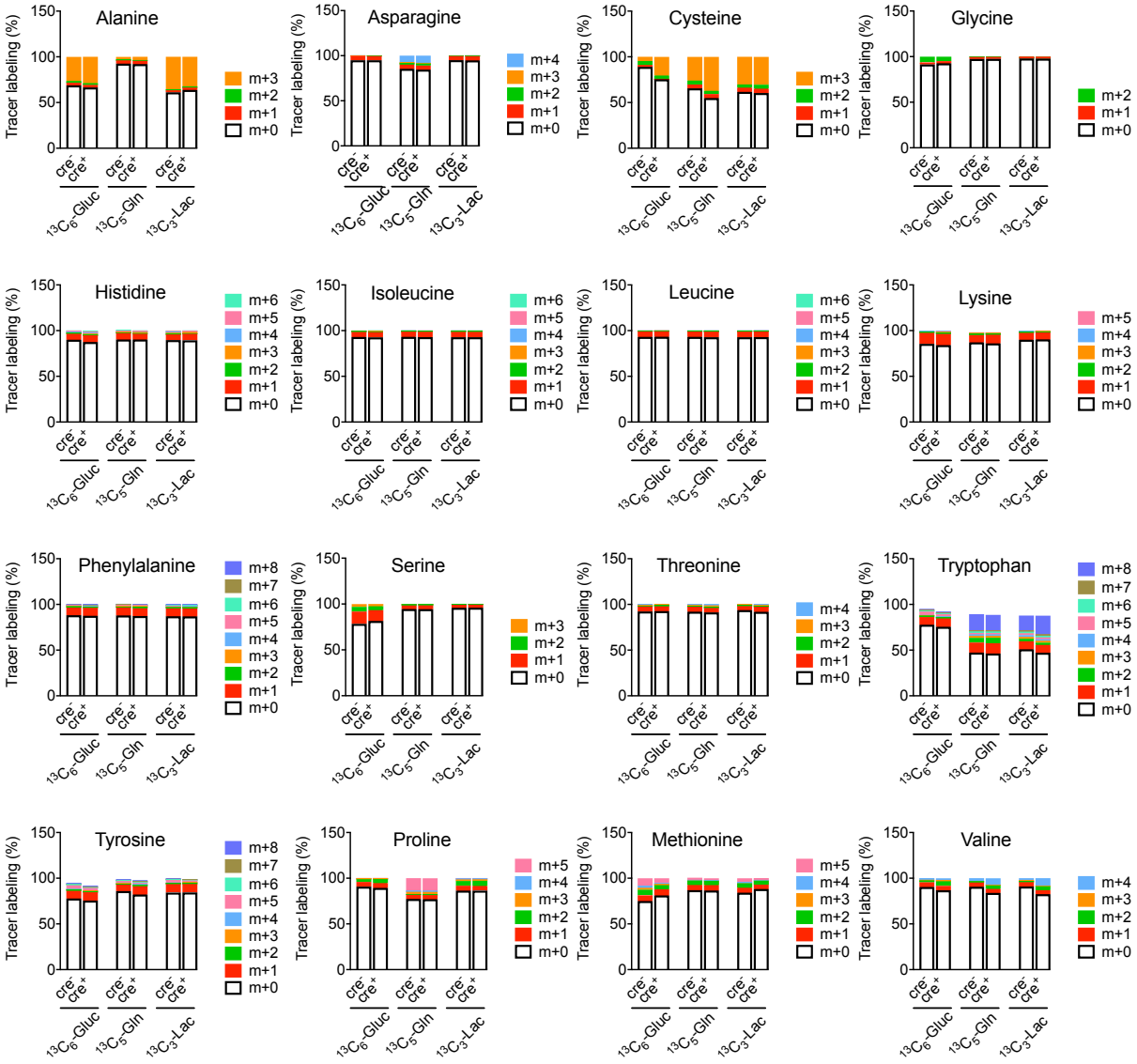

Supplementary Figure 1: Stable isotype labeling of proteinogenic amino acids in in vitro cultivated wildtype and Got1-deficient P14 cells. *Bar graphs showing the label distribution of the mean of three biological replicates.*

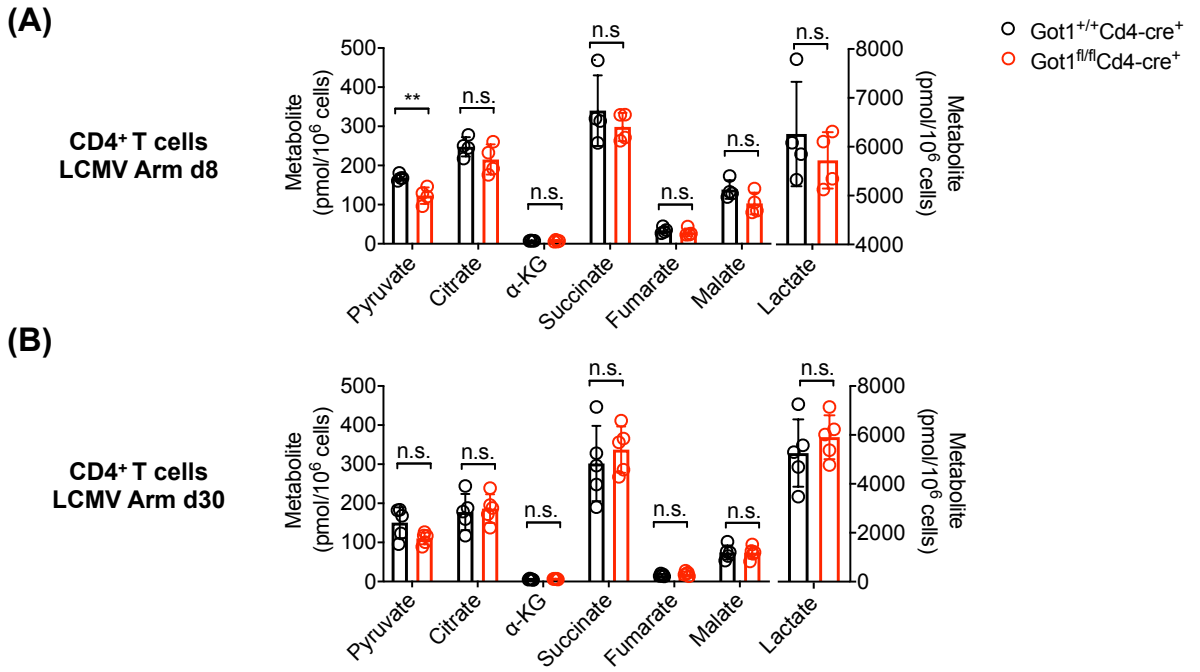

Supplementary Figure 2: MS quantification revealed altered organic acid levels in Got1-deficient CD4+ T cells *A: Samples obtained from T cells after LCMV Arm infection, 8 dpi B: Samples obtained from T cells after LCMV Arm infection, 30 dpi. Accumulated data from 2 experiments with 4-5 mice in total. n.s. = p>0.05; ** = p<0.01. P values were calculated by two-tailed unpaired Student's t-tests.*

List of figures

Figure 1.1: Schematic representation of TCR, BCR and MHC. 3
Figure 1.2: Overview over $CD4^+$ T cell subsets 5
Figure 1.3: Kinetics of CTLs (blue line) over time following a viral infection (red line) 6
Figure 1.4: Simplified representation of key T cell receptor signaling pathways 7
Figure 1.5: T cell metabolism in different T cell subsets 9
Figure 1.6: Inhibitory receptors interfere with T cell activation 12
Figure 1.7: The MAS connects cytosolic and mitochondrial metabolism. 16
Figure 4.1: Overview of the investigated Got1-deficient mouse lines 56
Figure 4.2: Immune characterization of naïve wildtype and Got1-deficient mice 57
Figure 4.3: GOT1 expression in $CD8^+$ T cells requires antigenic stimulation 59
Figure 4.4: GOT1 expression in $CD8^+$ T cells requires TCR stimulation 59
Figure 4.5: GOT1 expression in $CD8^+$ T cells is independent of inflammatory stimuli 60
Figure 4.6: Got1 is expressed in antigen-specific TILs 61
Figure 4.7: Got1 is required for effector cell responses following LCMV Arm infection 63
Figure 4.8: Got1 is not required for memory formation following LCMV Arm infection 65
Figure 4.9: Got1 is required for effector cell responses following LCMV cl-13 infection 67
Figure 4.10: Got1 is required for chronic infection with LCMV cl-13 69
Figure 4.11: Got1 deficiency correlates with tumor growth 70
Figure 4.12: Got1 deficiency exacerbated exhaustion of donor TILs in B16-gp33 tumors 72
Figure 4.13: Got1-deficiency exacerbated exhaustion of co-transferred donor TILs in B16-gp33 tumors. 74
Figure 4.14: Got1-deficiency exacerbated exhaustion of donor TILs in YUMM-gp33 tumors 76
Figure 4.15: Got1-deficiency exacerbated exhaustion of co-transferred donor TILs in YUMM-gp33 tumors. 78
Figure 4.16: MS quantification revealed altered organic acid levels in Got1-deficient $CD8^+$ T cells 79
Figure 4.17: Changes of NAD^+ and NADH levels in wildtype and Got1-deficient $CD8^+$ T cells 80
Figure 4.18: Stable isotype labeling of in vitro cultivated wildtype and Got1-deficient P14 cells. 82
Figure 4.19: Seahorse electron flow (A) and coupling assay (B) showed similar results for in vitro activated wildtype and Got1-deficient T cells 83
Figure 4.20: Got1 deficiency influences cell persistence and apoptosis after nutrient restriction in vitro 85

Figure 4.21: Got1 deficiency influences mitochondrial function and ROS after nutrient restriction in vitro 86
Figure 4.22: GOT1 deficiency affects OCR under nutrient-restricted conditions in vitro 87
Figure 4.23: GOT1-associated phenotypes can be rescued in vitro] 89
Figure 4.24: Antitumoral function can be improved by pre-treatment of Got1-deficient P14 cells 91
Figure 4.25: Flow cytometry analysis of recovered pre-treated wildtype or Got1-deficient P14 cells from B16-gp33 tumors or spleens 92
Figure 5.1: GOT1 maintains metabolic fitness to antagonize T cell exhaustion 111
Supplementary Figure 1: Stable isotype labeling of proteinogenic amino acids in in vitro cultivated wildtype and Got1-deficient P14 cells 127
Supplementary Figure 2: MS quantification revealed altered organic acid levels in Got1-deficient $CD4^+$ T cells 128

List of tables

Table 1: Overview over used chemicals and reagents. Standard chemicals that are not listed were purchased from Sigma-Aldrich/Merck KGaA (Darmstadt, Germany). 19
Table 2: Commercially available kits used in the study. 23
Table 3: Overview over used buffers and solutions and the respective composition. 24
Table 4: Cell culture medium composition for immortalized cell lines. 26
Table 5: Fluorescence-labeled antibodies for flow cytometry and used dilutions. 27
Table 6: Biotinylated and HRP-conjugated antibodies and respective dilutions. 29
Table 7: Unconjugated antibodies and respective dilutions. 29
Table 8: Overview over used enzymes, proteins and peptides. 30
Table 9: Immortalized cell lines for tumor implantation and virus replication. 31
Table 10: Viral strains for in vivo infections. 31
Table 11: Used mouse lines. 31
Table 12: Overview over consumables used in the study. 32
Table 13: Instruments for analysis and experiments. 33
Table 14: Used software and software versions. 35
Table 15: PCR program for qRT-PCR reaction. 44
Table 16: Portal injections for the mitochondrial stress test [in Seahorse medium + 6.7 mM-10 mM glucose]. 47
Table 17: Portal injections for the glycolytic stress test [in plain Seahorse medium]. 47
Table 18: Assay program mitochondrial and glycolytic stress tests. 47
Table 19: Portal injections for the mitochondrial coupling assay. 48
Table 20: Assay program for coupling and electron flow assay. 48
Table 21 Portal injections for the mitochondrial coupling assay. 49
Table 22: Standard PCR program for genotyping. 52
Table 23: Primer for Got1$^{flox/flox}$ genotyping (row 1-6), Cd4-cre genotyping (row 7, 8), P14 genotyping (row 9-12). 52
Table 24: Standard flow cytometry staining for genotyping. 53

Abbreviations

AA	Antimycin A
ADP	Adenosin diphosphate
AICD	Activation-induced cell death
Akt	Proteinkinase B
AMPK	AMP-activated protein kinase
AnxV	Annexin V
AOA	(Aminooxy)acetic acid
AP-1	Activating protein 1
APC	Antigen presenting cell
APS	Ammonium persulfate
Arm	Armstrong
ATAC	Assay for transposase-accessible chromatin sequencing
BCR	B cell receptor
BFA	Brefeldin A
BHK	Baby hamster kidney cells
BSA	Bovine serum albumin
CaM	Calmodulin
CaN	Calcineurin
CCR7	Chemokine receptor 7
CD	Cluster of differentiation
cl-13	Clone 13
CsA	Cyclosporin A
CTL	Cytotoxic T lymphocytes
CTLA-4	Cytotoxic T-lymphocyte-associated Protein 4
CXCR5	CXC chemokine receptor type 5
DAG	Diacylglycerol
DC	Dentritic cell
2-DG	2-Deoxyglucose
dpi	days post infection
DTAB	Dodecyltrimethylammoniumbromide
ECAR	Extracellular acidification rate
EOMES	Eomesodermin
ER	Endoplasmic reticulum
ETC	Electron transport chain
FACS	Fluorescence activated cell sorting

FAO	Fatty acid oxidation
FBS	Fetal bovine serum
FCCP	Carbonyl cyanide 4-(trifluoromethoxy)phenylhydrazone
fl	Flox
G3P	Glycerol-3-phosphate shutlle
GC/MS	Gas chromatography/mass spectrometry
GOT1	Glutamic oxaloacetic transaminase 1
GOT2	Glutamic oxaloacetic transaminase 2
gp33	Glycoprotein 33-41
GRP94	Heat shock protein 90kDa beta member
GSH	Glutathione
GSSG	Oxidized GSH
HBV/HCV	Hepatitis B/C virus
HIF-1α	Hypoxia-inducible factor 1α
HIV	Human immunodeficiency virus
HLA	Human leukocyte antigen
ICB	Immune checkpoint blockade
IFN	Interferon
IκB	Inhibitor of NFκB
IL	Interleukin
ILC	Innate lymphoid cell
ILL	Innate like lymphocytes
i.p.	Intraperitoneal
IP_3	Inositol 1,4,5-trisphosphate
ITAM	Immunoreceptor tyrosine-based activation motif
ITIM	Immunoreceptor tyrosine-based inhibition motif
ITSM	Immunoreceptor tyrosine-based switch motif
i.v.	Intravenous
IMPC	International Mouse Phenotyping Consortium
α-KG	α-Ketoglutarate
KLRG1	Killer cell lectin-like receptor subfamily G member 1
LAG-3	Lymphocyte-activation gene 3
LAT	Linker for activation of T cells
LCMV	Lymphocytic choriomeningitis virus
MΦ	Macrophage
MAIT	Mucosal-associated invariant T cells
MAPK	Mitogen-activated protein kinase

MAS	Malate aspartate shuttle
1x MAS	1x Mitochondrial assay solution
MDH	Malate dehydrogenase
MDSC	Myeloid derived suppressor cell
MFI	Mean fluorescence intensity
MHC	Major histocompatibility complex
mLN	Mesenteric lymph nodes
MTBSTFA	N-tert-Butyldimethylsilyl-N-methyltrifluoroacetamide
mTOR	Mechanistic target of Rapamycin
MOI	Multiplicity of infection
MPEC	Memory precursor effector cells
NAC	N-Acetyl-L-cysteine
NAD	Nicotinamide adenine dinucleotide (reduced NADH; oxidized NAD^+)
NADP	NAD phosphate (reduced NADPH; oxidized $NADP^+$)
NFAT	Nuclear factor of activated T cells
NK	Natural killer cell
NKT	Natural killer T cell
NOD	Nucleotide-binding oligomerization domain
NR	Nicotinamide Riboside
n.s.	Not significant
OAA	Oxaloacetate
OCR	Oxygen consumption rate
OM	Oligomycin
OVA	Ovalbumin
OXPHOS	Oxidative phosphorylation
PAMP	Pathogen-associated molecular patterns
PBS	Phosphate-buffered saline
PD-1	Programmed cell death protein 1
PDK1	Phosphoinositide-dependent kinase 1
pfu	Plaque forming units
PI	Propidium iodide
PIP_2	Phosphatidylinositol-4,5-bisphosphate
PIP_3	Phosphatidylinositol-3,4,5-triphosphate
PKCθ	Protein kinase Cθ
PLCγ1	Phospholipase C-γ 1
PLP	Pyridoxal 5'-phosphate
PMP	Plasma Membrane Permeabilizer

PRR	Pattern recognition receptor
pS6	p70S6 kinase
PTEN	Phosphatase and tensin homolog
Rapa	Rapamycin
RasGRP	Ras guanyl nucleotide-releasing protein
ROS	Reactive oxygen species
Rot	Rotenone
rpm	Rotation per minute
RT	Room temperature
s.c.	Subcutaneous
SD	Standard deviation
SLEC	Short lived effector cells
TAE	Tris acetate EDTA buffer
TAM	Tumor-associated macrophage
T-BET	T-box transcription factor TBX21
TCA cycle	Tricarboxylic acid cycle
TCF1	T cell factor 1
T_{CM}	Central memory T cell
TCR	T cell receptor
T_{EM}	Effector memory T cell
T_{Ex}	Exhausted T cell
T_{FH}	Follicular helper cell
T_H1	T helper 1 cell
T_H2	T helper 2 cell
T_H17	T helper 17 cell
TIGIT	T cell immunoreceptor with Ig and ITIM domains
TIL	Tumor infiltrating lymphocyte
TIM-3	T-cell immunoglobulin and mucin-domain containing-3
TLR	Toll-like receptor
TME	Tumor microenvironment
TMPD	N, N, N′, N′-tetramethyl-p-phenylenediamine (TMPD)
TOX	Thymocyte selection-associated HMG box protein
T_{Reg}	Regulatory T cell
T_{RM}	Tissue resident memory cell
UPLC	Ultra performance liquid chromatography
YUMM	Yale university mouse melanoma
ZAP70	Zeta-chain-associated protein kinase 70

List of publications

Journal articles:

Parts of this thesis are in preparation for re-submission:
Nina Weisshaar, Alaa Madi, Joschka Hey, Jingxia Wu, Sicong Ma, Gernot Poschet, Michael Buettner, Philipp Secker, Hannah Byren, Maren Baumeister, Alessa Mieg, Kerstin Mohr, Tilo Schlimbach, Marvin Hering, Helena Borgers, Christoph Plass, Rafael Carretero, Guoliang Cui: "The Malate-aspartate Shuttle Antagonizes $CD8^+$ T Cell Exhaustion"

Jingxia Wu, **Nina Weisshaar,** Agnes Hotz-Wagenblatt, Alaa Madi, Sicong Ma, Alessa Mieg, Marvin Hering, Kerstin Mohr, Tilo Schlimbach, Helena Borgers, and Guoliang Cui: "Skeletal Muscle Antagonizes Antiviral $CD8^+$ T Cell Exhaustion"; Accepted for publication in Science Advances, June 2020

Jingxia Wu, Alaa Madi, Alessa Mieg, Agnes Hotz-Wagenblatt, **Nina Weisshaar**, Sicong Ma, Kerstin Mohr, Tilo Schlimbach, Marvin Hering, Helena Borgers, and Guoliang Cui: "T Cell Factor 1 Suppresses $CD103^+$ Lung Tissue-Resident Memory T Cell Development"; Cell Reports 31, 107484, April 7, 2020; https://doi.org/10.1016/j.celrep.2020.03.048

Jingxia Wu, Sicong Ma, Roger Sandhoff, Yanan Ming, Agnes Hotz-Wagenblatt, Vincent Timmerman, Nathalie Bonello-Palot, Beate Schlotter-Weigel, Michaela Auer-Grumbach, Pavel Seeman, Wolfgang N. Löscher, Markus Reindl, Florian Weiss, Eric Mah, **Nina Weisshaar**, Alaa Madi, Kerstin Mohr, Tilo Schlimbach, Rubí M.-H. Velasco Cárdenas, Jonas Koeppel, Florian Grünschläger, Lisann Müller, Maren Baumeister, Britta Brügger, Michael Schmitt, Guido Wabnitz, Yvonne Samstag, Guoliang Cui: "Loss of Neurological Disease HSAN-I-Associated Gene SPTLC2 Impairs $CD8^+$ T Cell Responses to Infection by Inhibiting T Cell Metabolic Fitness"; Immunity 50, Issue 5, P1218-1231.E5, April 02, 2019; https://doi.org/10.1016/j.immuni.2019.03.005

Nina Weisshaar, Alaa Madi, Guoliang Cui: "Early TCR Signaling Sweetens Effector Function through PDHK1"; Trends in Endocrinology and Metabolism 29, Issue 9, P595-597, March 31 2018; https://doi.org/10.1016/j.tem.2018.03.016

Conference publications:

1st symposium on Cancer-Immuno-Oncology (Lübeck, Germany, 10/2018):
Nina Weisshaar, Guoliang Cui: “Investigating a potential role of Got1 in T cell exhaustion.”;
Proceedings on Cancer-Immuno-Oncology 1, Issue 1, Nov 03, 2018;
https://doi.org/10.18416/CIO.2018.1810040

Conference abstracts:

Immunometabolism: Fundamentals to Perspective New Therapies (Boston, USA, 06/2019)
Nina Weisshaar, Guoliang Cui: “Investigating a potential role of Got1 in T cell exhaustion.”

Prizes:

09/2018: **PhD Poster Presentation Prize** by the Helmholtz International Graduate School for Cancer Research, Heidelberg, Germany